Adaptive RAKE Receiver Structures for Ultra Wide-Band Systems

A Thesis Submitted to the College

of Graduate Studies and Research

In Partial Fulfillment of the Requirements

For the Degree of Master of Science

In the Department of Electrical Engineering

University of Saskatchewan

Saskatoon

By

Quan Wan

PERMISSION TO USE

In presenting this thesis in partial fulfillment of the requirement for a Postgraduate degree from University of Saskatchewan, I agree that the Libraries of this University may make it freely available for inspection. I further agree that permission for copying of this thesis in any manner, in whole or in part, for scholarly purposes may be granted by the professor or professors who supervised my thesis work or, in their absence, by the Head of the Department or the Dean of the College in which my thesis work was done. It is understood that any copying for publication or use of this thesis or parts thereof for financial gain shall not by allowed without my written permission. It is also understood that due recognition shall be given to me and to the University of Saskatchewan in any scholarly use which may be make of any material in my thesis.

Request for permission to copy or to make other use of material in this thesis in whole or part should be addressed to:

Head of the Department of Electrical Engineering

University of Saskatchewan

Saskatoon, Saskatchewan, S7N 5A9

Abstract

Ultra wide band (UWB) is an emerging technology that recently has gained regulatory approval. It is a suitable solution for high speed indoor wireless communications due to its promising ability to provide high data rate at low cost and low power consumption. Another benefit of UWB is its ability to resolve individual multi-path components. This feature motivates the use of RAKE multi-path combining techniques to provide diversity and to capture as much energy as possible from the received signal.

Potential future and rule limitation of UWB, lead to two important characteristics of the technology: high bit rate and low emitting power. Based on the power emission limit of UWB, the only choice for implementation is the low level modulation technology. To obtain such a high bit rate using low level modulation techniques, significant inter-symbol interference (ISI) is unavoidable.

Three N (N means the numbers of fingers) fingers RAKE receiver structures are proposed: the N-selective maximal ratio combiner (MRC), the N-selective MRC receiver with least-mean-square (LMS) adaptive equalizer and the N-selective MRC receiver with LMS adaptive combiner.

These three receiver structures were all simulated for N=8, 16 and 32. Simulation results indicate that ISI is effectively suppressed. The 16-selective MRC RAKE receiver with LMS adaptive combiner demonstrates a good balance between performance, computation complexity and required length of the training sequence.

Due to the simplicity of the algorithm and a reasonable sampling rate, this structure is feasible for practical VLSI implementations.

Acknowledgements

This thesis could not come through without the help of many wonderful people around me. First of all, I would like to express my deepest sense of gratitude to my supervisor, Dr. Anh Dinh, for his patient guidance, valuable advice and tremendous technical and moral support. Working with him has been a true privilege. His diligence, insights and enthusiasm demonstrate great scholars and dedicated teachers. His ideas and inspirations have greatly helped the development of my thesis. I really appreciate the countless times that he spent on discussions and feedback on my work.

I would like to acknowledge TRLabs for supporting this research in the past two years. I would also like to acknowledge my colleagues at TRLabs for making my graduate studies and research work enjoyable and productive. The creation of the outstanding research environment at TRLabs in Saskatoon is due to their tireless efforts.

Finally, I would like to express my sincere gratitude to my father who always encouraged me to face new challenges and never hesitated to provide me with ease and comfort towards my educations.

Dedication

To my dear parents

To my wife, Ying Cui, who has always been there for me and filled my life with love and happiness

To my dear son, YingJia Wan

Table of Contents

List of Tables

List of Figures

List of Acronyms

AV	audio and video
BER	bit error rate
CMOS	complementary metal oxide semiconductor
DD	decision-directed
DFE	decision-feedback equalizer
DSSS	direct-sequence spread-spectrum
FCC	Federal Communication Commission
FIR	finite impulse response
IF	intermediate frequency
ISI	inter-symbol interference
LAN	local area network
LMS	least-mean-square
LOS	line of sight
LTI	linear time-invariant
MB	multi-band
ML	maximum-likelihood
MRC	maximal ratio combiner
MSE	mean-square-error
NLOS	non-line of sight
OFDM	orthogonal frequency division multiplexing
PAM	pulse amplitude modulation

PAN	personal area network
PPM	pulse position modulation
RF	radio frequency
RMS	root-mean-square
SS	spread spectrum
THSS	time-hopping spread-spectrum
TR	transmitted reference
UWB	ultra wideband
WAN	wide area network
WPAN	wireless personal area networks

Chapter 1 Introduction

In this chapter, a brief history of ultra wideband (UWB) technology is described first and then motivations of the research are given. Description of the problems and objectives are also contained in this chapter.

1.1 Historical background

The concept of UWB communications originated in the early days of radio. In the 1900's, the Marconi spark gap transmitter (the beginning of radio) communicated by spreading a signal over a very wide bandwidth. This use of spectrum did not allow for sharing. The communication world abandoned wideband communications in favour of narrowband in order to share the available bandwidth. The government of each country governs spectrum allocation and provides guidelines for radiated power in the bandwidths of narrowband communication systems and for incidental out of band radiated power.

The origin of ultra wideband technology stems from work in time-domain electromagnetic begun in 1962 to fully describe the transient behaviour of a certain class of microwave networks through their characteristic impulse response [1, 2]. The concept was indeed quite simple. Instead of characterizing a linear time-invariant (LTI) system by the more conventional means of a swept frequency response (i.e., amplitude and phase measurements versus frequency), an LTI system could alternatively be fully characterized by its response to an impulsive excitation -- the so-called impulse response h(t). In particular, the output y(t) of such a system

to any arbitrary input x(t) could be uniquely determined by the well-known convolution integral:

$$y(t) = \int_{-\infty}^{\infty} h(u)x(t-u)du \tag{1.1}$$

However, it was not until the advent of the sampling oscilloscope (Hewlett-Packard 1962) and the development of techniques for sub-nanosecond pulse generation, to provide suitable approximations to an impulse excitation, that the impulse response of microwave networks could be directly observed and measured. Once impulse measurement techniques were applied to the design of wideband, radiating antenna elements [1, 2], it quickly became obvious that short pulse radar and communication systems could be developed with the same set of tools. While at the Sperry Research Center, part of the Sperry Rand Corporation, Ross applied these techniques to various applications in radar and communications [1, 2].

The invention of a sensitive, short pulse receiver to replace the cumbersome time-domain sampling oscilloscope further accelerated system development. In 1973, Sperry was awarded the first UWB communications patent. Through the late 1980's, this technology was alternately referred to as base-band, carrier-free or impulse communications. The term "ultra wideband" was not applied until 1989 by the U.S. Department of Defence. By that time, UWB theory, techniques and many hardware approaches had experienced nearly 30 years of extensive development. By 1989, for example, Sperry had been awarded over 50 patents in the field covering UWB pulse generation and reception methods, for applications such as communications, radar, automobile collision avoidance, positioning systems, liquid level sensing and altimetry [2].

On February 14th, 2002, the Federal Communication Commission (FCC) in the US approved the use of this very controversial ultra-wideband technology for commercial applications [3]. The targeted applications for UWB technology are those that traditionally suffered from the multi-path fading effects like indoor high-speed communications and positioning, ground penetrating radars, through-wall and medical imaging systems or other security systems. In issuing its rules for UWB, the FCC commissioners said that they were taking extreme care to avoid any possible interference and believe that after a trial period, the commission will be able to broaden the UWB applications permitted. UWB proponents believe that UWB pulses will not cause interference with other narrowband applications because the pulses continuously change frequencies and operate at extremely low power levels.

1.2 Motivation

According to FCC's definition, ultra wideband radio is a communication system which utilizes a signal whose fractional bandwidth is greater than 0.2 or which occupies 500 MHz or more of the spectrum.

Typical UWB radios communicate using sub-nanosecond pulses without a carrier. The reason why a communication scheme using narrow pulse signals has been proposed is because of their novel properties which possess advantages over conventional narrow-band or wide-band signals. A UWB signal supplies that bandwidth at a lower center frequency, which is advantageous for operation in heavy multi-path environments and for penetration of materials. Resolvable multi-

path and the penetration capability enable a vision of potential UWB radio applications in complex multi-path environments, including indoor wireless local area network (LAN). Furthermore, the absence of a sinusoidal carrier may allow a simpler radio architecture because no intermediate frequency (IF) stage is necessary.

The benefits of an increasingly mobile lifestyle introduced by wireless technologies in cell phones and home PCs resulted in a greater demand for the same benefits in other consumer devices. Consumers have enjoyed the increased convenience of wireless connectivity. They will soon demand it for video recording and storage devices, for real-time audio and video (AV) streaming, interactive gaming, and AV conferencing services as the need for digital media becomes more predominate in the home. Many technologies used in the digital home, such as digital video and audio streaming, require high bandwidth connections to communicate. Considering the number of devices used throughout the digital home, the bandwidth demand for wireless connectivity among these devices becomes very large indeed. The wireless networking technologies developed for wireless connecting PCs, such as Wi-Fi (IEEE 802.11a, b, g) and Bluetooth technology are not optimized for multiple high-bandwidth usage models of a digital home. Although data rates can reach 54 Mbps for Wi-Fi, for example, the technology has limitations in a consumer electronics environment, including power consumption and bandwidth. When it comes to connecting multiple consumer electronic (CE) devices in a short-range network, or wireless personal area networks (WPAN), a wireless technology is required to support multiple high data rate streams, consume

very little power, and maintain low cost, while fitting into a very small physical package, such as a PDA or a cell phone. The emerging UWB wireless technology and silicon developed for UWB applications offer a compelling solution.

1.3 Problems and objectives

UWB differs substantially from conventional narrowband radio frequency (RF) and spread spectrum technologies (SS), such as Bluetooth Technology and 802.11a/g. UWB uses an extremely wide band of RF spectrum to transmit data. In doing so, UWB is able to transmit more data in a given period of time than traditional technologies. The potential data rate over a given RF link is proportional to the bandwidth of the channel and the logarithm of the signal-to-noise ratio as stated in the Hartley-Shannon law

$$C = B\log_2(1+\frac{S}{N}) \tag{1.2}$$

where:

C = Maximum channel capacity, in bits per second.

B = Channel bandwidth, in Hertz.

S = Signal power, in watts.

N = Noise power, in watts.

RF design engineers typically have little control over bandwidth parameters as they are dictated by FCC regulations that stipulate the allowable bandwidth of the signal for a given radio type and application. Bluetooth Technology, 802.11a/g Wi-Fi, cordless phones, and numerous other devices are relegated to the unlicensed frequency bands at 900 MHz, 2.4 GHz, and 5.1 GHz.

Each radio channel is constrained to occupy only a narrow band of frequencies, relative to what is allowed for UWB. UWB is a unique and new usage of a recently legalized frequency spectrum. UWB radios can use frequencies from 3.1 GHz to 10.6 GHz—a band more than 7 GHz wide. Each radio channel can have a bandwidth of more than 500 MHz. To allow for such a large signal bandwidth, the FCC put in place severe broadcast power restrictions. By doing so, UWB devices can make use of an extremely wide frequency band while not emitting enough energy to be noticed by nearby narrower band devices, such as the 802.11a/g radios. This spectrum sharing allows devices to obtain very high data throughput, but they must be within close proximity. Strict power limits mean the radios themselves must be low power consumers. Because there is no need to emit a high power signal, it is feasible to develop cost-effective CMOS implementations of UWB radios in place of expensive high power components. With the characteristics of low power, low cost, and very high data rates at a limited range, UWB is positioned to address the market for high-speed WPAN.

Potential future and rule limitation of UWB, lead to two important characteristics of the technology: high bit rate and low emitting power. Based on the power emission limit of UWB, the only choice for implementation is using low level modulation technology. To obtain such a high bit rate using low level modulation techniques, the required symbol period is very small. According to the UWB channel model from IEEE P802.15 [4], there is a root-mean-square (RMS) delay spread of approximately 15ns for a 4-10 meter range with a non line-of-sight transmission. This spread indicates that a significant inter-symbol interference (ISI)

is unavoidable. The traditional RAKE receiver structure to collect multi-path energy in UWB systems does not combat ISI very well. Some published results on UWB have neglected this problem as most performance analyses employ a RAKE receiver under the assumption that channel delay spreads are much less than system symbol time [5, 24, 27, 29].

Still for a 4-10 meter range with a non line-of-sight transmission in the UWB channel model from IEEE P802.15, the average number of significant paths capturing greater than 85% energy is more than sixty. How could the multi-path signal's energy be captured effectively for a reasonable cost? How could the dense multi-path channel parameters be measured in the high data rate application environment?

The first objective is to find a method to estimate the channel parameters and gather multi-path energy with the low computation complexity. The second objective is to find suitable equalization technologies to suppress the significant inter-symbol interference. The overall objective of this research is to propose low cost UWB receiver structures with low complexity and a low sampling rate that can achieve satisfactory performance under a significant ISI.

In this thesis, the sample and effective sliding correlation algorithm is applied for UWB channel estimation. An analog and digital hybrid implementation of a RAKE receiver structure is proposed. Two schemes for suppressing ISI, LMS equalization and LMS combining, are developed. Simulations are performed using the popular simulation tool, MATLAB Simulink®. According to the simulation results, the objectives are achieved.

1.4 Thesis overview

This chapter provides a brief historical background on UWB communication systems. Motivation, problems and objectives are also discussed. The rest of this thesis is organized as follows.

Chapter 2 provides a definition of UWB signal. Advantages of this technology are also discussed. Existing UWB system schemes are briefly reviewed and channel characterization of UWB is introduced. Chapter 3 deals with signal processing technologies in the presence of multi-path, RAKE multi-path combining techniques and different equalization techniques. Chapter 4 describes the proposed receiver structures. Chapter 5 focuses on simulation set-up. This chapter also provides analysis and discussion of the simulation results. Finally, conclusions on the accomplished research objectives are summarized and research topics for future work are suggested in Chapter 6.

Chapter 2 UWB Communication Technology

In this chapter, the official definition and advantages of UWB are given. Basic concepts of several current main stream UWB system schemes are introduced subsequently. Finally UWB channel modes are described.

2.1 Definition of UWB

The UWB technology was often referred to as base-band, carrier-free or short impulse. But there was not a clear definition of UWB until the Federal Communications Commission's Report and Order [3], issued on Feb 2002, gives an official definition for UWB. According to this definition, an UWB signal is any signal whose fractional bandwidth is greater than 0.20 or occupies 500 MHz or more of the spectrum. The formula proposed by the FCC for calculating fractional bandwidth is

$$2(f_H - f_L)/(f_H + f_L),$$

where f_H is the upper frequency of the –10 dB emission point and f_L is the lower frequency of the –10 dB emission point. The center frequency of the transmission was defined as the average of the upper and lower –10 dB points, i.e., $(f_H + f_L)/2$. Meanwhile UWB signals must meet the spectrum mask shown in Fig. 2-1 and Fig. 2-2.

According to the FCC's rules, there is 7.5 GHz bandwidth (3.1 GHz—10.6 GHz) available for UWB communications and measurement systems. The allowed power emission level is -41.3 dBm/MHz. The equipment must be designed to

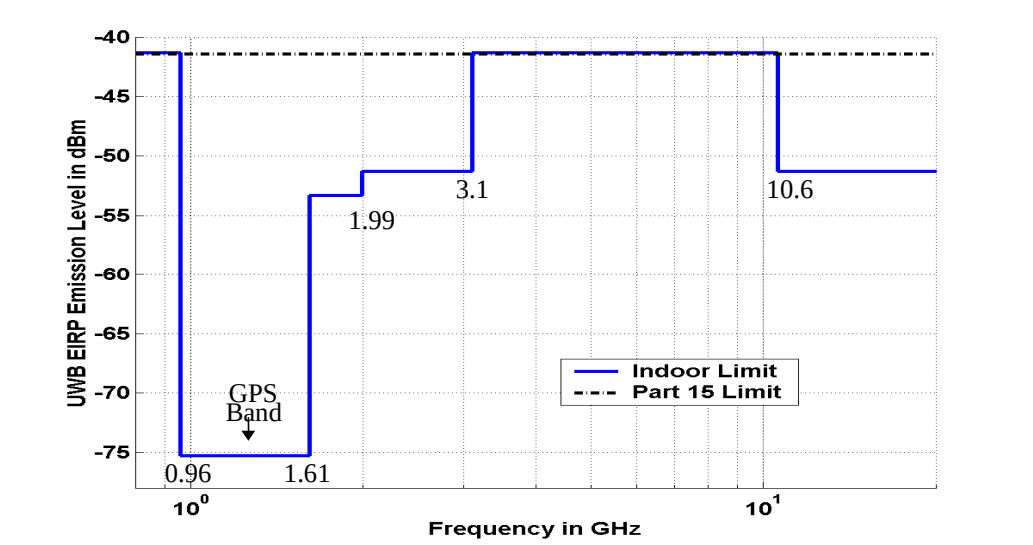

Figure 2-1: UWB emission limit for indoor systems

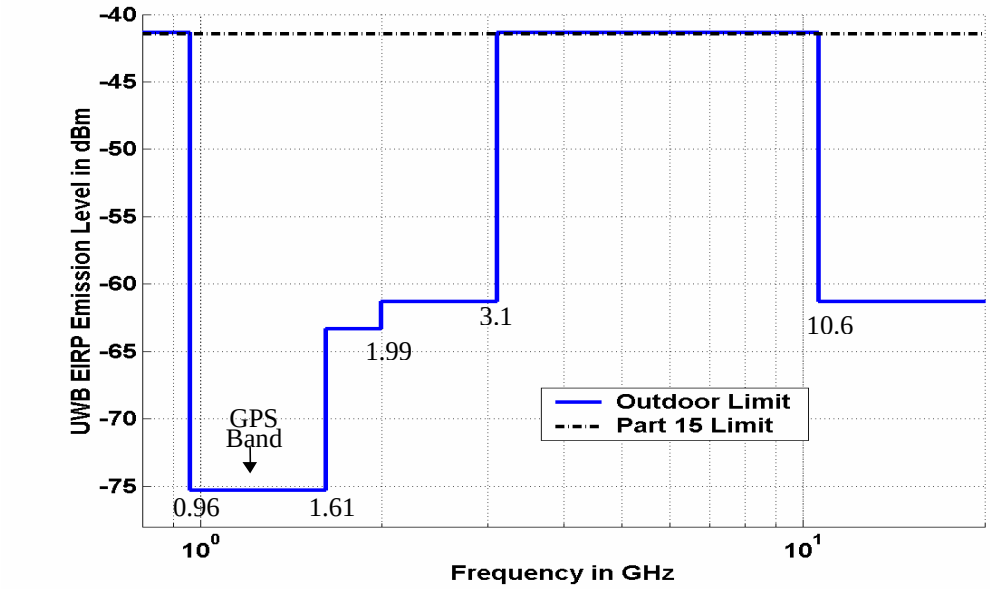

Figure 2-2: UWB emission limit for outdoor hand-held systems

ensure that the operation can only occur indoors or it must consist of hand held devices that may be employed for such activities as peer-to-peer operation. A comparison with the other unlicensed bands currently available in the US is shown in Table 1.

Table 2-1: Unlicensed bands

Unlicensed bands	**Frequency of operation**	**Bandwidth**
ISM at 2.4GHz	2.4000-2.4835 GHz	83.5MHz
U-NII at 5GHz	5.15-5.35GHz 5.725-5.825GHz	300MHz
UWB	3.1-10.6GHz	7,500MHz

Given the recent spectral allocation and the new definition of UWB adopted by FCC, UWB is not only just considered as a technology anymore, but also available spectrum for unlicensed use. This means that any transmission signal that meets the FCC requirements for UWB spectrum is acceptable. This, of course, is not just restricted to impulse radios or high speed spread spectrum radios pioneered by companies so far, but opened to any technology that utilizes more than 500MHz spectrum in the allowed spectral mask.

2.2 Advantages of UWB

Because UWB waveforms are of such short time duration, they have some unique properties. In communications, for example, UWB pulses can be used to provide extremely high data rate performance in multi-user network applications. For radar applications, these same pulses can provide a very fine range resolution and a precision distance and positioning measurement capability.

These short duration waveforms are relatively immune to multi-path effects compared to normal narrow band systems as observed in mobile and in-building

environments. As a result, UWB systems are particularly well suited for high-speed wireless applications.

As bandwidth is inversely related to pulse duration, the spectral extent of these waveforms can be made quite large. With proper engineering design, resultant energy densities (i.e., transmitted Watts of power per unit Hertz of bandwidth) can be quite low. This low energy density is translated into a low probability of detection RF signature. The low probability of detection signature is of particular interest for military applications; meanwhile, it also produces minimal interference to proximity systems and minimal RF health hazards, which is a significant benefit for both military and commercial applications.

Among the most important advantages of UWB technology, however, are those of low system complexity and low cost. UWB systems can be made nearly "all-digital," with minimal RF or microwave electronics. Because of the inherent RF simplicity of UWB designs, these systems are highly frequency adaptive, enabling them to be positioned anywhere within the RF spectrum. This feature avoids interference to existing services, while fully using the available spectrum.

In summary, UWB presents a compelling solution to many of the challenges facing today's wireless industry and applications. These include the following [30]:

- **Low radiated power:** UWB is limited by regulation to power levels that are a tiny fraction of other radio technologies, with possible health benefits and adaptation to sensitive environments, such as hospitals and airports.

- **Speed -** The same UWB device can scale from speeds far in excess of current communication networks, to very low speed (and low power) applications, such as meter reading.
- **Multiple channels -** UWB can support hundreds of simultaneous channels, compared to three for 802.11b, or ten for 802.11a.
- **Simultaneous networking -** This technology can function as a personal area network (PAN), a local area network (LAN), and a wide area network (WAN), simultaneously. It is the equivalent of Bluetooth, 802.11, and 3G converging, but in a single network, with a single device.
- **Lower cost and complexity -** Devices using RF spectrum require a real radio receiver and so are more complex in terms of components, higher cost, and consume significantly more power than UWB which operates at lower power, and requires fewer components.
- **Greater security -** The inherent digital nature of UWB transmission, coupled with its operation in the lower power level, makes UWB perhaps the most secure means of wireless transmission available.
- **Co-existence -** Because UWB signals can co-exist with conventional RF carriers, the technology will open up vast new communication possibilities by creating a new communication medium that peacefully coexists with existing technologies.

UWB is an RF wireless technology and, as such, is still subject to the same laws of physics as other RF technologies. Thus, there are obvious tradeoffs to be made in

signal-to-noise ratio versus bandwidth, range versus speed, and average power levels, and so on.

2.3 Existing UWB system schemes

There are four popular UWB system schemes: time-hopping spread-spectrum ultra wideband (THSS-UWB); direct-sequence spread-spectrum ultra wideband (DSSS-UWB); multi-band orthogonal frequency division multiplexing ultra wideband (MB-OFDM-UWB) and transmitted reference ultra wideband (TR-UWB).

- Time-hopping spread-spectrum ultra wideband

In THSS-UWB, the transmitted signal $S_{TH}(t)$ for one user using binary antipodal modulation can be defined as [6]

$$S_{TH}(t) = \sum_{j=-\infty}^{\infty} w_{tr}(t - jT_f - c_j T_c)(1 - 2D_{\lfloor j/N_S \rfloor}) \tag{2.1}$$

where $w_{tr}(t)$ denotes the transmitted pulse form that has a maximum amplitude of one, a duration of T_c and is transmitted with a repetition period T_f. The position of a transmitted pulse within each repetition period is determined by a pseudorandom code c_j which selects one of the N slots, each having a duration of T_c. The pseudorandom code c_j takes integer value between 0 and $N-1$ and it is assumed that $NT_c \le T_f$. Moreover, $D \in \{0,1\}$ is a data stream and $\lfloor x \rfloor$ denotes the integer part of *x*. A new bit starts with $j = 0 \bmod N_S$. Each information bit is transmitted with N_S pulses and has a duration of $T_S = N_S T_f$. Figure 2-3 shows the time divisions.

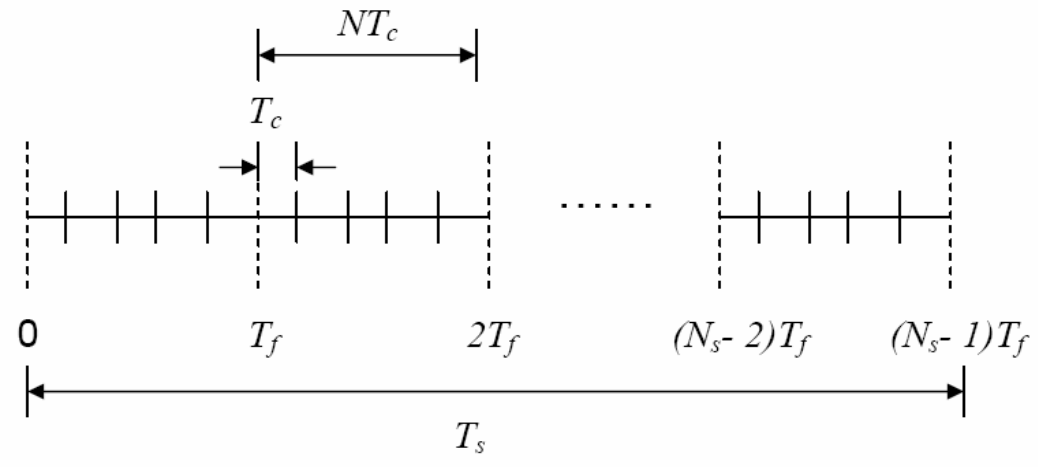

Figure 2-3: Time divisions in THSS-UWB scheme

- Direct-sequence spread-spectrum ultra wideband

A DSSS-UWB system is basically identical to an ordinary DSSS system except that the bandwidth spreading effect is achieved by pulse shaping. Similar to THSS-UWB above, DSSS-UWB is defined as

$$S_{DS}(t) = \sum_{j=-\infty}^{\infty} w_{tr}(t - jT_m) n_j (1 - 2D_{\lfloor j/N_{DS} \rfloor}) \tag{2.2}$$

where n_j is a pseudorandom code that takes values {±1}. Each information bit consists of N_{DS} pulses and has a duration of $T_b = N_{DS} T_m$.

The flexibility provided by the FCC ruling greatly expands the design options for UWB communication systems. Designers are free to use a combination of sub-bands within the spectrum to optimize system performance, power consumption and design complexity. UWB systems can still maintain the same low transmit power as if they were using the entire bandwidth by interleaving the symbols across these sub-bands [7].

- Multi-band orthogonal frequency division multiplexing ultra wideband

The MB-OFDM-UWB system transmits data simultaneously over multiple carriers spaced apart at precise frequencies by mean of OFDM modulation techniques. Beneficial attributes of MB-OFDM include high spectral flexibility and resiliency to RF interference and multi-path effects.

Regardless of present or future spectral allocations and emissions restrictions in various regions of the world, MB-OFDM is capable of complying with local regulations by dynamically turning off certain tones or channels using software. This flexibility, not demonstrated by other system schemes, enables worldwide adoption of UWB systems.

- Transmitted reference ultra wideband

To circumvent the drawbacks of RAKE receivers, e.g. channel estimation or finding a suitable template pulse form for correlation, TR-UWB schemes are well suited. A TR-UWB system transmits a doublet every T_S seconds. The first pulse of each doublet is information free, and the second delayed pulse that is modulated by pulse amplitude modulation (PAM), or pulse position modulation (PPM) and delayed by T_d seconds carries the user's information. Denote the pulse by $w_{tr}(t)$ with duration T_p and the binary PAM symbol by $D \in \{0,1\}$. The transmitted signal can be described by [8]

$$S_{TR}(t) = \sum_{j=-\infty}^{\infty} [w_{tr}(t - jT_S) + (1 - 2D_j) w_{tr}(t - jT_S - T_d)] \qquad (2.3)$$

Reasonably assume $T_d > T_p$ and $T_d + T_p < T_S$, meaning the first and second pulses do not interfere each other before propagating through a channel. However, large pulse spacing inevitably sacrifices data rate for good performance, especially when

the channel spread is very large [4]. Meanwhile, the first pulse may severely interfere with the second pulse and cause inter-pulse interference.

2.4 Channel characterization of UWB

The IEEE UWB channel model is based on the Saleh–Valenzuela model where multi-path components arrive in clusters [4, 9]. In this model, a lognormal distribution was used rather than a Rayleigh distribution for the multi-path gain magnitude. In addition, independent fading is assumed for each cluster as well as each ray within the cluster. Therefore, the multi-path model consists of the following discrete time impulse response:

$$h_i(t) = X_i \sum_{l=0}^{L} \sum_{k=0}^{K} \alpha_{k,l}^{i} \delta(t - T_l^i - \tau_{k,l}^i) \tag{2.4}$$

where $\{\alpha_{k,l}^{i}\}$ are the multi-path gain coefficients, $\{T_l^i\}$ is the delay of the l^{th} cluster, $\{\tau_{k,l}^{i}\}$ is the delay of the k^{th} multi-path component relative to the l^{th} cluster arrival time $\{T_l^i\}, \{X_i\}$ represents the log-normal shadowing, and i refers to the i^{th} realization of the channel. Finally, the model uses the following definitions:

T_l = the arrival time of the first path of the l-th cluster.

$\tau_{k,l}$ = the delay of the k-th path within the l-th cluster relative to the first path arrival time, T_l.

Λ = cluster arrival rate.

λ = ray arrival rate, i.e., the arrival rate of the paths within each cluster.

By definition, $\tau_{0,l} = 0$. The distribution of cluster arrival time and the ray arrival time are given by

$$p(T_l \mid T_{l-1}) = \Lambda \exp[-\Lambda(T_l - T_{l-1})], l > 0 \tag{2.5}$$

$$p(\tau_{k,l} \mid \tau_{(k-1),l}) = \lambda \exp[-\lambda(\tau_{k,l} - \tau_{(k-1),l})], k > 0 \tag{2.6}$$

The channel coefficients are defined as follow:

$\alpha_{k,l} = p_{k,l}\xi_l\beta_{k,l}$,

$20\log 10(\xi_l\beta_{k,l}) \propto \text{Normal}(\mu_{k,l}, \sigma_1^2 + \sigma_2^2)$, or $\left|\xi_l\beta_{k,l}\right| = 10^{(\mu_{k,l}+n_1+n_2)/20}$

where $n_1 \propto \text{Normal}(0, \sigma_1^2)$ and $n_2 \propto \text{Normal}(0, \sigma_2^2)$ are independent and correspond to the fading on each cluster and ray respectively.

$$E\left[\left|\xi_l\beta_{k,l}\right|^2\right] = \Omega_0 e^{-T_l/\Gamma} e^{-\tau_{k,l}/\gamma} \tag{2.7}$$

where T_l is the excess delay of bin l and Ω_0 is the mean energy of the first path of the first cluster, and $p_{k,l}$ is equiprobable +/-1 to account for signal inversion due to reflections. The $\mu_{k,l}$ is given by

$$\mu_{k,l} = \frac{10\ln(\Omega_0) - 10T_l/\Gamma - 10\tau_{k,l}/\gamma}{\ln(10)} - \frac{(\sigma_1^2 + \sigma_2^2)\ln(10)}{20} \tag{2.8}$$

In the above equations, ξ_l reflects the fading associated with the l^{th} cluster, and $\beta_{k,l}$ corresponds to the fading associated with the k^{th} ray of the l^{th} cluster. Note that, a complex tap model is not adopted here. The complex base-band model is a natural fit for narrowband systems to capture channel behavior independently of carrier frequency, but this motivation breaks down for UWB systems where a real-valued simulation at RF may be more natural.

Finally, since the log-normal shadowing of the total multi-path energy is captured by the term, X_i, the total energy contained in the terms $\{\alpha_{k,l}^i\}$ is normalized to unity for each realization. This shadowing term is characterized by the following:

$20\log10(X_i) \propto \text{Normal}(0, \sigma_x^2)$.

As shown above, there are 7 key parameters that define the model:

Λ = cluster arrival rate.

λ = ray arrival rate, i.e., the arrival rate of path within each cluster.

Γ = cluster decay factor.

γ = ray decay factor.

σ_1 = standard deviation of cluster lognormal fading term (dB).

σ_2 = standard deviation of ray lognormal fading term (dB).

σ_x = standard deviation of lognormal shadowing term for total multi-path realization (dB).

These parameters are found by trying to match important characteristics of the channel. Since it is difficult to match all possible channel characteristics, the main characteristics of the channel that are used to derive the above model parameters are chosen to be the following:

- Mean excess delay
- RMS delay spread
- Number of multi-path components which is defined as the number of multi-path arrivals that are within 10 dB of the peak multi-path arrival

There are four distinguished models:

CM1: This model is based on line of sight (LOS) (0-4m) channel measurements.

CM2: This model is based on non-line of sight (NLOS) (0-4m) channel measurements.

CM3: This model is based on non-line of sight (NLOS) (4-10m) channel measurements.

CM4: This model is generated to fit a 25 nsec RMS delay spread to represent an extreme no-line of sight (NLOS) multi-path channel.

The following table lists some initial model parameters for a couple of different channel characteristics that were found through measurement data.

Table 2-2: The IEEE UWB channel characteristics [4]

Model Parameters	**CM 1**	**CM 2**	**CM 3**	**CM 4**
Λ (1/nsec)	0.0233	0.4	0.0667	0.0667
λ (1/nsec)	2.5	0.5	2.1	2.1
Γ	7.1	5.5	14.00	24.00
γ	4.3	6.7	7.9	12
σ_1 (dB)	3.3941	3.3941	3.3941	3.3941
σ_2 (dB)	3.3941	3.3941	3.3941	3.3941
σ_x (dB)	3	3	3	3
Model Characteristics				
Mean excess delay (nsec) (τ_m)	5.0	9.9	15.9	30.1
RMS delay (nsec) (τ_{rms})	5	8	15	25
NP_{10dB}	12.5	15.3	24.9	41.2
NP (85%)	20.8	33.9	64.7	123.3
Channel energy mean (dB)	-0.4	-0.5	0.0	0.3
Channel energy std (dB)	2.9	3.1	3.1	2.7

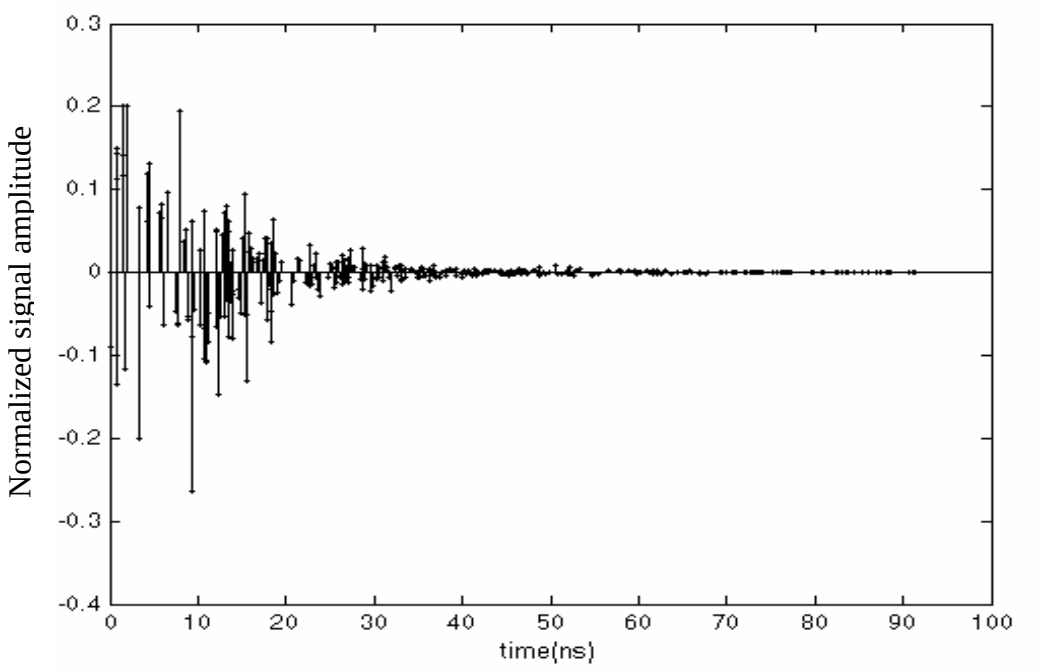

Figure 2-4: One realization of UWB channel model **CM1**

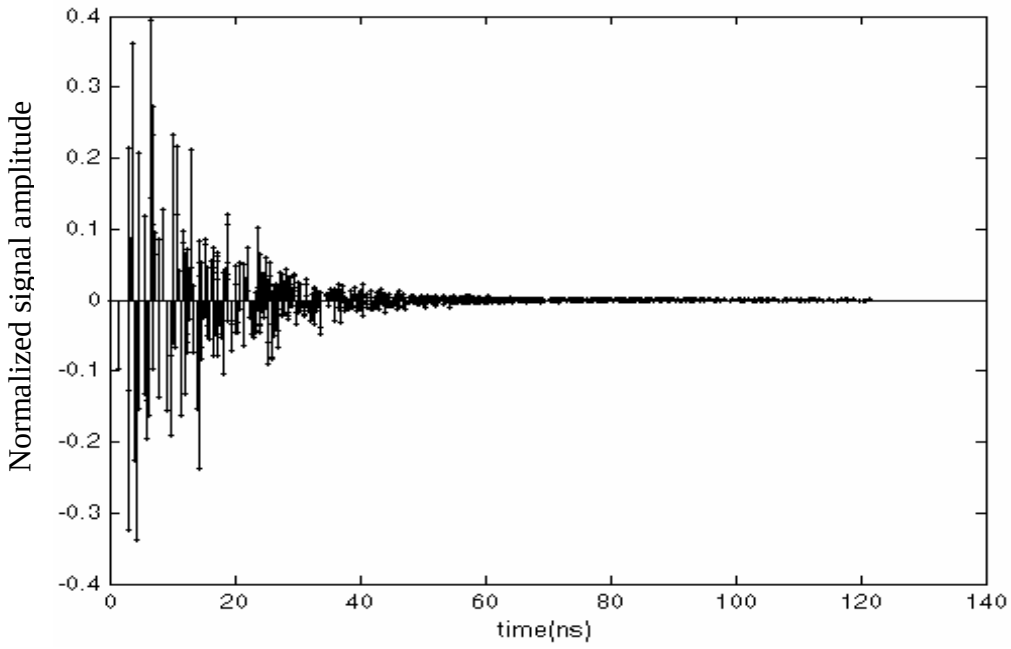

Figure 2-5: One realization of UWB channel model **CM2**

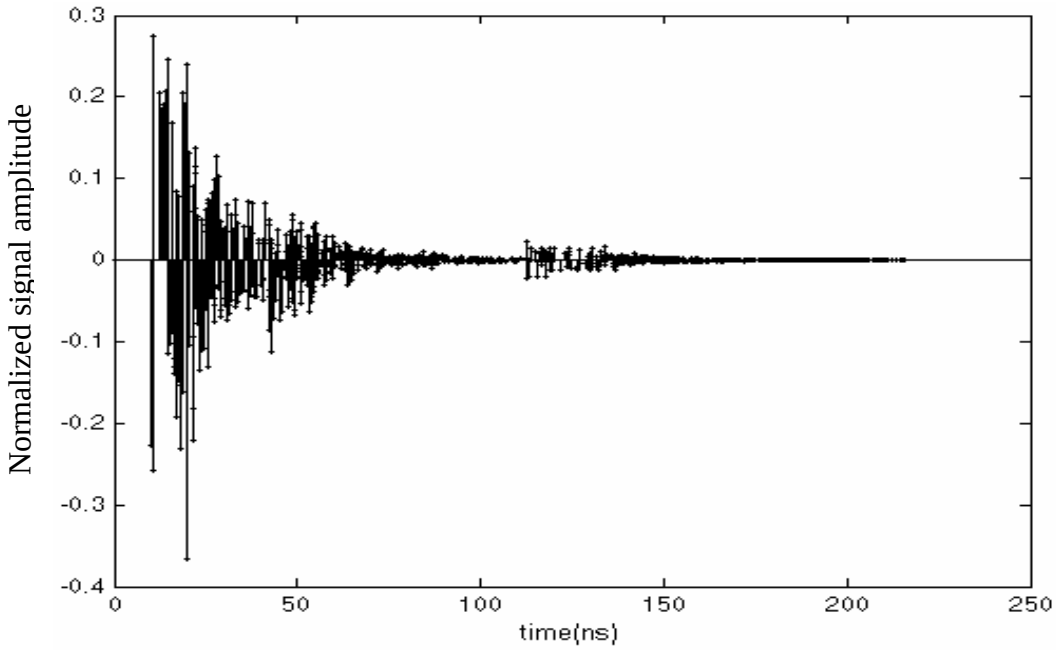

Figure 2-6: One realization of UWB channel model **CM3**

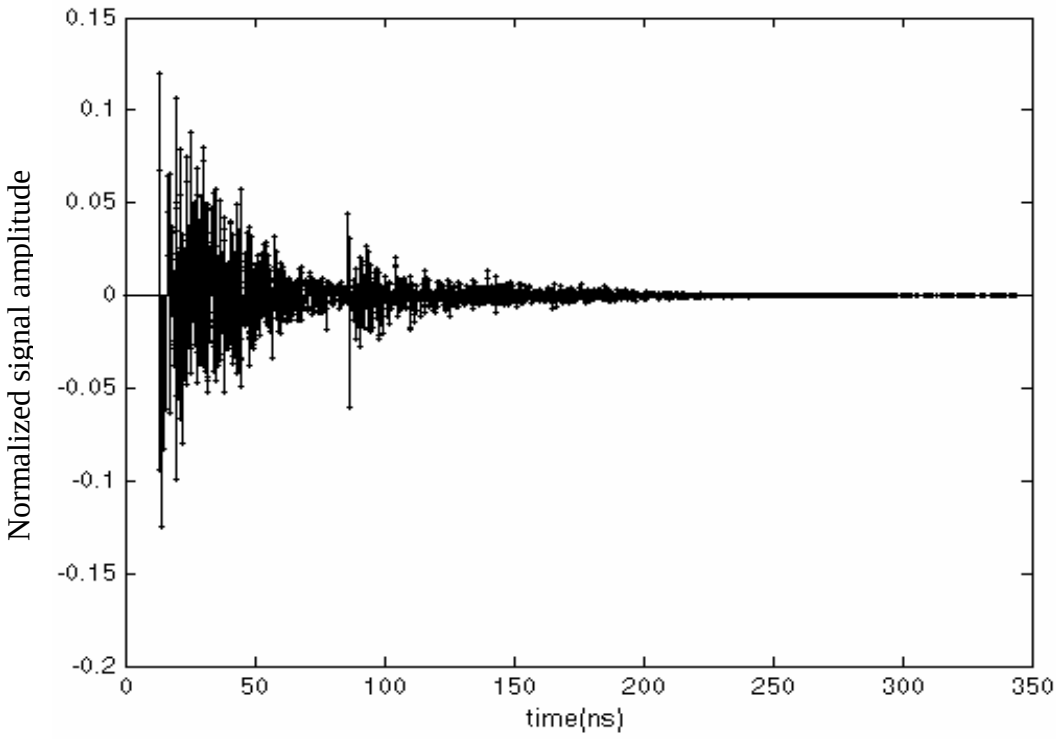

Figure 2-7: One realization of UWB channel model **CM4**

One realization of each channel model impulse response is shown below (continuous-time model). From Figure 2-3 the multi-path delay spread for **CM1** is about 90 ns. For **CM2** in Figure 2-4 the multi-path delay spread increase to about 120 ns. For CM3 in Figure 2-5 this value is about 200ns and for CM4 in Figure 2-6 it is almost 330ns.

Chapter 3 Receiver Signal Processing in the Presence of Multi-path

In this chapter, introduction of the RAKE receiver is given at the beginning. Then a description of ISI and some of the most used methods to combat ISI are introduced subsequently.

3.1 RAKE receiver

The extremely large bandwidth of UWB signals means that the UWB channel is highly frequency selective. According to the introduction of UWB channel model in Chapter 2, a large number of multi-path components arrive at the receiver with different time delays. This means that large losses in the receiver's performance will occur if a method of combating this frequency selective dense multi-path is not employed. However, the extremely narrow pulses used for UWB transmission lead to inherent path diversity (i.e., independent fading of different multi path components). This implies that the received UWB signal contains a significant number of resolvable multi path components which suggests a RAKE type receiver to coherently combine them [5, 10]. This significantly reduces the fading effects and the resulting reduction of fading margins in link power budgets leads to reduced transmission power requirements.

The RAKE receiver was invented by Price and Green in 1958 [11]. The receiver is used to achieve multi-path diversity by collecting signal energy from each received path using a delay line structure [12]. In spread spectrum communications,

the bandwidth of the spread signal is usually larger than the channel coherence bandwidth. If the bandwidth of the transmitted signal is large enough, it is possible to resolve multi-path components into separate signals. In such a case, the actual channel can be modeled as a tapped delay line with time varying tap coefficients [13].

Now suppose that W is the bandwidth occupied by real band-pass signal, then the band occupancy of the equivalent low-pass signal $s_l(t)$ is $|f| \le \frac{1}{2}W$. Since $s_l(t)$ is band-limited to $|f| \le \frac{1}{2}W$, according to the sampling theorem $s_l(t)$ can be expressed as

$$s_l(t) = \sum_{n=-\infty}^{+\infty} s_l(\frac{n}{W}) \frac{\sin[\pi W(t - n/W)]}{\pi W(t - n/W)} \tag{3.1}$$

The Fourier transform of $s_l(t)$ is

$$S_l(f) = \begin{cases} \frac{1}{W} \sum_{n=-\infty}^{\infty} s_l(n/W) e^{-j2\pi f n/W} & (|f| \le \frac{1}{2}W) \\ 0 & (|f| > \frac{1}{2}W) \end{cases} \tag{3.2}$$

The noiseless received signal through a frequency-selective channel is expressed in the form

$$r_l(t) = \int_{-\infty}^{\infty} C(f;t) S_l(f) e^{j2\pi f t} df \tag{3.3}$$

where $C(f;t)$ is the time-variant transfer function. Substitution for $S_l(f)$ from (3.2) into (3.3) yields

$$r_l(t) = \frac{1}{W} \sum_{n=-\infty}^{\infty} s_l(n/W) \int_{-\infty}^{\infty} C(f;t) e^{j2\pi f(t - n/W)} df$$

$$= \frac{1}{W} \sum_{n=-\infty}^{\infty} s_l(n/W) c(t - n/W; t) \tag{3.4}$$

where $c(\tau; t)$ is the time-variant impulse response. It is observed that equation (3.4) has the form of a convolution sum. Hence, it can be expressed in an alternative form as:

$$r_l(t) = \frac{1}{W} \sum_{n=-\infty}^{\infty} s_l(t - n/W) c(n/W; t) \tag{3.5}$$

It is convenient to define a set of time-variable channel coefficients as

$$c_n(t) = \frac{1}{W} c(\frac{n}{W}; t) \tag{3.6}$$

Then Equation (3.5) expressed in terms of these channel coefficients become

$$r_l(t) = \sum_{n=-\infty}^{\infty} c_n(t) s_l(t - n/W) \tag{3.7}$$

The form for the received signal in Equation (3.7) implies that the time-variant frequency-selective channel can be modeled or represented as a tapped delay line with tap spacing 1/W and tap weight coefficients $\{c_n(t)\}$. In fact, it is deduced from Equation (3.7) that the low-pass impulse response for the channel is

$$c(\tau; t) = \sum_{n=-\infty}^{\infty} c_n(t) \delta(\tau - n/W) \tag{3.8}$$

and the corresponding time-variant transfer function is

$$C(f; t) = \sum_{n=-\infty}^{\infty} c_n(t) e^{-j2\pi f n/W} \tag{3.9}$$

Thus, with an equivalent low-pass-signal having a bandwidth $\frac{1}{2}W$, one achieves a resolution of 1/W in the multi-path delay profile. Since the total multi-

path spread is T_m, for all practical purposes, the tapped delay line model for the channel can be truncated at $L = \lfloor T_m W \rfloor + 1$ taps. Then the noiseless received signal can be expressed in the form

$$r_l(t) = \sum_{n=1}^{L} c_n(t) s_l(t - n/W) \tag{3.10}$$

The truncated tapped delay line model is shown in Figure 3-1. The time-variant tap weights $\{c_n(t)\}$ are complex-valued stationary random processes. Since $\{c_n(t)\}$ represent the tap weights corresponding to the L different delays $\tau = n/W$, $n = 1,2,\ldots,L$, the uncorrelated scattering assumption implies that $\{c_n(t)\}$ are mutually uncorrelated. When $\{c_n(t)\}$ are Gaussian random processes, they are statistically independent.

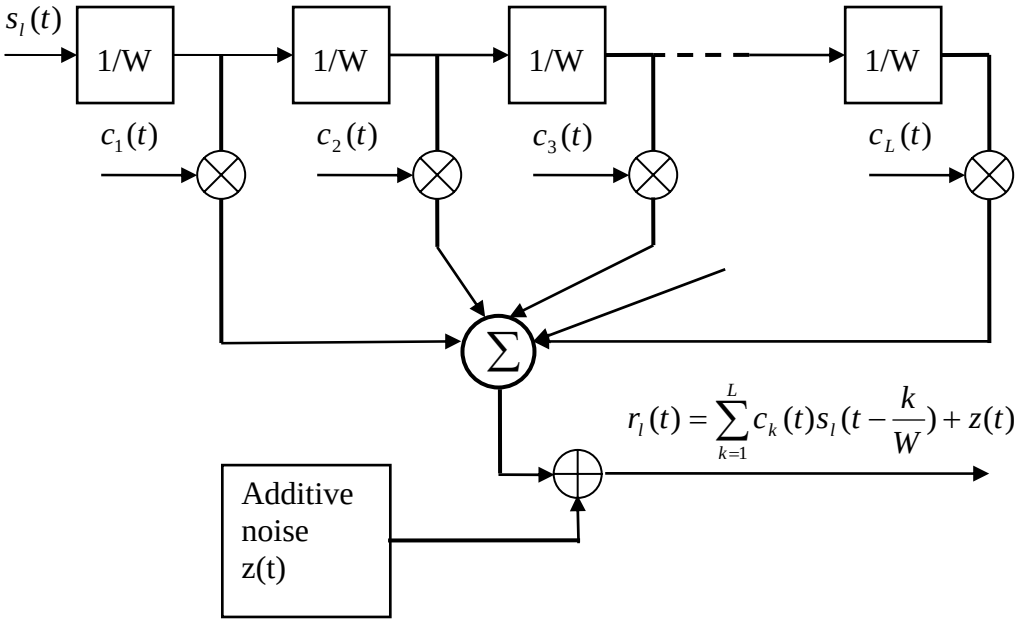

Figure 3-1: Tapped delay line model of frequency-selective channel

Now consider the problem of digital signaling over a frequency-selective channel that is modeled by a tapped delay line with statistically independent time-variant tap weights $\{c_n(t)\}$.

Binary signaling over the channel is considered. There are two equal-energy signals $s_{l1}(t)$ and $s_{l2}(t)$, which are either antipodal or orthogonal. Their time duration T is selected to satisfy the condition $T >> T_m$. Thus, one may neglect any inter-symbol interference due to multi-path. Since the bandwidth of the signal exceeds the coherent bandwidth of the channel, the received signal is expressed as

$$r_l(t) = \sum_{k=1}^{L} c_k(t) s_{li}(t - k/W) + z(t)$$

$$= v_i(t) + z(t), \quad 0 \le t \le T \quad i = 1,2 \tag{3.11}$$

where $z(t)$ is a complex-valued zero-mean white Gaussian noise process. Assume for the moment that the channel tap weights are known, then the optimum demodulator consists of two filters matched to $v_1(t)$ and $v_2(t)$. The demodulator output is sampled at the symbol rate and the samples are passed to a decision circuit that selects the signal corresponding to the largest output. An equivalent optimum demodulator employs cross correlation instead of matched filtering. In either case, the decision variables for coherent detection of the binary signals can be expressed as

$$U_m = \mathrm{Re}\left[\int_0^T r_l(t) v_m^*(t)\, dt\right]$$

$$= \mathrm{Re}\left[\sum_{k=1}^{L} \int_0^T r_l(t) c_k^*(t) s_{lm}^*(t - k/W)\, dt\right], \quad m = 1,2 \tag{3.12}$$

Figure 3-2 illustrates the operations involved in the computation of the decision variables. In this realization of an optimum receiver, the two reference signals are delayed and correlated with the received signal $r_l(t)$.

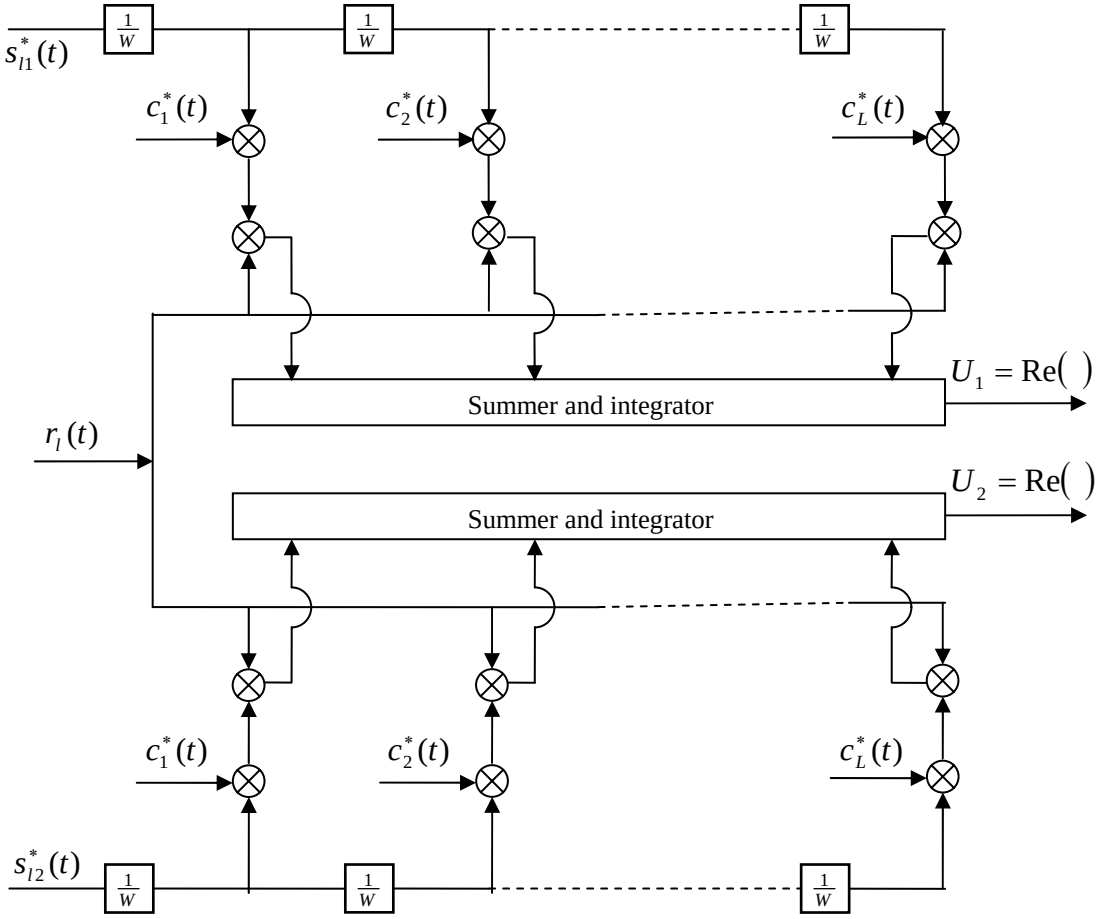

Figure 3-2: Optimum demodulator for wideband binary signals

Under the condition that the fading is sufficiently slow, within any one signaling interval, $c_k(t)$ is treated as a constant and denoted as c_k. If the binary signals are antipodal, then $s_{l1}(t) = -s_{l2}(t)$. Thus the decision variables in (3.12) may be expressed in the form

$$U = \mathrm{Re}\left[\sum_{k=1}^{L} c_k^* \int_0^T r_l(t) s_{l1}^*(t - k/W)dt \right] \tag{3.13}$$

Suppose the transmitted signal is $s_{l1}(t)$, then the received signal is

$$r_l(t) = \sum_{k=1}^{L} c_k s_{l1}(t - k/W) + z(t) \qquad 0 \le t \le T \tag{3.14}$$

Substitution of Eq.(3.14) into Eq.(3.13) yields

$$U = \mathrm{Re}\left[\sum_{k=1}^{L} c_k^* \sum_{n=1}^{L} c_n \int_0^T s_{l1}(t - n/W) s_{l1}^*(t - k/W)dt \right]$$

$$+ \mathrm{Re}\left[\sum_{k=1}^{L} c_k^* \int_0^T z(t) s_{l1}^*(t - k/W)dt \right] \tag{3.15}$$

If inter-pulse interference is neglected, the resulting signals have the property

$$\int_0^T s_{l1}(t - n/W) s_{l1}^*(t - k/W)dt = 0, \qquad k \ne n \tag{3.16}$$

Then Eq.3.15 can be simplified to

$$U = \mathrm{Re}\left[\sum_{k=1}^{L} |c_k|^2 \int_0^T s_{l1}(t - k/W) s_{l1}^*(t - k/W)dt \right]$$

$$+ \mathrm{Re}\left[\sum_{k=1}^{L} c_k^* \int_0^T z(t) s_{l1}^*(t - k/W)dt \right]$$

$$= \mathrm{Re}\left(\varepsilon \sum_{k=1}^{L} \alpha_k^2 + \sum_{k=1}^{L} \alpha_k N_k \right) \tag{3.17}$$

where $c_k = \alpha_k e^{-j\phi_k}$ and

$$\varepsilon = \int_0^T s_{l1}(t - k/W) s_{l1}^*(t - k/W)dt \tag{3.18}$$

$$N_k = e^{j\phi_k} \int_0^T z(t) s_{l1}^*(t - k/W)dt \tag{3.19}$$

In effect, the tapped delay line demodulator attempts to collect the signal energy from all received signal paths that fall within the span of the delay line and carry the same information. Its action is somewhat analogous to an ordinary garden rake and, consequently, the name "RAKE demodulator" has been coined for this demodulator structure by Price and Green [11].

It is apparent that the tapped delay line model with statistically independent tap weights provides L replicas of the same transmitted signal at the receiver. Hence, a receiver that processes the received signal in an optimum manner will achieve the performance of an equivalent L^{th}-order diversity communication. The L replicas of the transmitted signal at the receiver can be considered as carrying the same information-bearing signal passed through L diversity channels. Each channel is assumed to be frequency-nonselective and slowly fading. The fading processes among the L diversity channels are assumed to be mutually statistically independent. The signal in each channel is corrupted by an additive zero-mean white Gaussian noise process. The noise processes in the L channels are assumed to be mutually statistically independent. Thus the equivalent low-pass received signals for the L channels can be expressed in the form

$$r_{lk}(t) = \alpha_k e^{-j\phi_k} s_{km}(t) + z_k(t), \quad k = 1,2,\ldots,L, \quad m = 1,2 \tag{3.20}$$

where $\left\{\alpha_k e^{-j\phi_k}\right\}$ represent the attenuation factors and phase shifts for the L channels, $s_{km}(t)$ denotes the m^{th} signal transmitted on the k^{th} channel, and $z_k(t)$ denotes the additive white Gaussian noise on the k^{th} channel. All signals in the set $\{s_{km}(t)\}$ have the same energy.

The optimum demodulator for the signal received from the kth channel consists of two matched filters, one having the impulse response

$$h_{k1}(t) = s_{k1}^{*}(T - t) \tag{3.21}$$

and the other having the impulse response

$$h_{k2}(t) = s_{k2}^{*}(T - t) \tag{3.22}$$

Of course, if BPSK is the modulation method used to transmit information, then $s_{k1}(t) = -s_{k2}(t)$. Consequently, only a single matched filter is required for BPSK. Following the matched filters is a combiner that forms the two decision variables. The combiner that achieves the best performance is one in which each matched filter output is multiplied by the corresponding complex-valued (conjugate) channel gain $\alpha_k e^{j\phi_k}$. The effect of this multiplication is to compensate for the phase shift in the channel and to weight the signal by a factor that is proportional to the signal strength. Thus, a strong signal carries a larger weight than a weak signal. After the complex-valued weighting operation is performed, two sums are formed. One consists of the transmitted 0. The second consists of the real part of the outputs from the matched filters corresponding to a transmitted 1. This optimum combiner is called a maximal ratio combiner (MRC) by Brennan [19]. Of course, the realization of this optimum combiner is based on the assumption that the channel attenuations $\{a_k\}$ and the phase shifts $\{\phi_k\}$ are known. A block diagram illustrating the model for the binary digital communication system described above is shown in Figure 3-3.

If the modulation is BPSK, the output of the maximal ratio combiner can be expressed as a single decision variable in the form

$$U = \mathrm{Re}\left(\varepsilon \sum_{k=1}^{L} \alpha_k^2 + \sum_{k=1}^{L} \alpha_k N_k \right) \tag{3.23}$$

where

$$\varepsilon = \int_0^T s_{k1}(t) s_{k1}^*(t) dt \tag{3.24}$$

$$N_k = e^{j\phi_k} \int_0^T z_k(t) s_{k1}^*(t) dt \tag{3.25}$$

It is noticed that Eq.3.23 is identical to the decision variable given in Eq.3.17, which corresponds to the output of the RAKE demodulation. Consequently, the RAKE demodulator with perfect estimates of the channel tap weights is equivalent to a maximal ratio combiner in a system with L[th]-order diversity.

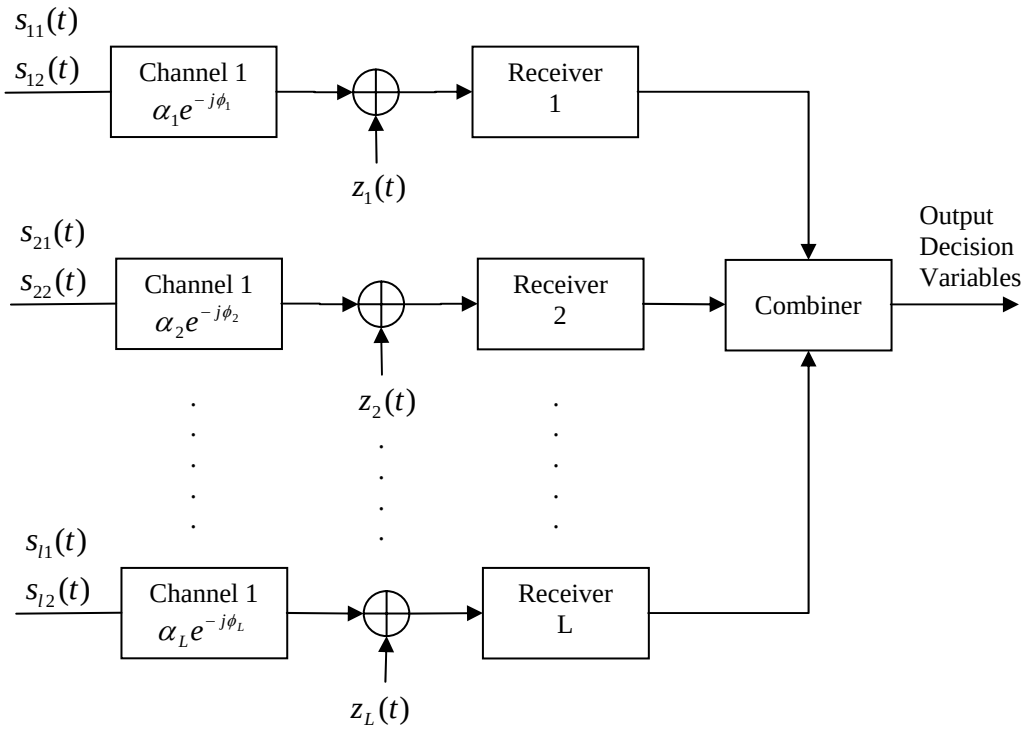

Figure 3-3: Model of binary digital communication system with L[th]-order diversity.

3.2 Combating ISI

The RAKE demodulator described above is an optimum demodulator based on the condition that the bit interval $T_b >> T_m$, i.e., there is negligible ISI. When the condition is not satisfied, the RAKE demodulator output is corrupted. If ISI is left uncompensated, high error rate will occur. The detailed information about the equivalent discrete-time model for a channel with ISI is in Appendix A. The solution to the ISI problem is to design a receiver that employs a means for compensating or reducing the ISI in the received signal. The compensator for the ISI is called an equalizer. From the potential future and rule limitation of UWB, it is well known that there are two important characteristics of UWB: high bit rate and low emitting power. Based on the power emission limit of UWB one can only choose low level modulation technology. To obtain such high bit rate with low level modulation techniques, the result is very small symbol period. According to the UWB channel models from IEEE P802.15 [4], there is a RMS delay spread of approximately 15ns for a 4-10 meter range with a non line-of-sight transmission. This spread indicates that a significant inter-symbol interference is unavoidable. In such a case, an equalizer is required to suppress ISI. At the receiver, after the signal is demodulated to base-band, it may be processed by the RAKE, followed by an equalizer to suppress the ISI. The RAKE output is sampled at bit rate, and these samples are passed to the equalizer. This structure is shown in Figure 3-4. There are several types of equalization methods being extensively used. One is based on the maximum-likelihood (ML) sequence detection criterion, which is optimum from a probability of error viewpoint. A second equalization method is based on the use of

a linear filter with adjustable coefficients. A third equalization method that is described exploits the use of previously detected symbols to suppress ISI in the present symbol being detected; this is called decision-feedback equalization. All these equalization methods are now described in detail.

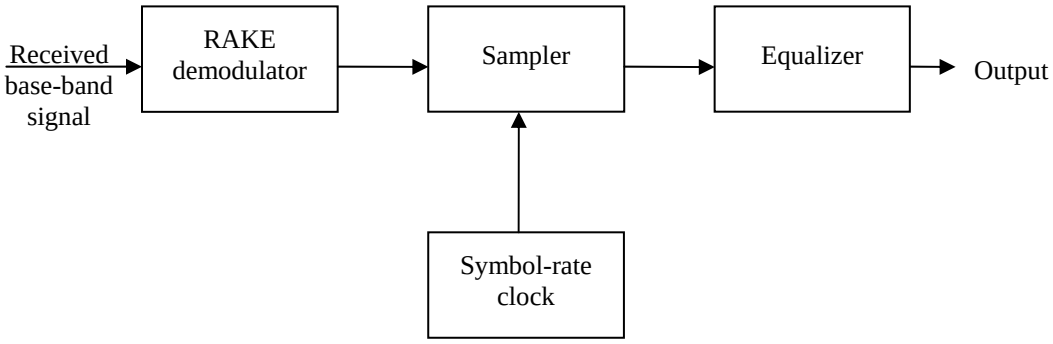

Figure 3-4: Receiver structure for processing signal corrupted by ISI

3.2.1 Optimum maximum-likelihood receiver

The received base-band signal can be expressed as

$$r_l(t) = \sum_n I_n h(t - nT) + z(t) \tag{3.26}$$

where $\{I_n\}$ is the information sequence, $h(t)$ represents the response of the channel to the input signal pulse $g(t)$ and $z(t)$ represents the additive white Gaussian noise. The maximum-likelihood estimates of the symbols $\mathrm{I}_p \equiv \lfloor I_1, I_2, \ldots, I_p \rfloor$ are those that maximize this quantity:

$$CM(\mathrm{I}_p) = 2\,\mathrm{Re}\left(\sum_n I_n^* y_n \right) - \sum_n \sum_m I_n^* I_m x_{n-m} \tag{3.27}$$

where

$$y_n \equiv y(nT) = \int_{-\infty}^{\infty} r_l(t) h^*(t - nT) dt \tag{3.28}$$

$$x_n \equiv x(nT) = \int_{-\infty}^{\infty} h^*(t) h(t + nT) dt \tag{3.29}$$

In any practical system, it is reasonable to assume that ISI affects a finite number of symbols. Consequently, ISI observed at the output of the demodulator may be viewed as the output of a finite state machine. This implies that the channel output with ISI can be represented by a trellis diagram, and the maximum-likelihood estimate of the information sequence $\mathrm{I}_p \equiv \lfloor I_1, I_2, \ldots, I_p \rfloor$ is simply the most probable path through the trellis given the received demodulator output sequence $\{y_n\}$. Clearly, the Viterbi algorithm provides an efficient means for performing the trellis search.

3.2.2 Linear equalization

The maximum likelihood signal estimation for a channel with ISI has a computational complexity that grows exponentially with the length of the channel time dispersion. If the size of the symbol alphabet is *M* and the number of interfering symbols contributing to ISI is *L*, the Viterbi algorithm computes M^{L+1} metrics for each new received symbol. In most channels of practical interest, such a large computational complexity is prohibitively expensive to implement.

One suboptimum channel equalization approach is the linear equalization that employs a linear transversal filter. This filter structure has a computational complexity that is a linear function of the channel dispersion length *L*. This linear transversal filter equalization structure is shown in Figure 3-4. Its input is the

demodulator output sequence $\{v_k\}$ and its output is the estimate of the information sequence $\{I_k\}$. This process can be expressed as

$$\hat{I}_k = \sum_{j=-K}^{K} c_j v_{k-j} \tag{3.30}$$

where $\{c_j\}$ are the 2K+1 complex-valued tap weight coefficients of the filter.

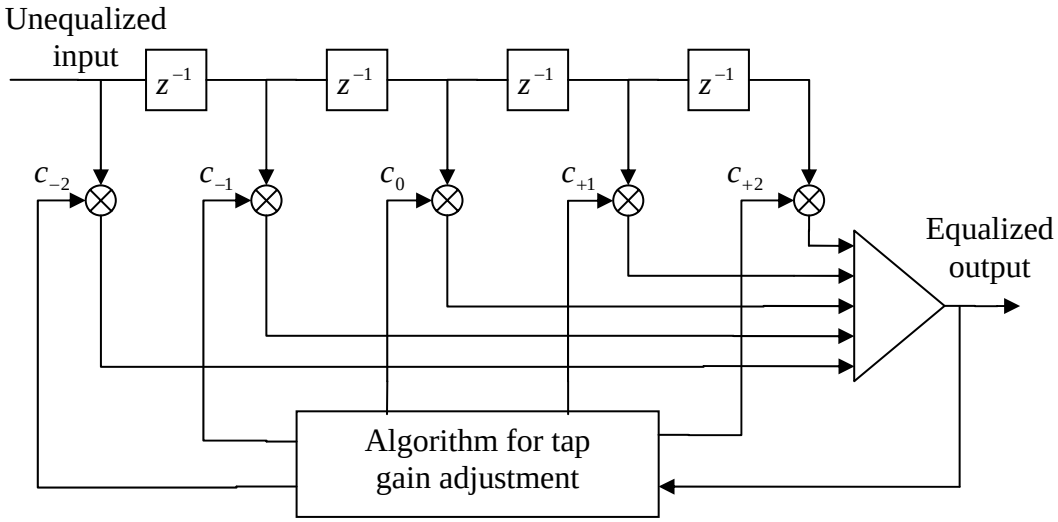

Figure 3-5: Linear transversal filter equalization structure

Here the problem is how to choose the tap weight coefficients $\{c_j\}$ to optimize system performance. Because the most meaningful measure of performance for a digital communication system is the average probability of error, it is desirable to choose the coefficients to minimize this performance index. However, the probability of error is a highly non-linear function of $\{c_j\}$. The probability of error as a performance index for optimizing the tap weight coefficients of the equalizer is

computationally complex. There are two criteria commonly used. One is the peak distortion criterion and the other is the mean-square-error criterion.

The peak distortion is simply defined as the worst-case inter-symbol interference at the output of the equalizer. The minimization of this performance index is called the peak distortion criterion. Firstly if one can use an equalizer that has an infinite number of taps, it is found that the equalizer is simply just an inverse filter to the equivalent discrete-time model of the channel and ISI can be completely eliminated. Such a filter is called a zero-forcing filter. Here the tedious formula derivation is left out and just the result is given. The detailed information about the equivalent discrete-time model for a channel with ISI and the zero-forcing filter is presented in Appendix A and Appendix B. Figure 3-6 depicts block diagram of the equivalent discrete-time channel and equalizer.

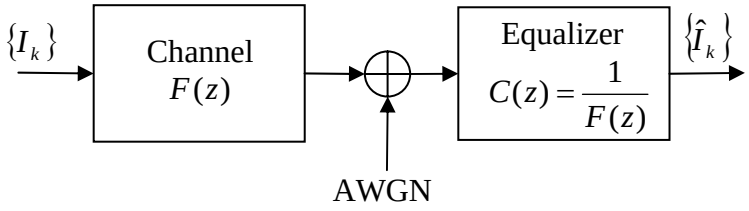

Figure 3-6: Block diagram of channel with zero-forcing equalizer

When the equalizer has a finite number of taps, the peak distortion is a convex function of the coefficients $\{c_j\}$. Its minimization can be carried out numerically using the method of steepest descent.

In MSE criterion, the tap weight coefficients $\{c_j\}$ of the equalizer are adjusted to minimize the mean square value of the error

$$J = E\left|\varepsilon_k\right|^2 = E\left|I_k - \hat{I}_k\right|^2 \tag{3.31}$$

where I_k is the information symbol transmitted in the k^{th} signaling interval and $\hat{I}_k$ is the estimate of that symbol at the output of the equalizer. J is a quadratic function of the equalizer coefficients $\{c_j\}$. This function can be easily minimized with respect to the $\{c_j\}$ to yield a set of linear equations for $\{c_j\}$. Alternatively, the set of linear equations can be obtained by invoking the orthogonal principle in mean square estimation. The optimum tap weight coefficient can be obtained by solving this set of linear equations. The detailed information of MSE linear equalizer is in Appendix C.

3.2.3 Decision-feedback equalization

The decision-feedback equalizer (DFE), depicted in Figure 3-7, consists of two filters, a feedforward filter and a feedback filter. Both have taps spaced at the symbol interval. Input to the feedforward section is the demodulator output sequence $\{v_k\}$. Input to the feedback filter is the sequence of decision on previously detected symbols. Functionally, the feedback filter is used to remove part of the inter-symbol interference from the present estimate caused by previously detected symbols. The equalizer output can be expressed as

$$\hat{I}_k = \sum_{j=-K_1}^{0} c_j v_{k-j} + \sum_{j=1}^{K_2} c_j \tilde{I}_{k-j} \tag{3.32}$$

where $\hat{I}_k$ is an estimate of the k^{th} information symbol, $\{c_j\}$ are the tap coefficients of the filter, and $\{\tilde{I}_{k-1},\ldots,\tilde{I}_{k-K_2}\}$ are previously detected symbols.

The equalizer is assumed to have $(K_1 + 1)$ taps in its feedforward section and K_2 taps in its feedback section. This equalizer is no longer linear because the feedback filter contains previously detected symbols $\{\tilde{I}_k\}$. Both the peak distortion criterion and the MSE criterion can be applied to optimize the tap coefficients $\{c_j\}$.

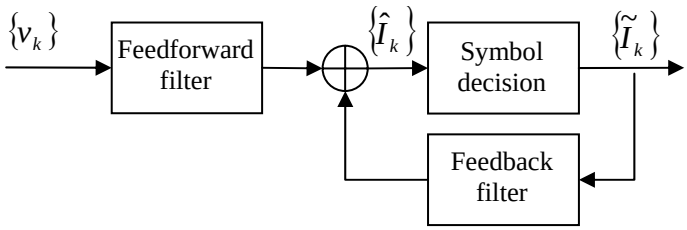

Figure 3-7: Structure of decision feedback equalizer

3.2.4 LMS adaptive equalization

In the introduction to equalization methods described previously, it is implicitly assumed that the channel characteristics, either impulse response or frequency response, are known at the receiver. However, in most communication systems that employ equalizers, the channel characteristics are unknown a priori and, in many cases, the channel response is time-variant. In such a case, the equalizers are designed to be adjustable to the channel response and, for time-variant channels, to be adaptive to the time variations in the channel response.

From the description of MSE criterion linear equalization, the optimum tap weight coefficient can be obtained by solving a set of linear equations. This optimum tap weight coefficient can also be recursively obtained by the method of steepest descent. This method is basic to the understanding of the least-mean-square (LMS)

adaptive equalization, so a brief introduction about the method of steepest descent is given[32].

Consider a cost function $J(\vec{w})$ that is a continuously differentiable function of some unknown weight vector $\vec{w}$. The function $J(\vec{w})$ maps the elements of $\vec{w}$ into real numbers. One wants to find an optimal solution $\vec{w}_o$ that satisfies the condition

$$J(\vec{w}_o) \le J(\vec{w}) \qquad \text{for any } \vec{w} \tag{3.33}$$

This is a mathematical statement of unconstrained optimization.

Starting with an initial guess denoted by $\vec{w}(0)$, generate a sequence of weight vectors $\vec{w}(1)$, $\vec{w}(2)$, …, such that the cost function $J(\vec{w})$ is reduced at each iteration of the algorithm; that is,

$$J\left(\vec{w}(n+1)\right) < J\left(\vec{w}(n)\right) \tag{3.34}$$

where $\vec{w}(n)$ is the old value of the weight vector and $\vec{w}(n+1)$ is its updated value. According to the method of steepest descent, the successive adjustments applied to the weight vector $\vec{w}$ are in the direction of steepest descent, in a direction opposite to the gradient vector of the cost function $J(\vec{w})$, which is denoted by $\nabla J(\vec{w})$. For convenience of presentation, it is written as:

$$\vec{g} = \nabla J(\vec{w}) = \frac{\partial J(\vec{w})}{\partial \vec{w}} = \begin{bmatrix} \dfrac{\partial J(\vec{w})}{\partial a_1} + j\dfrac{\partial J(\vec{w})}{\partial b_1} \\ \dfrac{\partial J(\vec{w})}{\partial a_2} + j\dfrac{\partial J(\vec{w})}{\partial b_2} \\ \vdots \\ \dfrac{\partial J(\vec{w})}{\partial a_M} + j\dfrac{\partial J(\vec{w})}{\partial b_M} \end{bmatrix} \tag{3.35}$$

where $\vec{w} = \left[a_1 + jb_1, \quad a_2 + jb_2, \quad \cdots \quad , a_M + jb_M\right]$ is a complex valued vector.

The steepest-descent algorithm can be described by

$$\vec{w}(n+1) = \vec{w}(n) - \frac{1}{2}\mu\vec{g}(n) \tag{3.36}$$

where n denotes the iteration, μ is a positive constant called the step-size parameter, and the factor ½ is introduced for mathematical convenience

Then the method of steepest descent is applied to the MSE linear equalization. Let Γ denote the (2K+1)-by-(2K+1) correlation matrix of the demodulator output sequence $\{v_k\}$:

$$\Gamma = E\left[V^*(k)V^T(k)\right] \tag{3.37}$$

where

$$V(k) = \left[v_{k-K}, v_{k-(K-1)}, \ldots, v_k, \ldots, v_{k+(K-1)}, v_{k+K}\right]^T \tag{3.38}$$

is the (2K+1)-by-1 demodulator output sequence $\{v_k\}$ vector at time k. Correspondingly, let P denote the (2K+1)-by-1 cross-correlation vector between the demodulator output sequence $\{v_k\}$ vector and the information signal I_k:

$$\mathrm{P} = E\left[V^*(k)I_k\right] \tag{3.39}$$

where

$$C = \left[c_K, c_{K-1}, \ldots, c_0, \ldots, c_{-(K-1)}, c_{-K}\right]^T \tag{3.40}$$

is the (2K+1)-by-1 equalizer coefficients vector. Equation (3-16) is rewritten here.

$$J = E\left|\varepsilon_k\right|^2 = E\left|I_k - \hat{I}_k\right|^2$$

$$= E\left[\varepsilon_k \varepsilon_k^*\right] = E\left[(I_k - \hat{I}_k)(I_k - \hat{I}_k)^*\right] \quad \text{, Substituting Equation (3.30).}$$

$$= E\left[\left|I_k\right|^2\right] - \sum_{j=-K}^{K} c_j^* E\left[v_{k-j}^* I_k\right] - \sum_{j=-K}^{K} c_j E\left[v_{k-j} I_k^*\right] + \sum_{j=-K}^{K}\sum_{i=-K}^{K} c_j c_i^* E\left[v_{k-j} v_{k-i}^*\right] \tag{3.41}$$

The gradient vector of the cost function J based on the equalizer coefficients vector C is (The detailed information about procedure of calculating this gradient vector is in Appendix D)

$$\nabla J(C) = -2\mathrm{P} + 2\Gamma C \tag{3.42}$$

For applying the steepest-descent algorithm, it is assumed that in Eq.3.42 the correlation matrix Γ and the cross-correlation vector P are known, so that the gradient vector $\nabla J(C)$ can be computed for a given value of the equalizer coefficients vector C. Thus, substituting Eq.3-20 into Eq.3-18, the update value of the equalizer coefficients vector C can be computed by using a simple recursive relation

$$C(n+1) = C(n) + \mu[\mathrm{P} - \Gamma C(n)], \qquad n = 0,1,2,\ldots, \tag{3.43}$$

This describes the mathematical formulation of the steepest-descent algorithm for the MSE linear equalization.

If it were possible to make exact measurements of the gradient vector $\nabla J(C)$ at each iteration *n*, and if the step-size parameter μ was suitably chosen, then the equalizer coefficients vector computed by using the steepest-descent algorithm would indeed converge to the optimum solution. In reality, however, exact measurements of the gradient vector are not possible, since that would require prior knowledge of both the correlation matrix Γ of the demodulator output sequence $\{v_k\}$ and the cross-correlation vector P between the demodulator output sequence $\{v_k\}$ vector and the information signal I_k. Consequently, the gradient vector must be estimated from the available data when this algorithm is operated in an unknown environment.

To develop an estimate of the gradient vector $\nabla J(C)$, the most obvious strategy is to substitute estimates of the correlation matrix Γ and the cross-correlation vector P in the formula of Eq.3-21. The simplest choice of estimators is to use instantaneous estimates for Γ and P that are based on sample values of the demodulator output sequence $\{v_k\}$ vector and the information signal I_k, defined respectively by

$$\hat{\Gamma} = V^*(k)V^T(k) \tag{3.44}$$

$$\hat{\mathrm{P}} = V^*(k)I_k \tag{3.45}$$

Correspondingly, the instantaneous estimate of the gradient vector is

$$\hat{\nabla} J(\hat{C}) = -2V^*(k)I_k + 2V^*(k)V^T(k)\hat{C} \tag{3.46}$$

Substituting the estimate of Eq.3.46 for the gradient vector $\nabla J(C)$ in the steepest-descent algorithm described in Eq.3.43, getting a new recursive relation for updating the tap-weight vector:

$$\begin{aligned}\hat{C}(n+1) &= \hat{C}(n) + \mu V^*(k)\left[I_k - V^T(k)\hat{C}(n)\right], \quad n = 0,1,2,\ldots, \\ &= \hat{C}(n) + \mu V^*(k)\left[I_k - \hat{I}_k\right]\end{aligned} \tag{3.47}$$

where

$$\hat{I}_k = \sum_{j=-K}^{K} c_j v_{k-j} = V^T(k)\hat{C}(n) \tag{3.48}$$

This recursive algorithm can be operated by the time index k and the result can be equivalently expressed in the form of three basic relations as follows:

1. Equalizer output:

$$\hat{I}_k = V^T(k)\hat{C}(k) \tag{3.49}$$

2. Estimation error:

$$e(k) = I_k - \hat{I}_k \tag{3.50}$$

3. Equalizer coefficients adaptation:

$$\hat{C}(k+1) = \hat{C}(k) + \mu V^*(k) e(k) \tag{3.51}$$

Equations (3.49) and (3.50) define the estimation error $e(k)$, the computation of which is based on the current estimate of the equalizer coefficients vector $\hat{C}(k)$. The iterative procedure is started with an initial guess $\hat{C}(0)$.

The algorithm described by Eq.3.49 through Eq.3.51 is the complex form of the adaptive least-mean-square (LMS) algorithm. In the above discussion, to obtain the estimation error $e(k)$, the receiver must have knowledge of the transmitted information sequence I_k. Such knowledge can be made available during a short training period in which a signal with a known information sequence is transmitted to the receiver for initially adjusting the equalizer tap weights. In practice, the training sequence is often selected to be a periodic pseudorandom sequence, such as a maximum length shift-register sequence. After the training period, a practical scheme for continuous adjustment of the equalizer tap weights may be used. One scheme is a decision-directed mode of operation in which decisions on the information symbols are assumed to be correct and used in place of I_k in forming the error signal $e(k)$. Another one is that a known pseudorandom-probe sequence is inserted in the information-bearing signal either additively or by interleaving in time and the tap weights adjusted by comparing the received probe symbols with

the known transmitted probe symbols. In the decision-directed mode of operation, the error signal becomes

$$\tilde{e}(k) = \tilde{I}_k - \hat{I}_k \tag{3.52}$$

where $\tilde{I}_k$ is the decision of the receiver based on the estimate $\hat{I}_k$.

As long as the receiver is operating at low error rates, an occasional error will have a negligible effect on the convergence of the algorithm. If the channel response changes, this change is reflected in the error signal $e(k)$. Hence, the equalizer tap weights will be changed to reflect the change in the channel. A similar change in the equalizer tap weights occurs if the statistics of the noise or the information sequence change. Thus, the equalizer is adaptive.

The convergence properties of the LMS algorithm given by Eq.3.49 through Eq.3.51 are governed by the step-size parameter μ. The necessary condition that has to be satisfied for the convergence of the LMS algorithm is:

$$0 < \mu < \frac{2}{\lambda_{\max}} \tag{3.53}$$

where $\lambda_{\max}$ is the largest eigenvalue of the correlation matrix Γ. The ratio $\lambda_{\max}/\lambda_{\min}$ ultimately determines the convergence rate. If $\lambda_{\max}/\lambda_{\min}$ is small, the step-size parameter μ can be selected so as to achieve rapid convergence. However, if the ratio $\lambda_{\max}/\lambda_{\min}$ is large, as is the case when the channel frequency response has deep spectral nulls, the convergence rate of the algorithm will be slow.

A significant feature of the LMS algorithm is its simplicity. Moreover, it does not require measurements of the pertinent correlation functions, nor does it require matrix inversion. Indeed, it is the simplicity of the LMS algorithm that has made it

the standard against which the other linear adaptive equalization algorithms are benchmarked.

Chapter 4 Proposed Receiver Structures

In this chapter, first basic requirements and considerations of the receiver are introduced. A simplified RAKE demodulation implementation and basic concept and method of channel estimation are discussed subsequently. Finally three receiver structures are proposed.

4.1 Basic requirements and considerations of receivers

The goal is to propose a low cost UWB receiver structure with data rate of at least 120 Mbps with low complexity at a reasonable sampling rate. There are several factors that must be considered first before selecting the receiver structure and algorithms.

1. Signal Bandwidth: UWB technology means a wide band signal and its advantage is also based on a wide band signal. But how wide is a good balance between performance and implementation difficulties? If the bandwidth is too wide, it will be very difficult to implement the analog front end. For the digital processing following the analog front end the wider bandwidth means a higher sampling rate and implementation cost.
2. Complexities of algorithms: The UWB technology is a potential solution for indoor short range high speed wireless connection. This means that the algorithms are also high speed algorithms and a good balance between speed, complexity and cost must be carefully considered.

First, RAKE demodulation methods are considered.

4.2 A simplified RAKE demodulation implementation

Here a single band impulse radio system with 1GHz bandwidth and antipodal PAM modulation is used. To simplify the analysis, only the base-band case is considered, and all signals are assumed to be real-valued. A model for this UWB transmission over a UWB channel is shown in Figure 4-1.

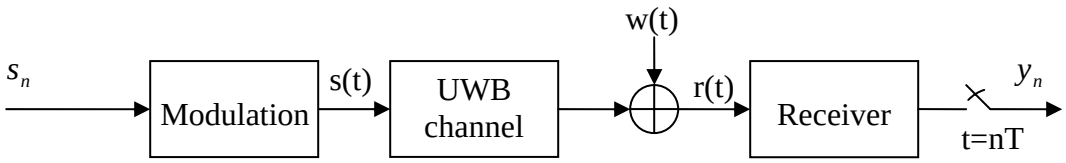

Figure 4-1: UWB transmission system model

The zero-mean +1 or -1 data symbols s_n are modulated with a unit energy pulse $p(t)$ to generate the signal $s(t)$. After antipodal PAM modulation, the signal goes through the UWB channel with L paths whose response is given by [4]:

$$h(t) = \sum_{l=0}^{L-1} \alpha_l \delta(t - \tau_l) \tag{4.1}$$

where α_l and τ_l are gain and delay introduced by the l^{th} path of the channel. The received signal can then be expressed as:

$$r(t) = \sum_{i=-\infty}^{+\infty} s_i \sum_{l=0}^{L-1} \alpha_l p(t - \tau_l - iT) + w(t) \tag{4.2}$$

where T is the symbol time and $w(t)$ is additive noise. The noise is assumed to be a zero-mean white noise that is uncorrelated with the data.

The channel is a dense multi-path channel according to the UWB channel characteristics described in Chapter 2. A RAKE receiver, the preferred structure for collecting multi-path energy seems a good choice. The traditional RAKE demodulation implementation is used here as described in Chapter 3. This structure is shown in Figure 4-2.

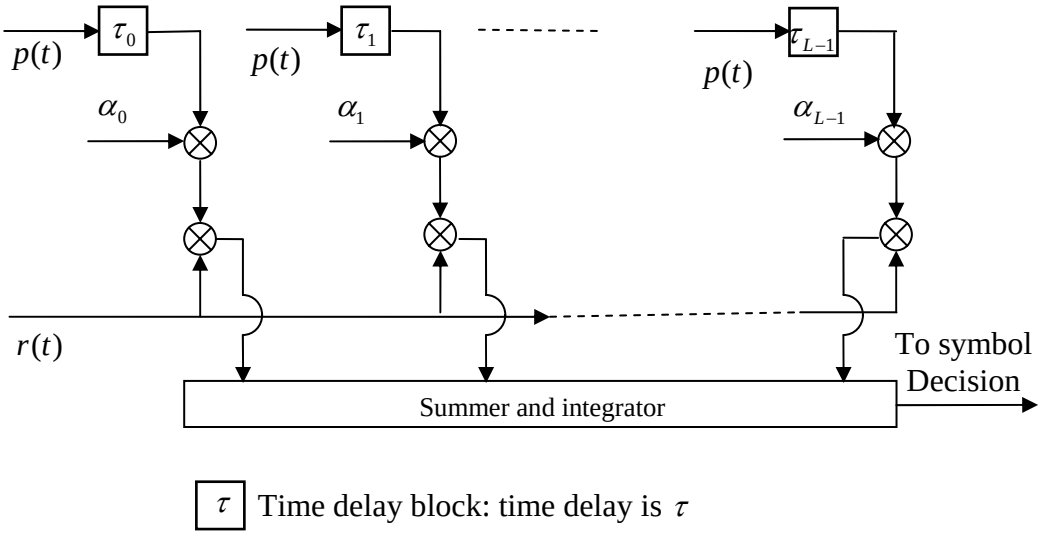

Figure 4-2: The traditional RAKE demodulation implementation

Otherwise the digital implementation of RAKE demodulation can be used as an alternative method. For digital implementation, the received signal $r(t)$ and the pulse signal $p(t)$ are sampled under the requirement of the Nyquist sampling criterion (at least 2 GHz) and then carry out the digital signal processing similar to the traditional RAKE demodulation implementation. The disadvantage of the traditional RAKE demodulation implementation is its high complexity. For the digital implementation of RAKE demodulation, the sampling rate is quite high.

The tapped delay line model described in Chapter 3 is restated briefly here. For a signal $s_l(t)$ having a bandwidth W when it is passed through a frequency-selective channel, the resolution of its multi-path delay profile is 1/W. Then the noiseless received signal can be expressed in the form

$$r_l(t) = \sum_{n=0}^{L-1} c_n(t) s_l(t - n/W) \tag{4.3}$$

The time-variant tap weights $\{c_n(t)\}$ are complex-valued stationary random processes. According to the UWB channel characteristics described in Chapter 2, these time-variant tap weights $\{c_n(t)\}$ are real-valued. Since the $\{c_n(t)\}$ represent the tap weights corresponding to the L different delays $\tau = n/W \quad n = 0,1,2,\ldots,L-1$, the uncorrelated scattering assumption implies that $\{c_n(t)\}$ are mutually uncorrelated.

This tapped delay line model can be applied here for the UWB channel. When a pulse signal having a bandwidth $W = 1GHz$ passes through the UWB channel, the impulse response of the UWB channel can be expressed in the form

$$h(t) = \sum_{l=0}^{L-1} \alpha_l \delta(t - l/W) \tag{4.4}$$

where α_l is the gain introduced by the l^{th} path of the channel. The received signal can then be expressed as:

$$r(t) = \sum_{i=-\infty}^{+\infty} s_i \sum_{l=0}^{L-1} \alpha_l p(t - l/W - iT) + w(t) \tag{4.5}$$

where T is the symbol time and $w(t)$ is additive noise. If TW is an integer, then the Eq.4.5 can be rewritten as:

$$r(t) = \sum_{i=-\infty}^{+\infty} s_i \sum_{l=0}^{L-1} \alpha_l \, p(t - (l + iTW)/W) + w(t) \tag{4.6}$$

If the traditional RAKE demodulation implementation shown in Figure 4-2 is used here, the symbol decision value can be expressed as:

$$y(n) = \int_{-\infty}^{+\infty} \left[\sum_{k=0}^{L-1} \alpha_k \, p(t - k/W - nT) \right] \cdot r(t) dt$$

$$= \sum_{i=-\infty}^{+\infty} s_i \sum_{k=0}^{L-1} \alpha_k \sum_{l=0}^{L-1} \alpha_l \delta(k + nTW - l - iTW) + \sum_{k=0}^{L-1} \alpha_k \int_{-\infty}^{+\infty} p(t - k/W - nT) \cdot w(t) dt \tag{4.7}$$

Here assuming that the system is perfectly synchronized, the pulse energy is 1 and no inter-pulse interference exists.If this signal is passed through a pulse $p(t)$-matched filter and sampling at the rate W. The result digital signal can be expressed as:

$$r(m) = \sum_{i=-\infty}^{+\infty} s_i \sum_{l=0}^{L-1} \alpha_l \delta(m - l - iTW) + \hat{w}(m) \tag{4.8}$$

where

$$\hat{w}(m) = \hat{w}(m/W) \tag{4.9}$$

and

$$\hat{w}(t) = \int_{-\infty}^{\infty} w(\tau) p(-t + \tau) d\tau \tag{4.10}$$

The sampled output were attenuated by the corresponded tap coefficients and then combined into a single test variable:

$$y(n) = \left[\sum_{k=0}^{L-1} \alpha_k \delta(m - k - nTW) \right] \cdot r(m)$$

$$= \sum_{i=-\infty}^{+\infty} s_i \sum_{k=0}^{L-1} \alpha_k \sum_{l=0}^{L-1} \alpha_l \delta(k + nTW - l - iTW) + \sum_{k=0}^{L-1} \alpha_k \int_{-\infty}^{+\infty} p(t - k/W - nT) \cdot w(t) dt \tag{4.11}$$

This result is identical with the value in Equation (4.7). From this mathematical procedure just described above, an analogue and digital hybrid processing method can be proposed to implement the RAKE demodulation. First, the received signal was passed through a pulse $p(t)$-matched filter and sampling at rate W. The sampled output were attenuated by the corresponded tap coefficients and then combined into a single test variable for final decision. This proposed simplified RAKE demodulation implementation structure is shown in Figure 4-3.

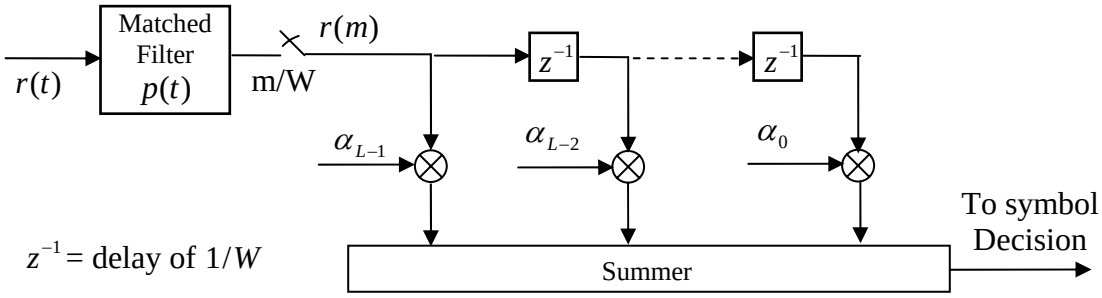

Figure 4-3: A simplified RAKE demodulation implementation

This proposed simplified RAKE demodulation implementation structure not only reduces high complexity of the traditional implementation but also avoid high Nyquist sampling rate. Another benefit is the convenience for channel estimation described in following section.

4.3 Channel estimation for RAKE demodulation

For implementing a RAKE receiver to capture signal energy spread over multiple paths, channel parameters such as arrival time, amplitude and phase of the fingers need to be known. However, in a dense multi-path UWB wireless environment,

channel information can not be known a priori. Therefore channel parameters must be estimated before any receiving processing can be implemented.

Channel parameters estimation in UWB communications has been previously addressed in [10, 14] to assess the signal energy capture in Rake receivers as a function of the number of fingers. In these papers, an UWB signal propagation experiment was performed in a typical office building. The isolated monocycle signal with bandwidth in excess of 1 GHz is transmitted through the channel and corresponding multi-path profiles were measured using a digital sampling oscilloscope and recorded. The authors use the ML technique as the optimization criterion to find delay, amplitude and phase of the fingers. The problem is to approximate the actual channel with a channel with L_c branches and to choose the propagation parameters in the latter in such a way that its output matches the recorded waveform as best as possible. Clearly, the degree of matching depends on L_c and the minimum value of L_c required for a good match establishes the number of fingers that a Rake receiver must possess to efficiently exploit the channel diversity.

Rather than from isolated pulses, channel estimation methods that derive channel parameters estimates from the information-bearing signal have been proposed [15]. In this paper there are two scenarios: either data-aided (DA) or non-data-aided (NDA) estimation was considered based on the maximum-likelihood (ML) criterion. The first instance is of interest during channel acquisition when a training sequence is available. Channel tracking can be pursued in a pilot-aided fashion, by periodically retransmitting the training sequence, or in a decision-

directed (DD) manner using the receiver decisions in place of the real data. On the other hand, NDA estimation is useful in broadcast networks where training sequences would impede the transmitter when new users enter the network.

Some words are useful about the practical implementation of the DA method. A possible approach is to organize the data pattern in groups, each consisting of a preamble of M pilot symbols followed by $Q \times M$ information symbols. The channel estimate from the pilots is used to detect the subsequent information data. In this context, the integer M must be large enough to guarantee adequate estimation accuracy (on the order of a hundred [15]). Integer Q is related to the transmission efficiency $Q/(Q+1)$ and should be as large as possible. However, with a time-varying channel, the product $Q \times M$ must be much smaller than the channel de-correlation.

Another approach is to employ a decision-directed (DD) technique. The symbol pattern still has a framed structure as before but the channel estimates are no longer "frozen" during the transmission of the data. Indeed, the detector decisions are taken in groups of M and are used in place of the true symbols to update the channel estimate. The advantage of this method is that it can track the channel and, in consequence, it allows using much larger values of Q.

The approaches described above all use a maximum-likelihood criterion to estimate the arrival time, amplitude and phase of the channel taps. The complexity of such an approach is too high for the practical implementation. Instead, the well known suboptimal estimation sliding correlation algorithm can be used. A similar approach for outdoor wireless communications has been presented by Viterbi in

[17] and also included in the Interim Standard 95 (IS-95) by the U.S. Telecommunications Industry Association (TIA) [18].

The sliding correlation algorithm cross-correlates the received pilot sequence with the known pilot sequence and then calculate gains and delays for the N largest amplitudes of the cross-correlated sequence. The sliding correlation algorithm is ML optimum for a one-tap channel or if the shifted versions of the received signal are mutually orthogonal. Unfortunately, neither of these requirements is met in the UWB channel mode, which results in sub-optimality of the sliding correlation approach.

The successive cancellation algorithm [16] can improve performance of the sliding correlation algorithm by using an iterative cancellation algorithm. The algorithm begins with the use of the sliding correlation algorithm to find the parameters of the strongest tap. The delayed version of the transmitted signal corresponding to the estimated tap is then subtracted from the received sequence and the algorithm is repeated. The number of iterations is equal to the number of taps to be estimated. Note that the successive cancellation algorithm introduces a longer computation delay than the sliding correlation algorithm. This delay is unendurable in the UWB high speed communication application environment. Therefore the simple and effective sliding correlation algorithm was finally chosen for the channel parameter estimation. This approach endures a small loss of performance as the cost. Another benefit of sliding correlation algorithm is that it just needs the digital sampled output of the pulse-matched filter which is available

as described in Section 4.2 and it makes the receiver structure much simpler and easier to implement without need for any extra hardware or measurement.

4.4 N-selective MRC RAKE receiver

The ultimate goal of a RAKE receiver is to construct correlators or filters that are matched to the set of received symbol waveforms corresponding to a train of transmitted pulses. Imperfect construction of the synthesized waveform in a UWB RAKE receiver degrades the performance of the receiver. The All_RAKE receiver is a RAKE receiver with unlimited resources (correlators) and instant adaptability, so that it can, in principle, perfectly construct matched filters or correlators reference signals that are identical to the set of received symbol waveforms. The All_RAKE is an optimal RAKE receiver structure and is not realizable. Due to complexity and performance, in practice, the suboptimal N-selective RAKE receivers that process only a subset of the available resolved multi-path components are used commonly [20]. These receivers diversity combine outputs of a fixed number of correlators, each selectively locked to a different resolved signal path. Of course the delay and amplitude parameters of each selected path must be estimated in advance.

From the result of the UWB signal propagation experiment in [10], some helpful advice can be obtained. Energy capture as a function of the number of single-path signal correlators is computed for each received waveform measurement. This can be used to estimate the performance of an N-selective RAKE receiver with coherent diversity combining with the correlator outputs, each

correlator matched to a basic building block waveform. The number of required correlators in an UWB N-selective Rake receiver versus percentage energy capture is plotted in Figure 4-4[10]. Note that in Fig. 4-4 the amount of captured energy made. Because of

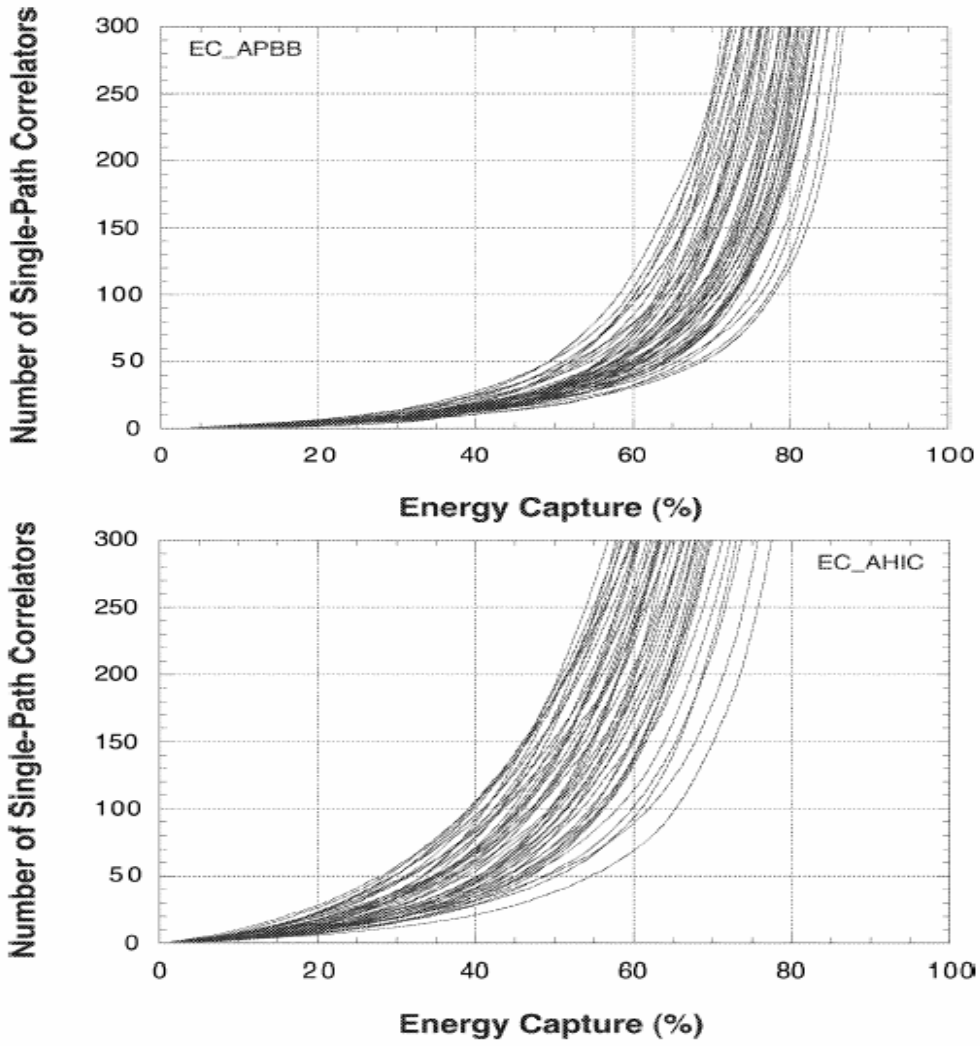

Figure 4-4: The number of single-path signal correlators in a UWB Rake receiver as a function of percentage energy capture for received waveforms in an office P (upper plot) and H (lower plot) representing typical “high SNR” and “low SNR” environment. In each plot, 49 measurement waveforms are used [10].

increases rapidly as the number of correlators increases from 0 to 50. However, this improvement becomes gradual as the number of correlators increases from 50 to 100. Beyond this point, only a negligible improvement in energy capture can be complexity constraints in practice, UWB N-selective RAKE receivers are designed to operate in the regions where the increases in energy capture as a function of the number of correlators is rapid. Fig. 4-4 also suggests that the number of dominant specular multi-path components is expected to be less than 50 for UWB signal transmissions in a typical modern office building. On the other hand, the number of dominant specular multi-path components is much larger than five.

From the UWB channel model from IEEE P802.15 [4], there is also some useful information about the relation between energy capture and the number of single-path signal correlators. IEEE P802.15 has four channel models:

CM1: this model is based on LOS (0-4m) channel measurements.

CM2: this model is based on NLOS (0-4m) channel measurements.

CM3: this model is based on NLOS (4-10m) channel measurements.

CM4: this model was generated to fit a 25 nsec RMS delay spread to represent an extreme NLOS multipath channel.

These characteristics data is the average value of the 100 actual realizations for each channel model. The situation is a little better than the result in [10]. The rapidly increasing region is from 0 to 40. **CM4** is almost the same as the “high SNR” scenario in [10].

Based on the experiment result in [10] and the channel characteristics from IEEE P802.15, the N-selective RAKE ought to diversity combine N multi-path

components where N can be chosen in the region from 5 to 40 depending on the performance requirement and channel situation.

Based on the proposed simplified RAKE demodulation implementation described in Section 4.2 and the sliding correlation channel estimation algorithm chosen in Section 4.3, an N-selective MRC RAKE receiver structure is proposed. This receiver structure includes a matched filter and sampling, a data-aided (DA) sliding correlation channel parameters estimation and a MRC combiner. In this receiver structure, the N strongest multi-path components were selected as N fingers of the RAKE receiver. From the sampled output of the pulse-matched filter, samples according to the N fingers were selected and weighted by their respective weight and finally combined together. The weight and their respective delay can be expressed as:

$$f(m) = \sum_{q=0}^{N-1} \beta_q \delta(m - \theta_q) \tag{4.12}$$

where β_q and θ_q are the weights and fingers delays respectively and $\theta_q \in [0, L-1]$ is an integer.

The block diagram of this proposed receiver structure is shown in Figure 4-5. The received signal $r(t)$ passes through the pulse $p(t)$ matched filter and the output is sampled at rate m/W and resulted in the discrete signal $r(m)$. During channel estimation period, the pilot sequence generator generates a pilot sequence the same as the one generated at the transmitter. The slide cross-correlator correlates the signal $r(m)$ with the pilot sequence and N maximum result gain and corresponding time delay are selected by the N-maximum selector as channel

parameters. When channel estimation is finished, the MRC combiner starts to

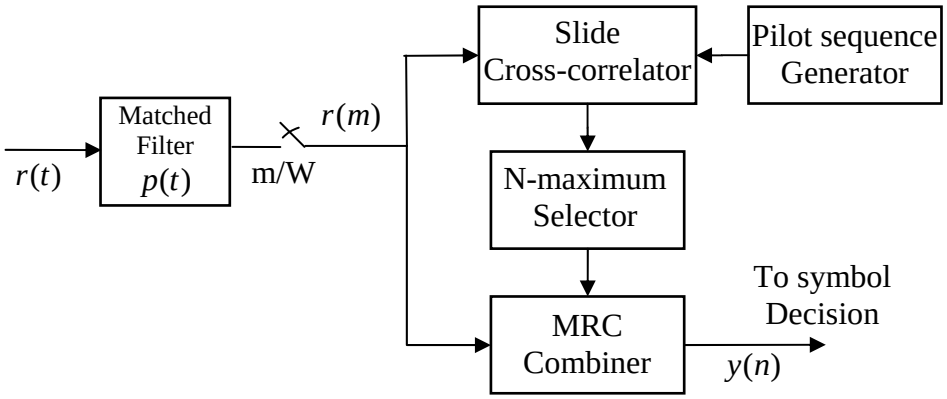

Figure 4-5: N- selective MRC RAKE receiver structure

implement the N diversity combining on signal $r(m)$ and creates a single value $y(n)$ for symbol decision.

4.5 N-selective MRC RAKE receiver with LMS adaptive equalizer

To obtain 110 Mbps per user in UWB with binary signalling, the required symbol period is less than 10 ns without considering coding or signal spreading. Meanwhile, several UWB indoor channel measurement campaigns and UWB channel model from IEEE P802.15 have demonstrated delay spreads far beyond this symbol time [4, 10, 21]. In other words, for high data rate systems significant inter-symbol interference (ISI) is unavoidable.

The N-selective MRC RAKE receiver structure described in Section 4.4, is an effective structure for collecting multi-path energy in UWB channel environment,

but does not combat ISI. Several published results on UWB ignored this fact as most performance analyses employ a RAKE receiver under the assumption that channel delay spreads are much less than the symbol time [5, 24, 27, 29].

For ISI interference, the optimal solution is the maximum-likelihood (ML) sequence detection. However, the computational complexity for ML detection limits it for practical applications. Suboptimum and more computationally effective solutions include linear equalization and decision-feedback equalization. According to the introduction of these two equalization techniques in Section 3.2, for implementing these equalizations an accurate channel characteristic must be obtained first. Optimum equalizer tap weight coefficients can be then obtained by solving a set of linear equations. The sliding correlation algorithm in the N-selective MRC RAKE receiver structure just obtained the parameters of the N strongest multi-path components. This is not sufficient to solve that set of linear equations. If these two equalization methods were implemented, some new channel estimation method through which the accurate parameters of the whole multi-path components can be obtained must be carried out.

Based on the above analysis, the LMS adaptive equalization is a suitable choice. First, the LMS adaptive equalization does not need to know the parameters of the entire multi-path components a priori. Then the LMS algorithm is very simple in implementation and capable of delivering a good performance. Another advantage is that the algorithm has the ability to track the slow variations of the channel. The cost for implementating the LMS equalization is an extra short training period in which a signal with a known information sequence is transmitted

to the receiver. This sequence is used initially to adjust the equalizer tap weights. A similar data pattern organization scheme for channel estimation described in Section 4.3 can be used. After the training period, a decision-directed (DD) scheme of operation in using receiver decisions in place of real data for continuous adjustment of the equalizer tap weights can be used. The channel variations now can be tracked continuously.

The LMS algorithm introduced in 3.2.4 is rewritten here.

- Equalizer output:

$$\hat{I}_k = Y^T(k)\hat{C}(k) \tag{4.13}$$

- Estimation error:

$$e(k) = I_k - \hat{I}_k \tag{4.14}$$

- Equalizer coefficients adaptation:

$$\hat{C}(k+1) = \hat{C}(k) + \mu Y^*(k)e(k) \tag{4.15}$$

where

$$Y(k) = \left[y(k-K), y(k-K+1), \ldots, y(k), \ldots, y(k+K-1), y(k+K)\right]^T \tag{4.16}$$

is (2K+1)-by-1 MRC RAKE demodulator output sequence $\{y(n)\}$ vector at time *k*.

$$C(k) = \left[c_K^{(k)}, c_{K-1}^{(k)}, \ldots, c_0^{(k)}, \ldots, c_{-(K-1)}^{(k)}, c_{-K}^{(k)}\right]^T \tag{4.17}$$

is the (2K+1)-by-1 equalizer coefficients vector at time k. Equations (4.11) and (4.12) define the estimation error $e(k)$, the computation of which is based on the current estimate of the equalizer coefficients vector $\hat{C}(k)$. The iterative procedure is started with an initial guess $\hat{C}(0)$.

When the LMS algorithm is implemented, stability of the algorithm is critical. The convergence properties of the LMS algorithm are governed by the step-size parameter μ. The necessary condition that has to be satisfied for the convergence of the LMS algorithm is:

$$0 < \mu < \frac{2}{\lambda_{\max}} \tag{4.18}$$

where $\lambda_{\max}$ is the largest eigenvalue of the correlation matrix Γ. Γ denotes the (2K+1)-by-(2K+1) correlation matrix of MRC RAKE demodulator output sequence $\{y(n)\}$ vector.

This bound for the step-size parameter μ is a required condition that has to be satisfied for the stability of zero-order solutions derived from the small-step-size theory.

Nevertheless, a derivation of the necessary and sufficient condition for the stability of LMS algorithm of arbitrary length remains an open problem. But if the step-size parameter μ is selected as a small value, this bound still can be used in practical application to guarantee the stability of the LMS algorithm.

To use the bound, the largest eigenvalue $\lambda_{\max}$ of the correlation matrix Γ is a prior condition. But there are some difficulties in obtaining the value of $\lambda_{\max}$. The suboptimal solution is to find another value larger than $\lambda_{\max}$ and related to the MRC RAKE demodulator output sequence $\{y(n)\}$ vector.

There are two properties of the eigenvalues of the correlation matrix Γ.

1. These eigenvalues are real and nonnegative.
2. The sum of these eigenvalues equals to the trace of matrix Γ.

From these two properties, the relation shown below can be obtained:

$\lambda_{\max} \le$ sum of eigenvalues of matrix Γ = trace of matrix $\Gamma = (2K+1)E[|y(n)|^2]$

In any practical system, it is reasonable to assume that the ISI affects a finite number of symbols. Eq.4.7 to Eq.4.9 are rewritten here.

$$r(m) = \sum_{i=-\infty}^{+\infty} s_i \sum_{l=0}^{L-1} \alpha_l \delta(m - l - iTW) + \hat{w}(m) \tag{4.19}$$

where

$$\hat{w}(m) = \hat{w}(m/W) \tag{4.20}$$

and

$$\hat{w}(t) = \int_{-\infty}^{\infty} w(\tau) p(-t+\tau) d\tau \tag{4.21}$$

If TW is a integer valued M, for any arbitrary value m,

$$m - l - iM = 0 \tag{4.22}$$

where i can be an arbitrary valued integer, the number of solutions for l can be obtained as following:

If $remainder(\frac{m}{M}) \le remaider(\frac{L}{M})$ then the number of solutions for l is $\left\lfloor \frac{L}{M} \right\rfloor$.

If $remainder(\frac{m}{M}) > remaider(\frac{L}{M})$ then the number of solutions for l is $\left\lfloor \frac{L}{M} \right\rfloor - 1$.

This solution means that any $r(m)$ is the sum of $\left\lfloor \frac{L}{M} \right\rfloor$ or $\left\lfloor \frac{L}{M} \right\rfloor - 1$ multi-path components and a noise component. If $\left\{ \alpha_1^{(m)}, \alpha_2^{(m)}, \ldots, \alpha_{\left\lfloor \frac{L}{M} \right\rfloor}^{(m)} \right\}$ is $\left\lfloor \frac{L}{M} \right\rfloor$ maximum multi-path components. The following relation can be obtained.

$$r(m) < \sum_{l=1}^{\left\lfloor \frac{L}{M} \right\rfloor} \left| \alpha_l^{(m)} \right| \tag{4-23}$$

Here the noise $\hat{w}(m)$ is neglected. Define $\{\beta_0, \beta_1, \ldots, \beta_{N-1}\}$ to be the N-selective MRC RAKE combining weights. Then

$$|y(n)| < \left(\sum_{q=0}^{N-1} |\beta_q| \right) \left(\sum_{l=1}^{\left\lfloor \frac{L}{M} \right\rfloor} \left| \alpha_l^{(m)} \right| \right) \tag{4.24}$$

$$E[|y(n)|^2] < \left(\left(\sum_{q=0}^{N-1} |\beta_q| \right) \left(\sum_{l=1}^{\left\lfloor \frac{L}{M} \right\rfloor} \left| \alpha_l^{(m)} \right| \right) \right)^2 \tag{4.25}$$

$$\lambda_{\max} < (2K+1) \left(\left(\sum_{q=0}^{N-1} |\beta_q| \right) \left(\sum_{l=1}^{\left\lfloor \frac{L}{M} \right\rfloor} \left| \alpha_l^{(m)} \right| \right) \right)^2 \tag{4.26}$$

So the step-size parameter μ can be chosen as:

$$\mu = \frac{2}{(2K+1) \left(\left(\sum_{q=0}^{N-1} |\beta_q| \right) \left(\sum_{l=1}^{\left\lfloor \frac{L}{M} \right\rfloor} \left| \alpha_l^{(m)} \right| \right) \right)^2} \tag{4.27}$$

Then the condition in Eq.4.16 is satisfied. Here $\{\beta_q\}$ and $\{\alpha_l\}$ can all be obtained directly from the channel estimation.

The receiver structure described above is shown in Figure 4-6. The step-size

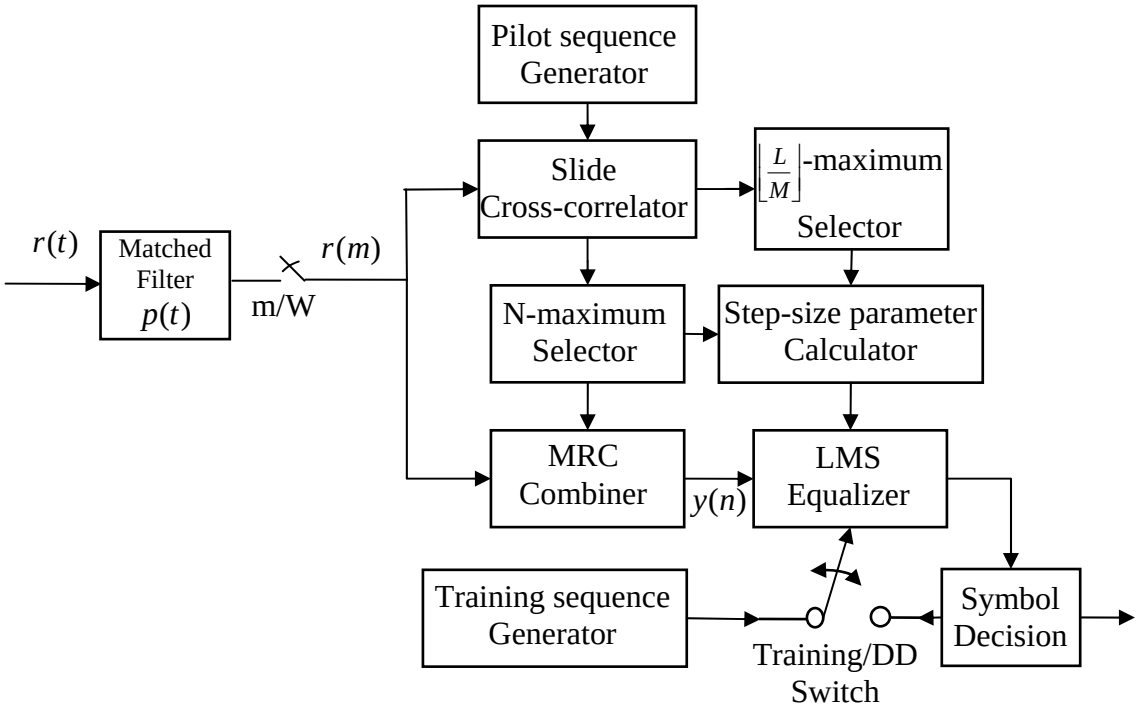

Figure 4-6: N-selective MRC RAKE receiver with LMS adaptive equalizer

parameter calculator calculates the step size parameter according to Eq.4.25. The training sequence generator generates the same training sequence as in the transmitter. During the training period, using the training sequence, the LMS equalizer adjusts the equalizer tap weights. After the training period, the LMS equalizer acts as a linear filter to suppress ISI and continuously adjust the equalizer tap weights using the receiver decisions.

4.6 N-selective RAKE receiver with LMS adaptive combiner

It is well known that the maximum-likelihood (ML) sequence detection is the optimal method in the presence of ISI. Since computational complexity grows exponentially with channel length, most channels of practical interest require too much computation for ML sequence detection to be feasible. Consequently, system designers typically resort to suboptimal schemes such as equalization techniques to compensate for ISI. The N-selective RAKE receiver with LMS adaptive equalizer schemes in Section 4.5 belongs to this type of solutions. A linear equalizer (strictly LMS adaptive equalizer is not a linear algorithm, but having a similar structure as the linear FIR filter except the feedback) and a RAKE demodulator are structurally quite similar, as both are linear combiners. Furthermore, an equalizer attempts to suppress ISI by minimizing metrics as MSE, while a MRC-RAKE ignores ISI and attempts to gather signal energy to maximize the SNR. The combination of these two, a RAKE demodulation structure where the combining weights are chosen to minimize MSE, thereby arrives at a RAKE that finds an optimal balance between the goals of gathering multi-path signal energy effectively and suppressing ISI.

The pulse $p(t)$ -matched filter's sampling output can be expressed as:

$$r(m) = \sum_{i=-\infty}^{+\infty} s_i \sum_{l=0}^{L-1} \alpha_l \delta(m - l - iTW) + \hat{w}(m) \tag{4.28}$$

where

$$\hat{w}(m) = \hat{w}(m/W) \tag{4.29}$$

and

$$\hat{w}(t) = \int_{-\infty}^{\infty} w(\tau) p(-t + \tau) d\tau \tag{4.30}$$

The RAKE's weights and their respective delay can be expressed as:

$$f(m) = \sum_{q=0}^{N-1} \beta_q \delta(m - \theta_q) \tag{4.31}$$

where β_q and θ_q are the weights and fingers delays respectively and $\theta_q \in [0, L-1]$ is an integer. Then output of the RAKE is

$$\begin{aligned} y(n) &= \sum_{q=0}^{N-1} \beta_q \delta(m - \theta_q - nTW) \sum_m r(m) \\ &= \sum_{q=0}^{N-1} \beta_q r(\theta_q + nTW) \\ &= \sum_{q=0}^{N-1} \beta_q \sum_{i=-\infty}^{+\infty} s_i \sum_{l=0}^{L-1} \alpha_l \delta(nTW + \theta_q - iTW - l) + \tilde{w}(n) \end{aligned} \tag{4.32}$$

where

$$\tilde{w}(n) = \sum_{q=0}^{N-1} \beta_q \hat{w}(\theta_q + nTW) \tag{4.33}$$

Here define

$$C_w = \begin{bmatrix} \beta_0 & \beta_1 & \cdots & \beta_{N-1} \end{bmatrix} \tag{4.34}$$

to be the vector of N-selective RAKE combining weights. Define $\Psi(n) \in R^N$ as:

$$\Psi(n) = \sum_{l=0}^{L-1} \alpha_l \begin{bmatrix} \delta(nTW + \theta_0 - l) \\ \delta(nTW + \theta_1 - l) \\ \vdots \\ \delta(nTW + \theta_{N-1} - l) \end{bmatrix} \tag{4.35}$$

Define $W(n) \in R^N$ as:

$$W(n) = \begin{bmatrix} \hat{w}(nTW + \theta_0) \\ \hat{w}(nTW + \theta_1) \\ \vdots \\ \hat{w}(nTW + \theta_{N-1}) \end{bmatrix} \tag{4.36}$$

Then the $y(n)$ can be expressed as:

$$y(n) = \sum_{i=-\infty}^{+\infty} s_i C_w \Psi(n-i) + C_w W(n) \tag{4.37}$$

The mean square error (MSE) of the system is given as:

$$J = E[|Gs_n - y(n)|^2] \tag{4.38}$$

where G is a constant gain. Because here every value is real number, this MSE can be expressed as:

$$J = E[(Gs_n)^2] - 2E[Gs_n y(n)] + E[y(n)^2] \tag{4.39}$$

Then every component in (4-30) is to be calculated:

$$E[(Gs_n)^2] = G^2 \sigma_s{}^2 \tag{4.40}$$

where $\sigma_s{}^2$ is the power of source symbols.

$$E[Gs_n y(n)]] = G\sigma_s{}^2 C_w \Psi(0) \tag{4.41}$$

in which it is assumed that data symbols s_n are uncorrelated mutually and $\hat{w}(t)$ is uncorrelated with data symbols s_n

$$E[y(n)^2] = \sum_{i=-\infty}^{\infty} \sigma_s{}^2 C_w \Psi(i) \Psi^T(i) C_w{}^T + C_w E[W(n) W^T(n)] C_w{}^T \tag{4.42}$$

Then Eq.4.37 can be finally expressed as:

$$J = G^2 \sigma_s{}^2 - 2G\sigma_s{}^2 C_w \Psi(0) + C_w \left(\sum_{i=-\infty}^{\infty} \sigma_s{}^2 \Psi(i) \Psi^T(i) + E[W(n) W^T(n)] \right) C_w{}^T \tag{4-43}$$

It is very clear from Eq.4.41 that J is in a quadratic form of C_w, and hence there exists an optimal value of C_w to minimize J. Here stochastic gradient approach can be used to adaptively find this optimal C_w. So in the sense of MSE,

there exits an optimal combining weight in the case of ISI. LMS algorithm can be used to adaptively find this value.

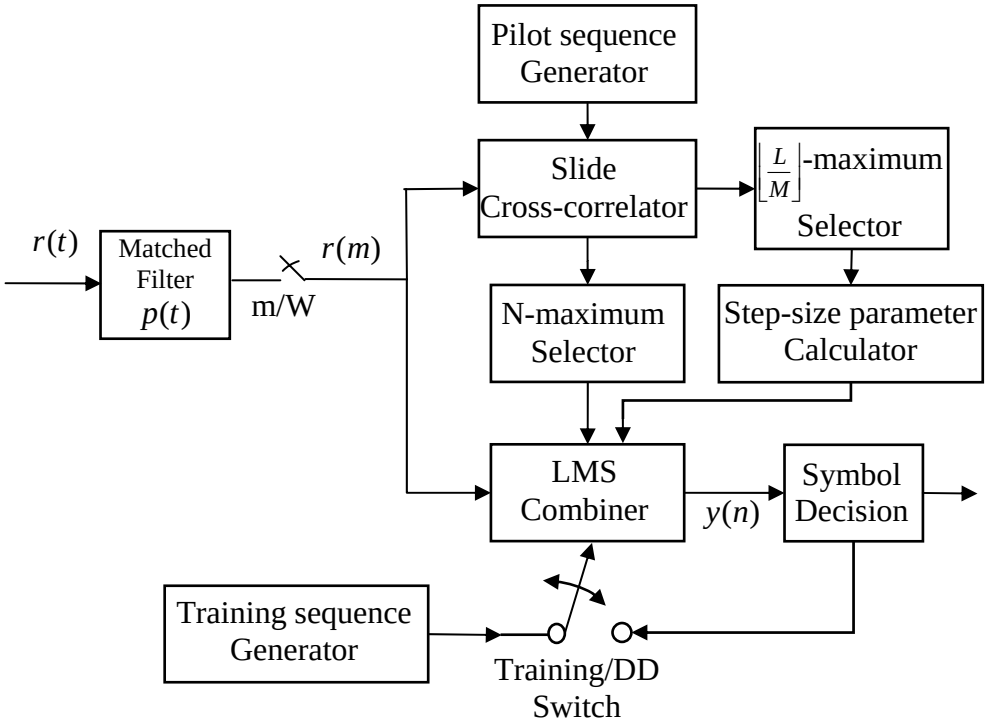

Figure 4-7: N-selective RAKE receiver with LMS adaptive combiner

A similar method described in Section 4.5 can be used to calculate the step-size parameter μ .

$$\mu = \frac{2}{N\left(\sum_{l=1}^{\lfloor \frac{L}{M} \rfloor} \left|\alpha_l^{(m)}\right|\right)^2} \tag{4. 44}$$

An implementation of the receiver structure described above is shown in Figure 4.7. The step-size parameter calculator calculates the step size parameter according to Eq.4.42. The LMS combiner gets initial combining parameters from the N-

maximum selector and implements diversity combining operation. Training sequence generator generates training sequence the same as in the transmitter. During training period, the LMS combiner adjusts the combining tap weights by using the training sequence. After training period, the LMS combiner adjusts combining parameters using the symbol decision results.

Chapter 5 Simulation Set-up and Results

In this chapter, first simulation set-up is described and then simulation results are provided. The chapter ends with the analysis and discussion of simulations and their results.

5.1 Simulation set-up

A personal computer equipped with MATLAB Simulink® was used as a platform for simulation. The block diagram of the simulation is shown in Figure 5-1 below.

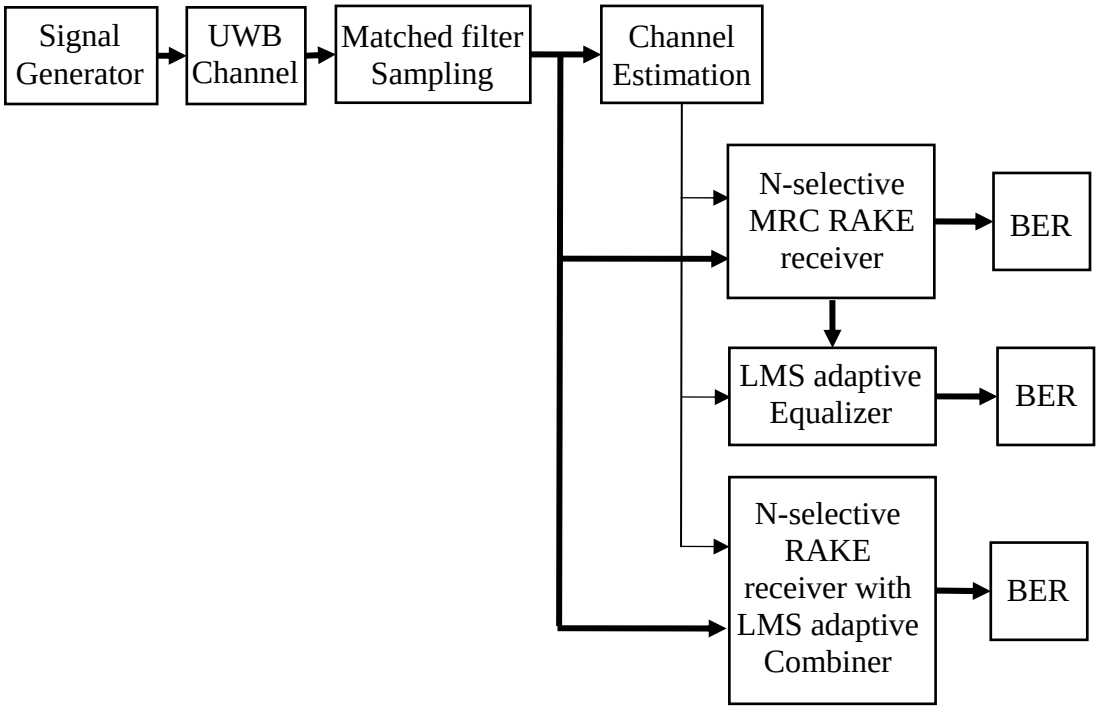

Figure 5-1: Block diagram of simulation

The detailed information of each block in Figure 5-1 is described in the following sectionss.

5.1.1 Signal generator

Functions of the signal generator include generating a pilot sequence for channel estimation, generating a training sequence for the LMS algorithm, generating the information sequence and modulating the data.

The pilot sequence for channel estimation must be large enough to guarantee adequate estimation accuracy. The sequence must have good autocorrelation properties. Here the most commonly used binary maximum-length shift-register pseudo-noise (PN) sequence was used [13].

The training sequence and the information sequence were the same random sequence (1 or -1) with the same probabilities.

Followings are some of the modulation parameters:

- The symbol time T is 8 ns and the bit rate is125 Mbps.
- The transmitted pulse p(t) is Gaussian mono-pulse with 1 GHz bandwidth.
- The modulation format is direct-sequence spread-spectrum ultra wideband with 4 pulses every symbol.

The Simulink® block diagram of the signal generator is shown in Figure 5-2. The Gaussian pulse generator generates a Gaussian mono-pulse p(t) and then generates a direct-sequence spread-spectrum pulse train symbol signal. The PN sequence generator generates a pilot sequence. The Bernoulli binary generator generates training sequence and information sequence. The three switch blocks are for timing control. The output 1 is the normal output and the output 2 is the reference signal to be used to calculate bit error rate.

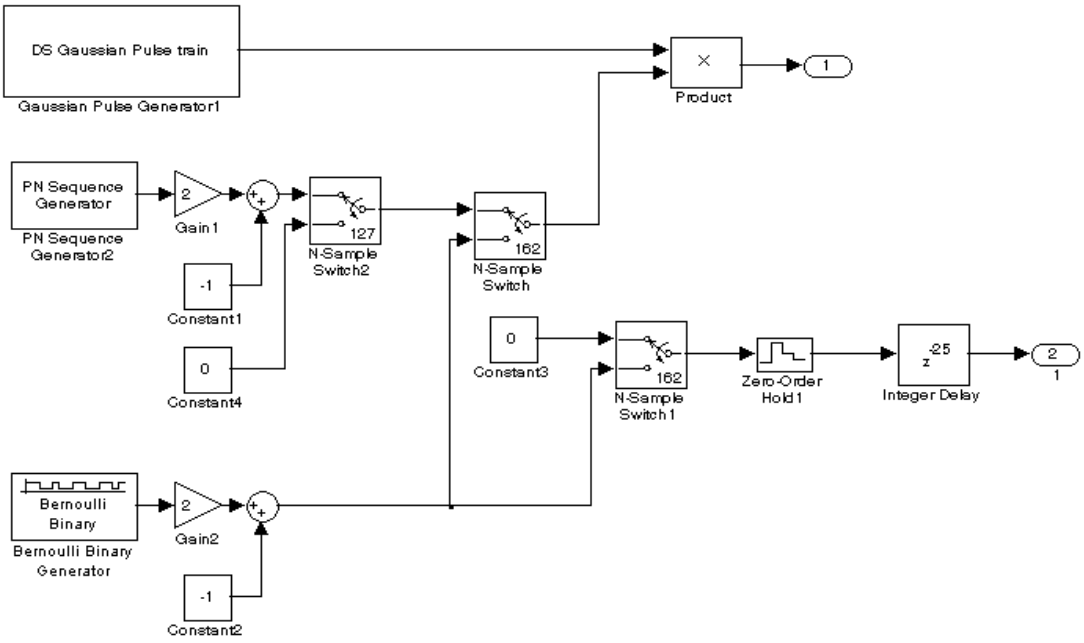

Figure 5-2: Simulink® block diagram of the signal generator

5.1.2 UWB channel

Functions of the UWB channel are simulating the UWB indoor dense multi-path channel with the channel impulse response calculated based on the UWB channel models from IEEE P802.15. This block also adds white Gaussian noise.

Block diagram of the UWB channel is shown in Figure 5-3. There are two blocks: the UWB multi-path channel (i.e. CM1-CM4 of IEEE P802.15) and the AWGN.

In Simulink® there is no block to be used for the UWB multi-path channel. Here S-functions (system-functions) are used to construct this UWB multi-path channel block. S-functions provide a powerful mechanism to extend the capabilities of Simulink®. S-functions allow the user to add custom built blocks to Simulink models.

According to the analysis in Section 4.2, the resolution of the UWB channel multi-path delay profile is 1/W. In simulation, since the signal bandwidth is 1 GHz, the multi-path resolution of the UWB multi-path channel is 1 ns.

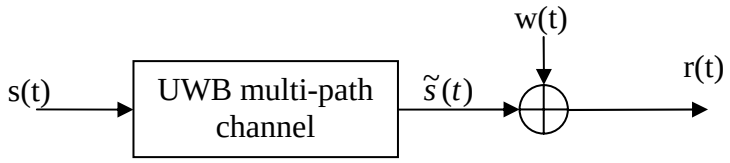

Figure 5-3: Block diagram of UWB channel

When how much noise was decided to add, the signal energy of $\tilde{s}(t)$ is required to be known prior. Normally, there is an assumption that when a signal passes through a multi-path channel, the energy of the signal will not change. But this is different from the UWB channel models in IEEE P802.15, when the signal passes through the channel, its energy is reduced. If this reduction has a fixed relation then the energy of $\tilde{s}(t)$ can be calculated based on the energy of s(t). If only one realization of the UWB multi-path channel is used in simulation, then the reduction is definitely a fixed relation. But for the accuracy of simulation, a sufficient larger number of channel realizations ought to be used. Every time the simulation was run, a channel realization is calculated and used in the run. Although using the same channel model defined with the same statistical parameters, the channel realization of every simulation is generated randomly by using the same statistical parameters. So the exact relation of this change cannot be obtained. The solution is using an average value of the signal energy of $\tilde{s}(t)$. Here, 100 realizations of one channel

model were calculated and then this average signal energy of $\tilde{s}(t)$ was used in simulation to decide how much noise to be added.

5.1.3 Matched filter sampling and channel estimation

The first processing unit in the receiver is the matched filter sampling. This block generates the pulse template signal, implements matched filter function and finally samples the output of the matched filter. The sampling rate is fixed at 1GHz. In practical environment, distortions from the air transmission and analog front end of the receiver cause variation of the pulse shape. When this variation is small, it can be neglected and the pulse template signal of matched filter can be generated as same as the pulse shape of the transmitter. When this variation is large, some methods must be used to compensate this effect. The focus of this research is studying the algorithm and receiver structure to improve the performance of system in UWB multi-path channel and combat the ISI. So here in this simulation, these distortions are neglected. The pulse template in matched filter is the same as the one in the transmitter.

The channel estimation block generates the pilot sequence the same as in the transmitter, fulfills the sliding correlation channel estimation algorithm and finally selects N maximum finger values.

Synchronization between the transmitter and the receiver is not considered in this simulation. The receiver and the transmitter use the same time base as they are in perfect synchronization.

M-file S-functions are written to implement the matched filter and the channel estimation blocks.

5.1.4 N-selective MRC RAKE receiver and LMS adaptive equalizer

The Simulink® block diagram of N-selective MRC RAKE receiver and LMS adaptive equalizer is shown in Figure 5-4.

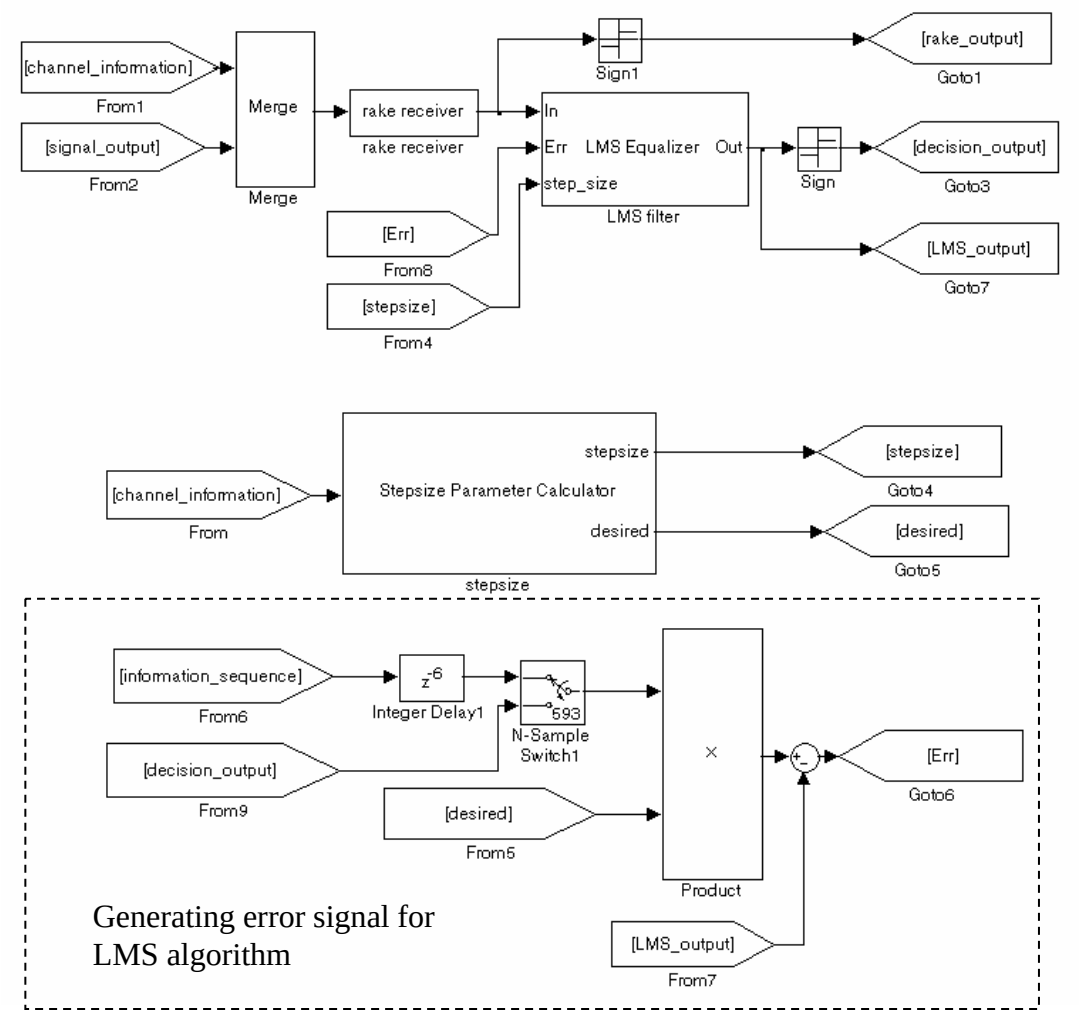

Figure 5-4: Simulink® block diagram of N-selective MRC RAKE receiver and LMS adaptive equalizer

In Figure 5-4, channel_information is the output of the channel estimation block; signal_output is the matched filter sampled output; information_sequence is the training sequence. These are three input signals. The RAKE receiver implements

the N-selective MRC RAKE receiving and its output is passed to the LMS equalizer. The step-size parameter calculator generates the step-size parameter and the desired value for the LMS equalizer. The parts in the dashed boundary area generate the error signal for the LMS algorithm based on the training sequence or the DD method. The RAKE receiver block, LMS equalizer block and the step-size parameter calculator block in Figure 5-4 are all implemented with the M-file S-functions. The rake_output is the system output without equalizer and the decision_output is the system output with equalizer.

5.1.5 N-selective RAKE receiver with LMS adaptive combiner

The Simulink® block diagram of N-selective RAKE receiver with LMS adaptive combiner is shown in Figure 5-5.

The difference here from Figure 5-4 is that the N-selective RAKE receiver with LMS adaptive combiner block replaces the N-selective MRC RAKE receiver and the LMS adaptive equalizer. Or in other words, the LMS adaptive combiner takes the place of the maximum ratio combiner (MRC) and the equalizer is not used. The N-selective RAKE receiver with LMS adaptive combiner block in Figure 5-5 implements the RAKE operation and at the same time updates the weighting parameters based on the LMS algorithm.

5.2 Simulation results

UWB channel models used in the simulation are from IEEE P802.15 which consists of four distinct channel models (CM1–CM4). Model CM3 representing a 4-10

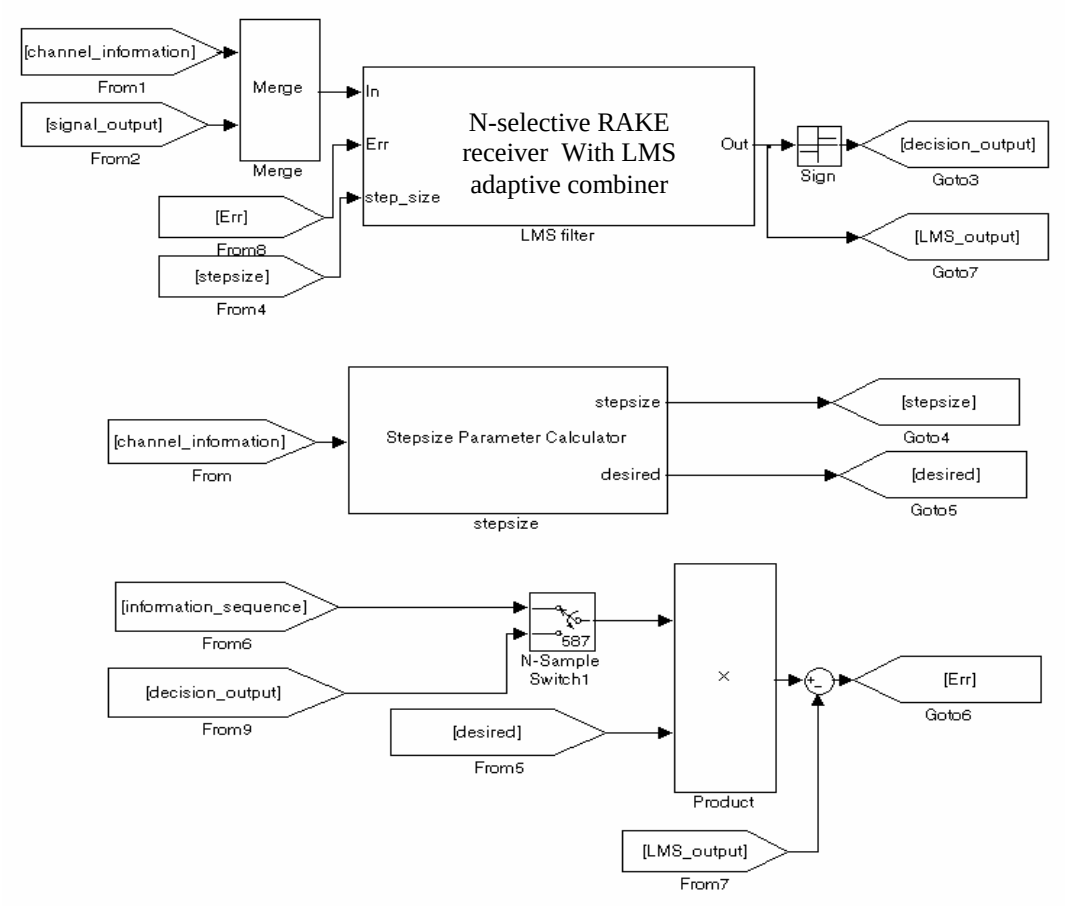

Figure 5-5: Simulink® block diagram of N-selective RAKE receiver with LMS adaptive combiner

meter range and a non line-of-sight channel is the best choice for real indoor communication environments. This channel model was used in the simulations.

According to the discussion about channel estimation in Section 4.3, it is well known that the pilot sequence for channel estimation must be long enough to guarantee adequate estimation accuracy. But in simulations how long would be enough? If it is too long, the estimation accuracy is obtained but the payload of the system is too high. So the optimum value of the length of the pilot sequence must be decided first. Simulations are good methods to test different lengths of the pilot sequence. For simulation accuracy, 100 channel realizations were used in

simulation for each length of the pilot sequence and finally an average value of bit error rate was calculated. The 8-finger MRC RAKE receiver structure was chosen in simulation. The simulation running time for this sample receiver structure was short and the optimal length of pilot sequence was decided by channel no matter what kind of receiver structure was used. Here the binary maximum-length shift-register pseudo-noise (PN) sequence was used. The lengths were 31, 63, 127 and 255 bits. The Es/N0 level was 10 dB. The result of simulation is shown in Figure 5-6.

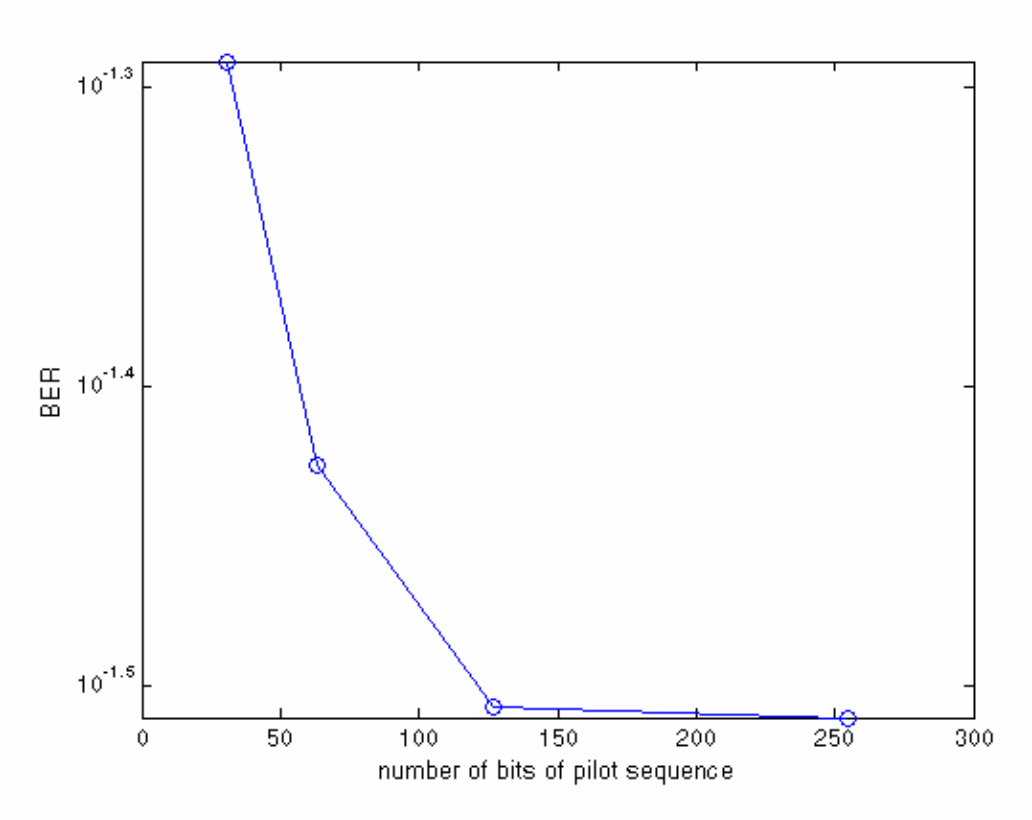

Figure 5-6: The BER for different pilot sequence

From the result it is very clear that between the 31 bits to 127 bits of the pilot sequence, the BER performance has a sharp increase. After 127 bits the BER

performance has almost no improvement as the length of the pilot sequence increased. Therefore a pilot sequence of 127 bits in length was used.

After the length of pilot sequence was decided, three cases of N-selective MRC RAKE receiver structures (N= 8, 16, 32) were simulated. The simulation results and curves fitted to them are shown in Figure 5-7.

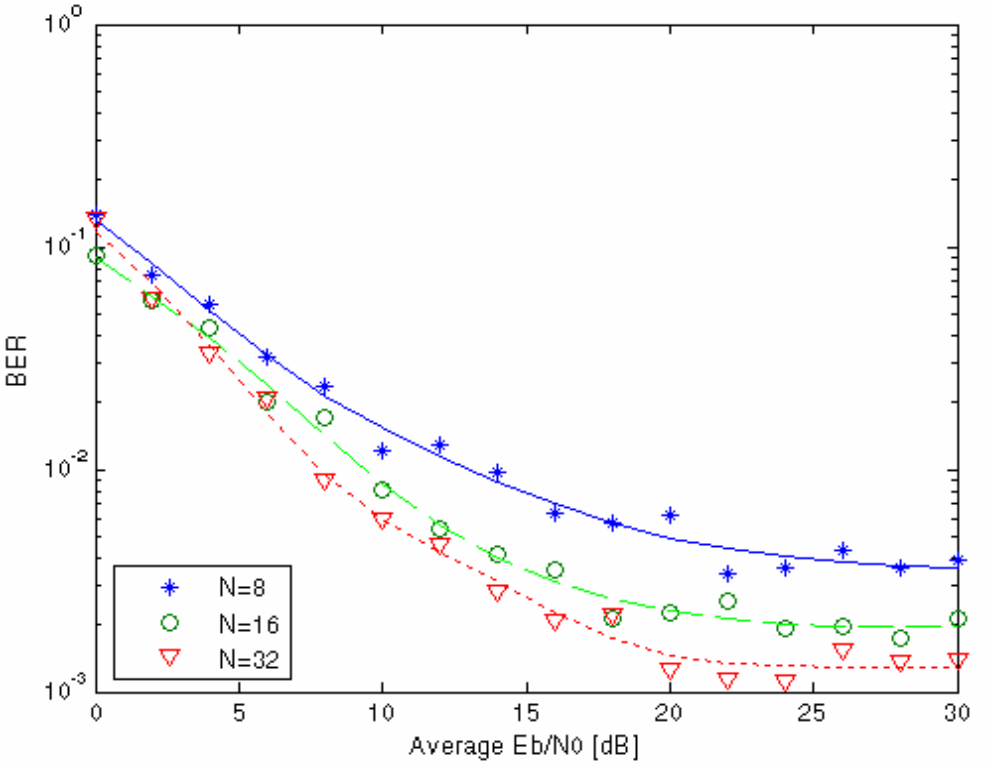

Figure 5-7: The BER for N-selective MRC RAKE receiver structures

Before simulating the LMS adaptive equalizer, some parameters must be obtained. The first one is the number of stages of the LMS equalizer. There still ought to be an optimum balance between the performance and complexity of the system. Simulations were used to test the equalizers with different number of stages. The index for comparing is the system bit error rate. For simulation

accuracy, 100 channel realizations were used in simulation for every number of stages and finally an average value of bit error rate is obtained. The 8-finger MRC RAKE receiver structure was chosen in this simulation. The Es/N0 level was 20 dB. For low Es/N0 level, the equalizer effect is not obvious. The result of the simulation is shown in Figure 5-8.

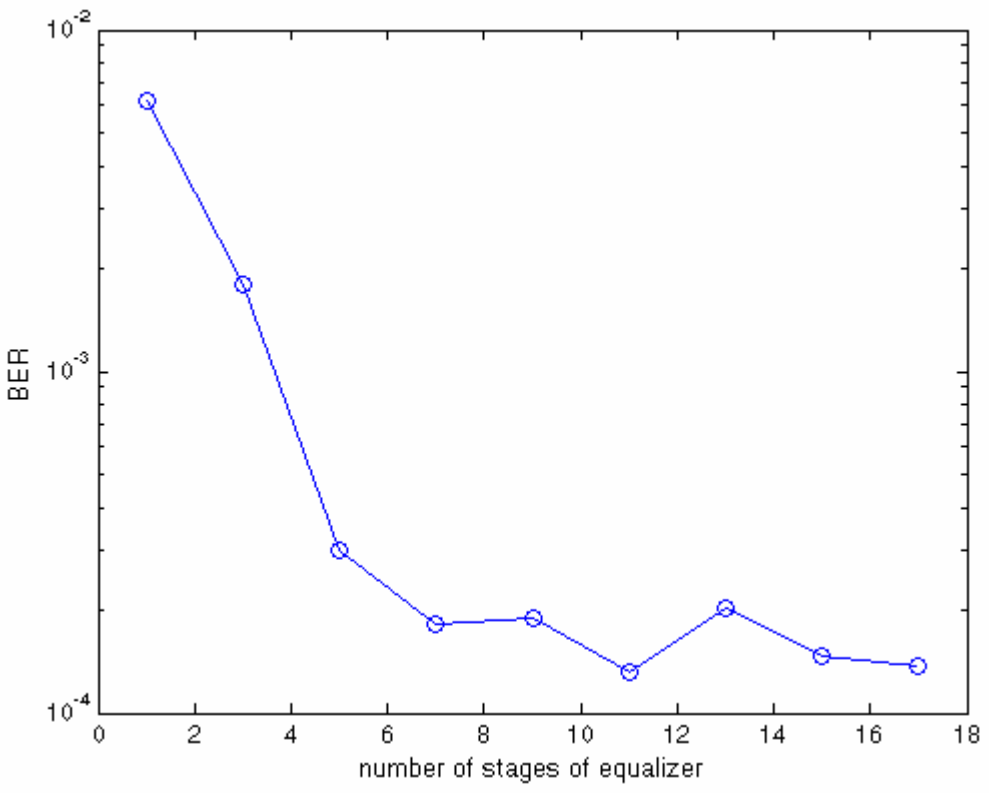

Figure 5-8: The BER for LMS equalizers with different stages

From Figure 5-8 it is very clear that system performance does not always increase with the number of stages of the LMS equalizer. The LMS equalizer with 11 stages is a reasonable choice for a good balance between performance and complexity of the system.

The second parameter which must be decided before simulating the LMS adaptive equalizer and the N-selective RAKE receiver with LMS adaptive combiner is the length of the training sequence. This goal is also pursued by using simulation. In this simulation the information sequence was used as a training sequence and the system did not switch to DD mode. The error signal of the LMS algorithm was recorded. According to the discussion of the LMS algorithm in Chapter 3, as the LMS algorithm approaches the optimum point step by step, the error signal decreases continuously and final when arriving optimum point the error signal will stop to decrease and stay at this value with a small fluctuation. By observing the error signals the optimum length of training sequence can be obtained. For the simulation accuracy, 100 simulations for every tap of receiver structures were run and the final result was the average value. The Es/N0 level was set at 20 dB.

Based on the results of simulations shown in Figure 5-9 and Figure 5-10, the length 400 of the training sequence for 8-selective MRC RAKE receiver with LMS adaptive equalizer and 8-selective RAKE receiver with LMS adaptive combiner was chosen.

Based on the results of simulations shown in Figure 5-11 and Figure 5-12, the length 600 of the training sequence for 16-selective MRC RAKE receiver with LMS adaptive equalizer and 16-selective RAKE receiver with LMS adaptive combiner was chosen.

Based on the results of simulations shown in Figure 5-13 and Figure 5-14, the length 800 of the training sequence for 32-selective MRC RAKE receiver with

LMS adaptive equalizer and 32-selective RAKE receiver with LMS adaptive combiner was chosen.

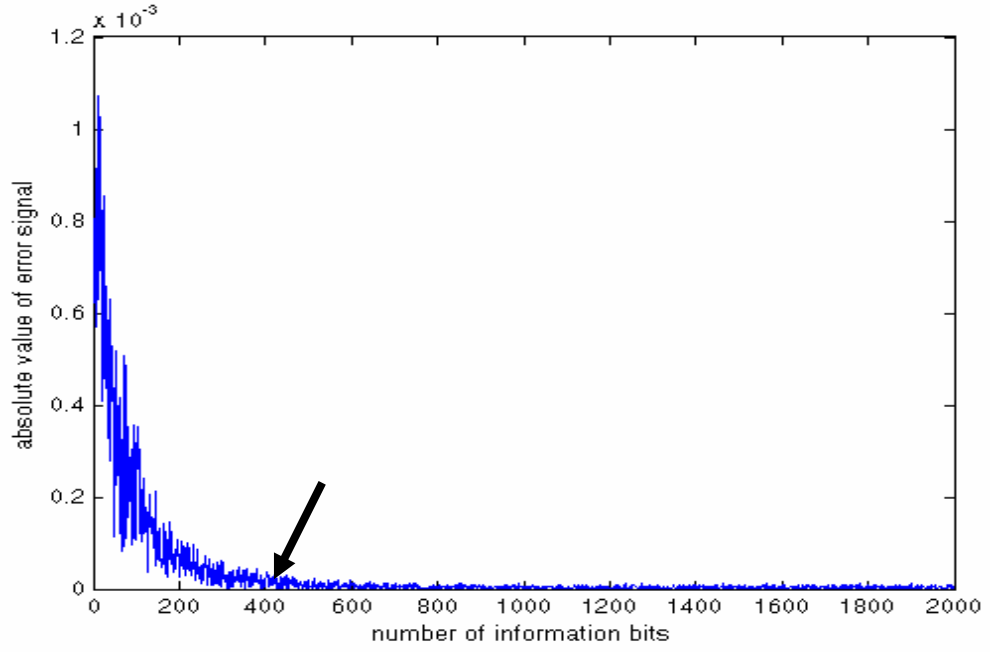

Figure 5-9: The error signal for 8-selective MRC RAKE receiver with LMS adaptive equalizer

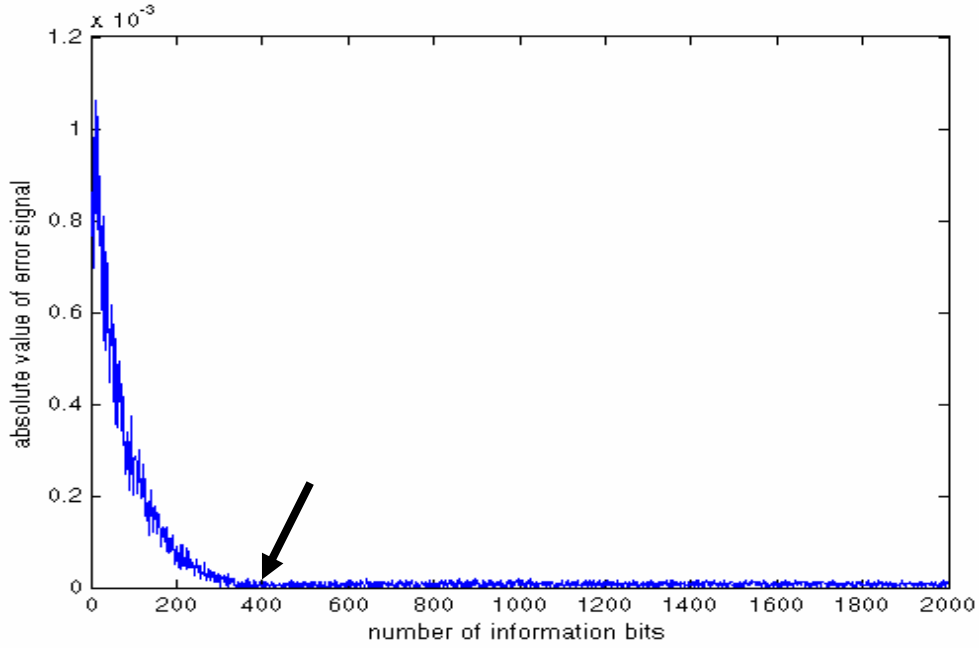

Figure 5-10: The error signal for 8-selective RAKE receiver with LMS adaptive combiner

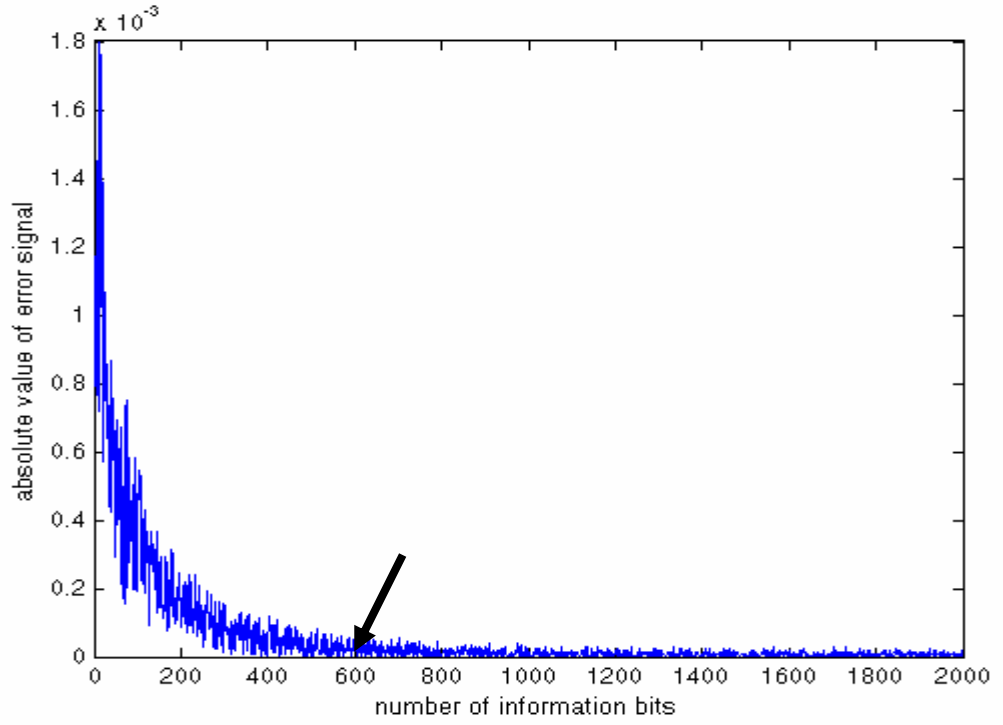

Figure 5-11: The error signal for 16-selective MRC RAKE receiver with LMS adaptive equalizer

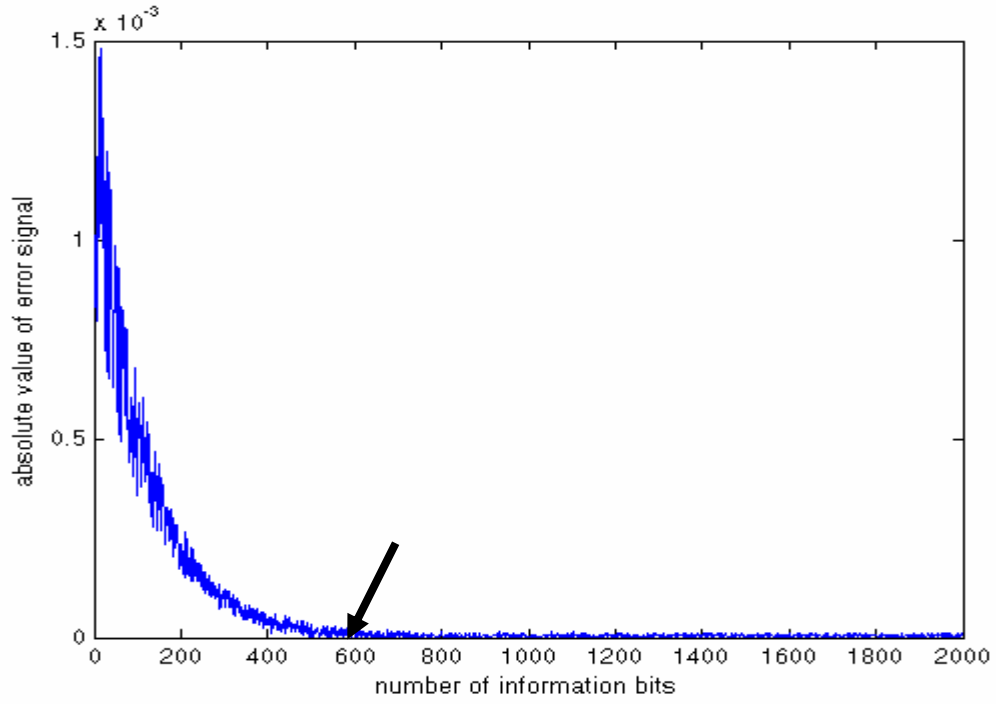

Figure 5-12: The error signal for 16-selective RAKE receiver with LMS adaptive combiner

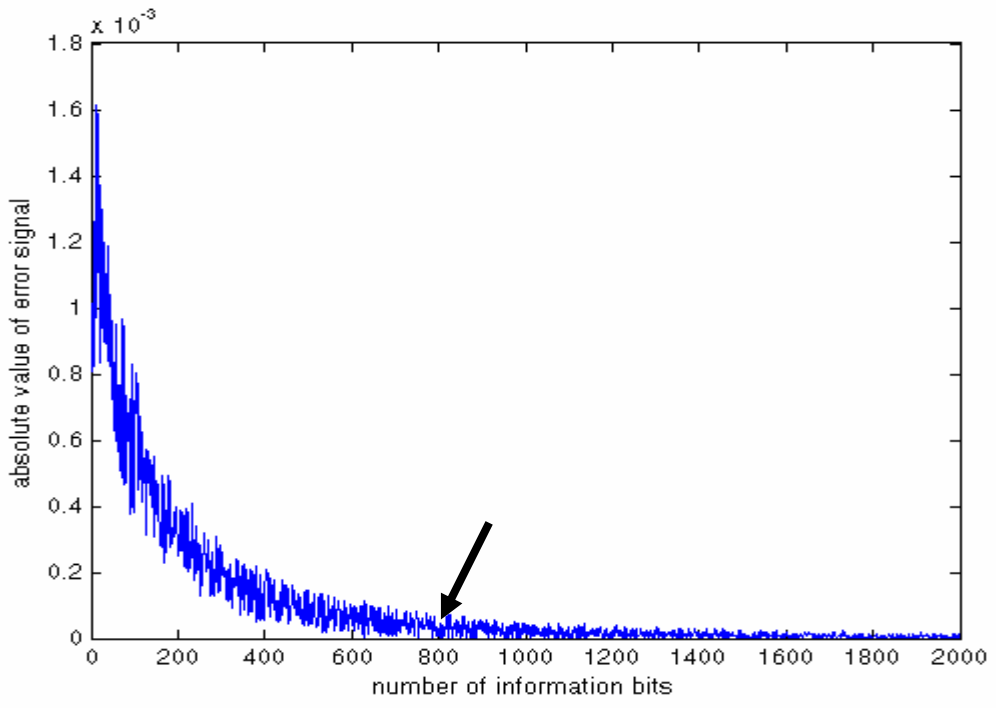

Figure 5-13: The error signal for 32-selective MRC RAKE receiver with LMS adaptive equalizer

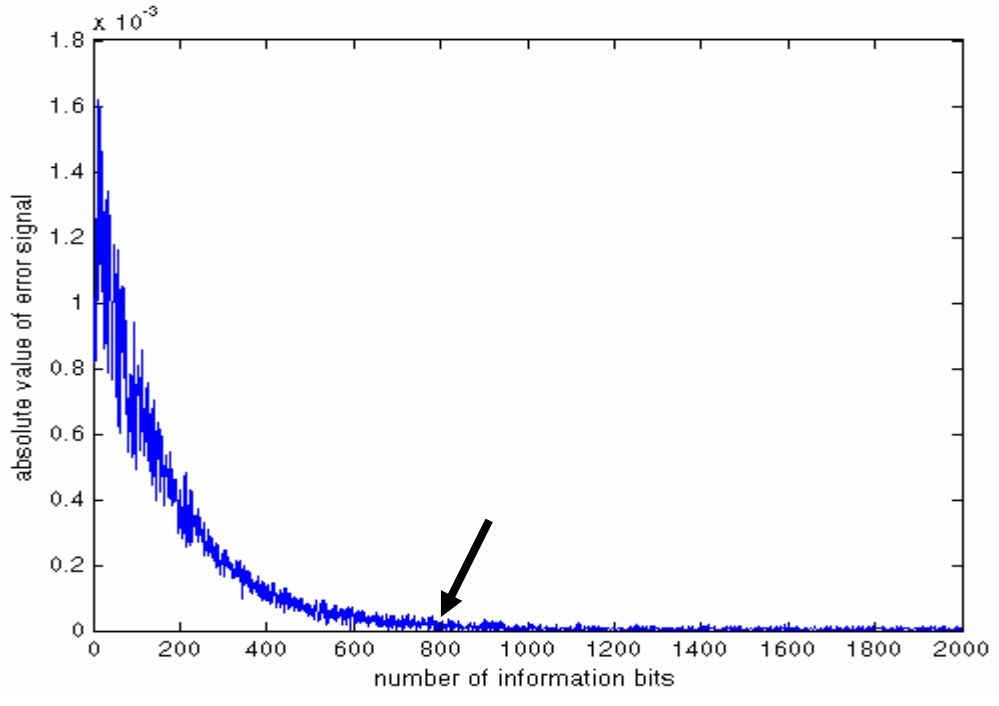

Figure 5-14: The error signal for 32-selective RAKE receiver with LMS adaptive combiner

Table 5-1: The Parameters of different receiver structures

Different receiver structures	**8E**	**8C**	**16E**	**16C**	**32E**	**32C**
Length of pilot sequence	127	127	127	127	127	127
Number of equalizer stages	11	N/A	11	N/A	11	N/A
Length of training sequence	400	400	600	600	800	800
Calculation complexity of processing one information bit	19 ⊗ 29 ⊕	8 ⊗ 16 ⊕	27 ⊗ 37 ⊕	16 ⊗ 32 ⊕	43 ⊗ 53 ⊕	32 ⊗ 64 ⊕

8E: 8-selective RAKE receiver with LMS adaptive equalizer.

8C: 8-selective RAKE receiver with LMS adaptive combiner.

16E: 16-selective RAKE receiver with LMS adaptive equalizer.

16C: 16-selective RAKE receiver with LMS adaptive combiner.

32E: 32-selective RAKE receiver with LMS adaptive equalizer.

32C: 32-selective RAKE receiver with LMS adaptive combiner.

⊗ : multiply operation.

⊕ : add operation.

Like the simulations of the N-selective MRC RAKE receiver structure, three cases of N-selective MRC RAKE receiver with LMS adaptive equalizer and N-selective RAKE receiver with LMS adaptive combiner (N= 8, 16, 32) were simulated.

When the calculation complexity is compared between the N-selective MRC RAKE receiver with LMS adaptive equalizer and the N-selective RAKE receiver

with LMS adaptive combiner, only the different parts will be considered not the

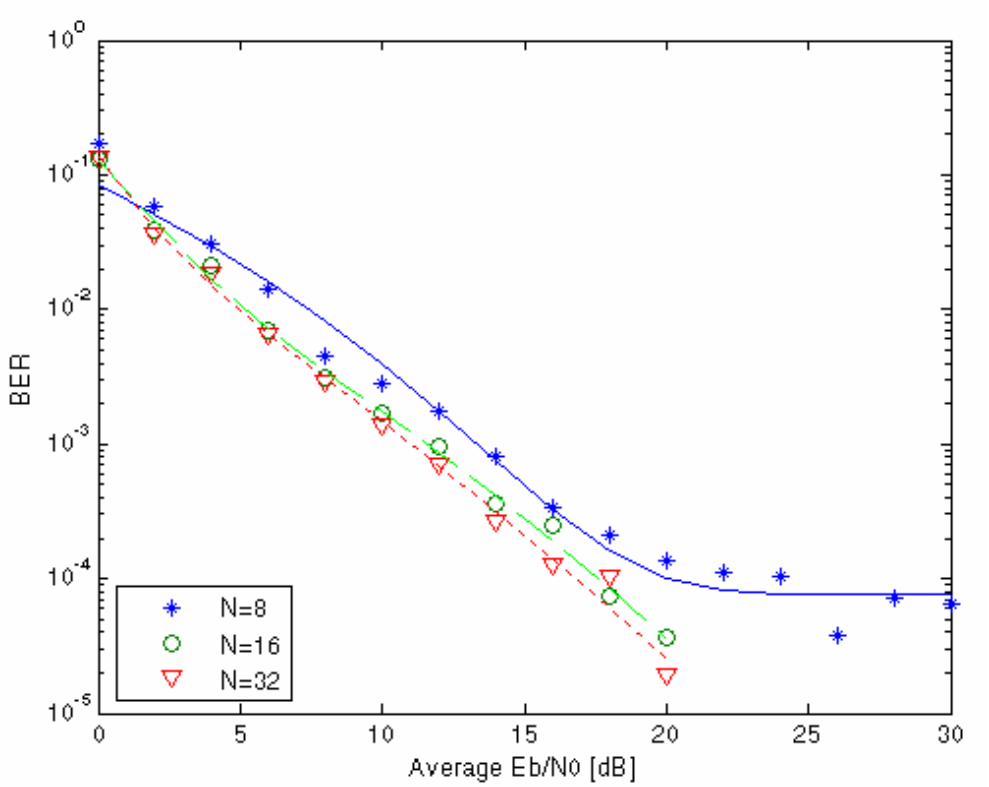

Figure 5-15: The BER for N-selective MRC RAKE receiver with LMS adaptive equalizer

common parts like matched filter, sampling, channel estimation, symbol decision etc. According to the RAKE MRC combining operation and LMS algorithm expressed in equations (4.11), (4.13), (4.14) and (4.15), the calculation for processing one information bit is: N-selective MRC RAKE receiver with LMS adaptive equalizer include N+11 multiply operations, 1 sum operation of N real numbers (equally N-1 add operations), 1 sum operation of 11 real numbers (10 add operations) and 1+11 add operations; N-selective RAKE receiver with LMS adaptive combiner include N multiply operations, 1 sum operation of N real

numbers (N-1 add operations) and 1+N add operations. The summary of parameters and calculation complexity is listed in Table 4.

The BER simulation results and curves fitted to them are shown in Figure 5-15 and Figure 5-16.

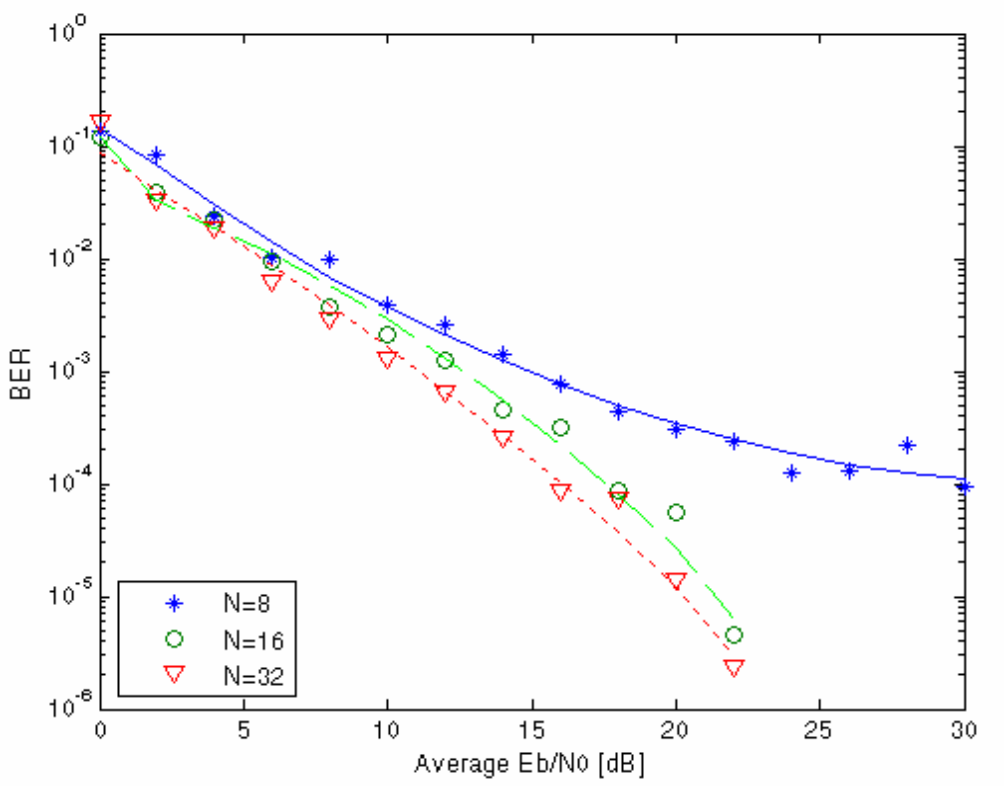

Figure 5-16: The BER for N-selective RAKE receiver with LMS adaptive combiner

5.3 Analysis and discussion

For the three cases of N-selective MRC RAKE receiver structures (N= 8, 16, 32), the result of the simulation is shown in Figure 5-17. System performance increases proportionally to N; this coincides with discussions in Chapter 3 on the RAKE receiver. When N increases, the receiver captures more signal energy leading to the decrease in BER. In another aspect, it is well known that BER will decrease as the

level of SNR or Es/N0 increase. From this simulation result, this is true when Es/N0 level is less than 20dB. However system performance does not improve when Es/N0 level is higher than 20dB. This can be explained as follows: The bit error rate is mainly determined by the ratio of the desired signal energy to the energy of any other interference signal. When Es/N0 level is less than 20dB, the main part of the interference signal is from noise signal. When the Es/N0 level increases, the ratio of the desired signal energy to the energy of any other interference signal increases leading to the decrease in BER. When the Es/N0 level is larger than 20dB, a large portion of the interference signal is from ISI. So the numerator and the denominator of this ratio will increase as Es/N0 level increases and the result is that this ratio almost has little change. This explanation can also be demonstrated by the simulation result shown in Figure 5-15 and Figure 5-16 because the N-selective MRC RAKE receiver with LMS adaptive equalizer and the N-selective RAKE receiver with LMS adaptive combiner both have some mechanism to suppress the ISI. Another significant outcome is that when the Es/N0 level is lower than 15dB, increasing N does not show an obvious performance improvement in BER. This exists particularly for 16-selective and 32-selective MRC RAKE receivers with LMS adaptive equalizer. It is also can be observed that the cases of N=16 and N=32 looks more promising to combat ISI than the case of N=8 when Es/N0 level is larger than 15dB. For the simulation result shown in Figure 5-8, the number of stages of the equalizer is 1 which means the system does not have an equalizer. The improvement is very obvious when the number of stages of the equalizer is 11.

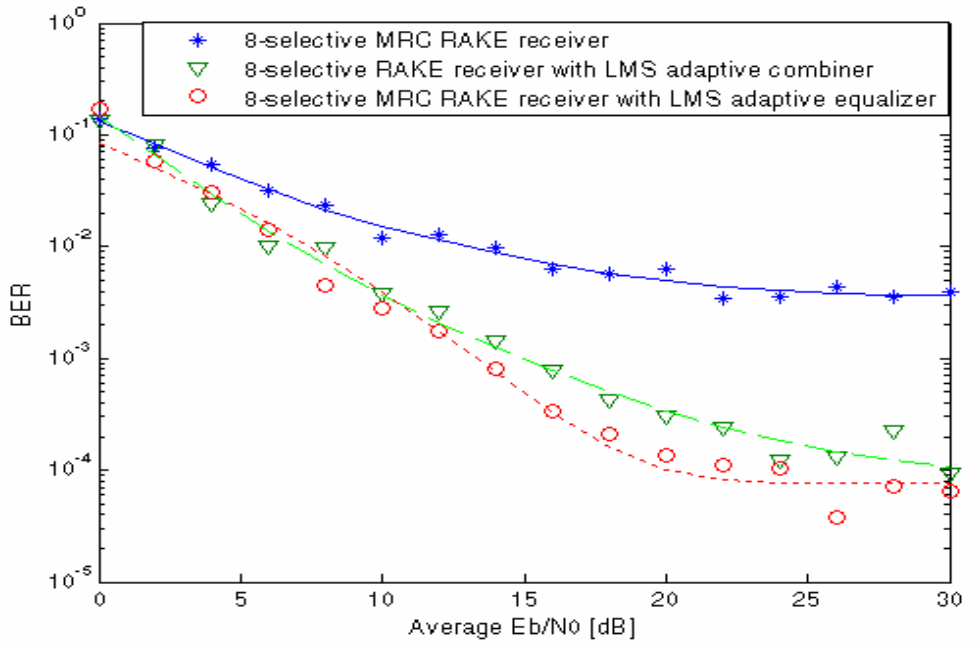

Figure 5-17: The BER for three different receiver structures with N=8

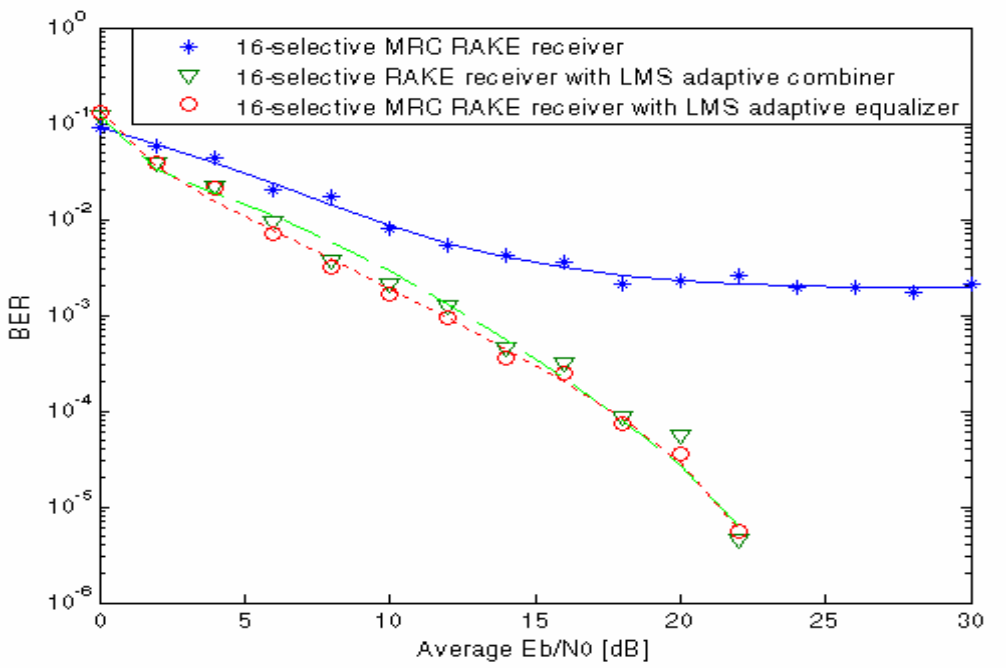

Figure 5-18: The BER for three different receiver structures with N=16

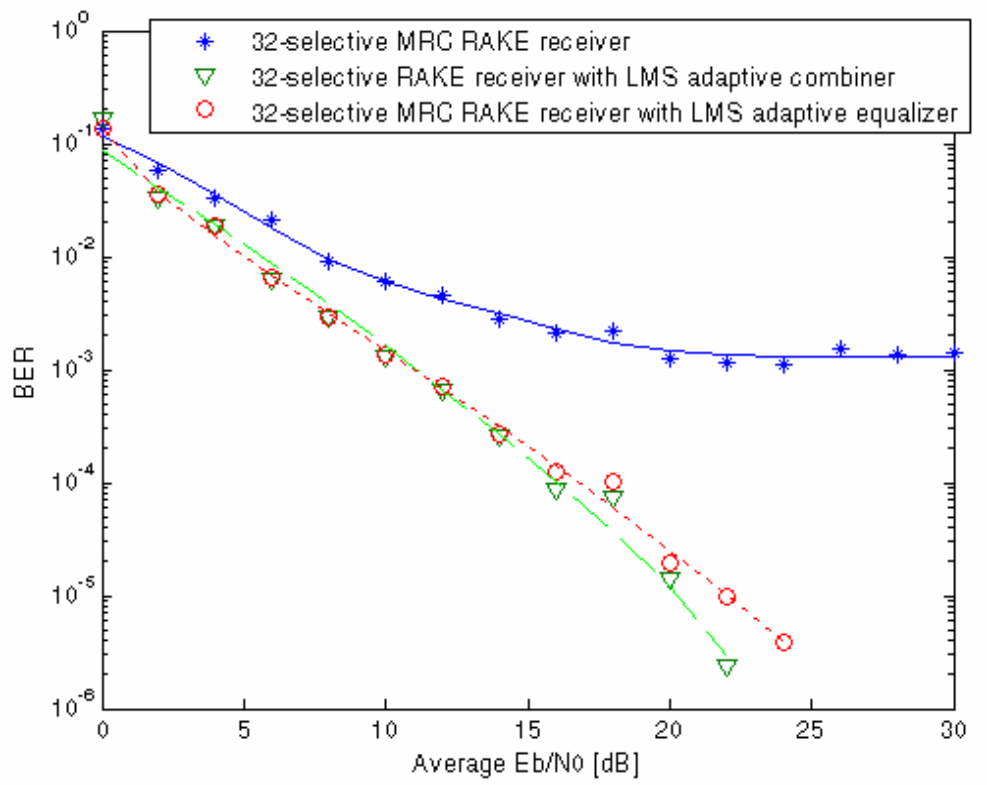

Figure 5-19: The BER for three different receiver structures with N=32

From the simulation results shown in Figure 5-17 to Figure 5-19, it is very clear that both the N-selective MRC RAKE receiver with LMS adaptive equalizer and the N-selective RAKE receiver with LMS adaptive combiner effectively suppress ISI and significantly improve system performance.

When either the LMS adaptive equalizer or LMS adaptive combiner is used to combat ISI, case N=16 obtains higher system performance improvement than the case N=8. The case N=32 does not obtain obvious system performance improvement over the case N=16 although the calculation complexity and the length of training sequence both are increased. The calculation complexity and the lengths of training sequence of different receiver structures are summarized in Table 4. For N=16, the LMS adaptive combiner and the LMS adaptive equalizer

both achieved almost same system performances. But the LMS adaptive combiner has simpler computation complexity. The case N=16 shows the best balance between performance, computation complexity and length of training sequence.

Chapter 6 Conclusions and Future Work

This chapter presents conclusions of the work that was accomplished in this thesis. Some topics for future work to continue the research in this area are also discussed.

6.1 Conclusions

Ultra wideband (UWB) technology has been proposed recently for use in wireless personal area networks. After gaining regulatory approval, the technology has moved from academic research topics into the mainstream of telecommunications. UWB is a suitable solution for high speed indoor wireless communications due to its promising ability to provide high data rate at low cost and low power consumption. Another benefit of UWB is its ability to resolve individual multi-path components. This feature motivates the use of RAKE multi-path combining techniques to provide diversity and capture as much energy as possible of the received signal.

UWB is being considered for use in wireless personal area networks (WPANs), where the required data rate can be as high as 110 Mbps per user. To obtain such a rate with very low power emission, significant inter-symbol interference (ISI) is unavoidable. Some published results on UWB have neglected this problem as most performance analyses employ a RAKE receiver under the assumption that channel delay spreads are much less than the system symbol time. The traditional RAKE receiver structure to collect multi-path energy in UWB systems does not combat ISI very well. There is a need to find effective methods to combat ISI.

In this thesis, three receiver structures were proposed and simulated. The first proposal is the N-selective MRC RAKE receiver structure. This is a mixed analog and digital implementation. The structure takes advantage of the unique characteristics of the UWB signal. The structure not only reduces the high complexity of the traditional analog RAKE demodulation implementation but also avoids the high Nyquist sampling rate in the digital implementation. A very simple and effective channel estimation algorithm (sliding correlation algorithm) is utilized and integrated into this receiver structure smoothly. From simulation results, this proposed receiver structure achieved a reasonable BER performance.

The second proposal is the N-selective MRC RAKE receiver with LMS adaptive equalizer. A LMS adaptive equalizer is added to the N-selective MRC RAKE receiver with the purpose of suppressing ISI. The channel estimation outcome provided by the N-selective MRC RAKE receiver is not very accurate. A fast equalization algorithm is essential in the UWB high speed application environment. This equalization algorithm ought to have the ability to track channel variance. The LMS adaptive equalizer is a good solution for all of these requirements. From simulation results, this proposed receiver structure indeed suppresses ISI effectively and exhibits a high BER performance improvement over the N-selective MRC RAKE receiver.

The third proposal is the N-selective MRC RAKE receiver with LMS adaptive combiner. The LMS adaptive equalizer and the MRC combiner have similar linear combing structure. The combination of these two parts, a RAKE combining structure where the combining weights are chosen to minimize the MSE, thereby

creates a RAKE combining that accomplishes the goals of gathering multi-path signal energy effectively and suppressing ISI simultaneously. The achievement of this new idea is demonstrated by simulation results.

From simulation results, the 16-selective MRC RAKE receiver with LMS adaptive combiner demonstrated the best balance between performance, computation complexity and length of training sequence among three receiver structures.

In summary, based on the proposed N-selective MRC RAKE receiver structures, two new receiver structures for suppressing ISI were proposed. These three receiver structures were all simulated for N=8, 16 and 32. From simulation results, ISI is suppressed effectively by these two new schemes. Due to the simplicity of the algorithm and a 1G Hz sampling rate, the 16-selective MRC RAKE receiver with LMS adaptive combiner is feasible for practical VLSI implementations.

6.2 Future work

In this research, many important issues have not been dealt with, or have been considered with simplified assumptions. Hence, there are some areas in which the work of this thesis can be extended. Some topics for future research following the direction of this thesis are issued here:

- The inter-pulse interference was neglected in the theory derivation in Chapter 4 and was not considered in this thesis. The methods for suppressing this interference could be studied. The scheme of using signal processing technologies

or designing pulse shape with better inter-pulse interference immunity properties could be considered.

- The UWB channel model is a static model and its parameters do not change during simulations. Adding some time-variant properties to the channel model and making it more close to the realistic indoor channel could be considered
- Constructing a hardware test-bed to verify the simulation is also very important and helpful for the future hardware implementation.
- Other adaptive filter algorithms could be considered instead of the LMS algorithm used in this thesis. System performance, computation complexity and difficulty of implementation could be analyzed.

Bibliography

[1] T. W. Barrett, “History of Ultra Wide Band (UWB) Radar & Communications Pioneers and Innovators,” *In Proc. Progress In Electromagnetic Symposium 2000 (PIERS2000)*, Cambridge, MA, July, 2000.

[2] R. J. Fontana, “A Brief History of UWB Communications,” *Multi-Spectral Solutions Inc.*.

[3] Federal Communications Commission, “First Report and Order, Revision of Part 15 of the Commission’s Rules Regarding Ultra-Wideband Transmission Systems,” *ET Docket 98-153*, Feb. 14, 2002.

[4] J. Foerster et al., “Channel modeling sub-committee report final,” IEEE P802.15 Wireless Personal Area Networks, P802.15-02/490r1-SG3a, Feb. 2003.

[5] J. D. Choi and W.E. Stark, “Performance of Ultra-Wideband Communications with Suboptimal Receivers in Multi-path Channels,” *IEEE Journal on Selected Areas in Communications*, vol. 20, pp. 1754-1766, Dec. 2002.

[6] M. Z. Win and R.A. Scholtz, “Ultra-wide bandwidth time-hopping spread-spectrum impulse radio for wireless multiple-access communications,” *IEEE Trans. Commun.*, vol. 48, pp. 679–689, Apr., 2000.

[7] Multi-Band OFDM Alliance, “Ultra wideband: High-speed, short-range technology with far-reaching effects,” *MBOA-SIG White Paper*, September, 2004, http://www.multibandofdm.org/papers/MBOA_UWB_White_Paper.pdf.

[8] R. T. Hoctor and H. W. Tomlinson, “Delay-hopped transmitted reference RF communications,” *Proc. 2002 UWBST*, pp. 265-270, May 2002.

[9] A Saleh and R. Valenzuela, “A statistical model for indoor multi-path propagation,” *IEEE Journal on Selected Areas in Communications*, vol. 5, pp. 128-137, Feb. 1987.

[10] M. Win, R. Scholtz, “Characterization of ultra-wide bandwidth wireless indoor channels: a communication-theoretic view,” *IEEE Journal on Selected Areas in Communications*, vol. 20, no. 9, pp. 1613-1627, Dec. 2002.

[11] R. Price, P. E. Green, “A Communication Technique for Multi-path Channels,” *Proc. IRE.*, vol. 46, pp. 555-570, Mar. 1958.

[12] G. L. Turin, “The effect of multipath and fading on the performance of direct sequence CDMA systems,” *IEEE Journal on Selected Areas in Communications*, vol. 2, pp. 597-603, Jul. 1994.

[13] J. G. Proakis, *Digital Communications*, 4th edition, McGraw Hill Inc., 2001.

[14] M. Z. Win and R. A. Sholtz, “On the energy capture of ultrawide bandwidth signals in dense multipath environments,” *IEEE Commun. Lett.*, vol. 2, pp. 245–247, Sep. 1998.

[15] V. Lottici, A. D’Andrea, and U. Mengali, “Channel estimation for ultra-wideband communications,” *IEEE Journal on Selected Areas in Communications*, vol. 20, no. 9, pp. 1638–1645, 2002.

[16] R. Fantacci and A. Galligani, “An Efficient RAKE Receiver Architecture with Pilot Signal Cancellation for Downlink Communications in DS-CDMA Indoor

Wireless Networks," *IEEE Transactions on Communications*, vol. 47, no. 6, June 1999, pp. 823-827.

[17] A. J. Viterbi, *CDMA, Principles of Spread Spectrum Communication.* Reading, MA: Addison Wesley, 1995.

[18] T. S. Rappaport, *Wireless Communications.* Upper Saddle River, NJ: Prentice Hall, 1996.

[19] Brennan, D. G. "Linear Diversity Combining Techniques," Proc. IRE., vol. 47, pp. 1075-1102.

[20] M. Z. Win and Z. A. Kostic´, "Virtual path analysis of selective Rake receiver in dense multipath channels," *IEEE Commun. Lett.*, vol. 3, pp. 308–310, Nov. 1999.

[21] J. Keignart and N. Daniele, "Subnanosecond UWB Channel Sounding in Frequency and Temporal Domain," in *Proc. IEEE Conf. Ultra Wideband Systems and Technol*., pp. 25-30, May 2002.

[22] Marvin K. Simon, Sami M. Hinedi, and William C. Lindsey, Digital Communication Techniques: Signal Design and Detection, Prentice Hall, Englewood Cliffs, New Jersey 07632, first edition, 1995.

[23] L. Zhao and A. M. Haimovich, "Performance of ultra-wideband communications in the presence of interference," in Proc. IEEE Int. Conf. Communications (ICC'01), Helsinki, Finland, June 2001, pp. 2948–2952.

[24] F. Ramirez-Mireles, "Performance of ultra wideband SSMA using timehopping And M-Ary PPM," IEEE J. Select. Areas Commun., vol. 19, pp. 1186–1196, June 2001.

[25] Rusch, L. A., C. Prettie, D. Cheung, Q. Li, and M. Ho, "*Characterization of UWB Propagation from 2 to 8 GHz in a Residential Environment*," IEEE Journal on Selected Areas in Communications, submitted December 2001.

[26] Madhow, U., "*Blind adaptive interference suppression for direct-sequence CDMA*," Proceedings of the IEEE , vol. 86, no. 10, pp. 2049-2069, Oct. 1998.

[27] Ramirez-Mireles, F., "*On the performance of ultra-wideband signals in gaussian noise and dense multipath*," IEEE Transactions on Vehicular Technology, vol. 50, no. 1, pp. 244-249, Jan 2001 .

[28] M. Z. Win and R. A. Scholtz, "Impulse radio: How it works," *IEEE Comm. Lett.*, vol. 2, pp. 36–38, Feb 1998.

[29] D. Cassioli, M. Z. Win, A. F. Molisch, and F. Vatelaro, "Performance of selective Rake reception in a realistic UWB channel," in Proc. ICC 2002, pp. 763–767, 2002.

[30] D. Barras, F. Ellinger, H. Jackel, "A comparison between ultra wideband and narrowband transceivers,"
http://www.ife.ee.ethz.ch/~ellinger/Homepage/UWB2002.pdf

[31] D. Porcino, W. Hirt, "Ultra-Wideband Radio Technology: Potential and Challenges Ahead," *IEEE Communications Magazines*, pp. 66-74, July 2003.

[32] Simon Haykin, *Adaptive Filter Theory*, 4th edition, Prentice Hall Inc., 2001.

Appendix A: Discrete-time model for a channel with ISI

The received base-band signal can be expressed as

$$r_l(t) = \sum_n I_n h(t - nT) + z(t) \tag{A.1}$$

where $\{I_n\}$ is the information sequence, $h(t)$ represents the response of the channel to the input signal pulse $g(t)$ and $z(t)$ represents the additive white Gaussian noise. Since the transmitter sends discrete-time symbols at a rate of $1/T$ symbols/s and the sampled output of the matched filter at the receiver is also a discrete-time signal with samples occurring at a rate of $1/T$ per second, the cascade of the analog filter at the transmitter with impulse response $g(t)$, the channel with impulse response $c(t)$, the matched filter at the receiver with impulse response $h^*(-t)$, and the sampler can be represented by an equivalent discrete-time transversal filter having tap gain coefficients $\{x_k\}$. This equivalent discrete-time transversal filter spans a time interval of $2LT$ seconds. Its input is the sequence of information symbols $\{I_k\}$ and its output is the discrete-time sequence $\{y_k\}$ given by Eq.A.1.

$$y_k = \sum_n I_n x_{k-n} + \upsilon_k \tag{A.2}$$

Where $$y_k \equiv y(kT) = \int_{-\infty}^{\infty} r_l(t) h^*(t - kT) dt \tag{A.3}$$

$$x_k \equiv x(kT) = \int_{-\infty}^{\infty} h^*(t) h(t + kT) dt \tag{A.4}$$

υ_k denotes the additive noise sequence at the output of the matched filter,

$$\upsilon_k = \int_{-\infty}^{\infty} z(t)h^*(t-kT)dt \tag{A.5}$$

In any practical system, it is reasonable to assume that ISI affects a finite number of symbols. Hence, it is can be assumed that $x_n = 0$ for $|n| > L$. The autocorrelation function of the additive noise sequence $\{\upsilon_k\}$ is:

$$\frac{1}{2}E(\upsilon_k^*\upsilon_j) = \frac{1}{2}E\left\{\left[\int_{-\infty}^{\infty} z(t)h^*(t-kT)dt\right]^*\left[\int z(t)h^*(t-jT)dt\right]\right\}$$

$$= \begin{Bmatrix} N_0 x_{j-k} & (|k-j| \le L) \\ 0 & (otherwise) \end{Bmatrix} \tag{A.6}$$

Hence, the noise sequence is correlated. Since it is more convenient to deal with the white noise sequence when calculating the error rate performance, it is desirable to whiten the noise sequence by further filtering the sequence $\{y_k\}$. Consequently, passage of the sequence $\{y_k\}$ through the digital noise-whitening filter results in an output sequence $\{v_k\}$ that can be expressed as

$$v_k = \sum_{n=0}^{L} f_n I_{k-n} + \eta_k \tag{A.7}$$

where $\{\eta_k\}$ is a white Gaussian noise sequence and $\{f_k\}$ is a set of tap coefficients of an equivalent discrete-time transversal filter having a transfer function $F(z)$.

In summary, the cascade of the transmitting filter $g(t)$, the channel $c(t)$, the matched filter $h^*(-t)$, the sampler, and the discrete-time noise-whitening filter can be represented as an equivalent discrete-time transversal filter having the set $\{f_k\}$ as its tap coefficients. The additive noise sequence $\{\eta_k\}$ corrupting the output of the discrete-time transversal filter is a white Gaussian noise sequence having zero-

mean and variance N_0. Figure A-1 illustrates the discrete-time model for a channel with ISI.

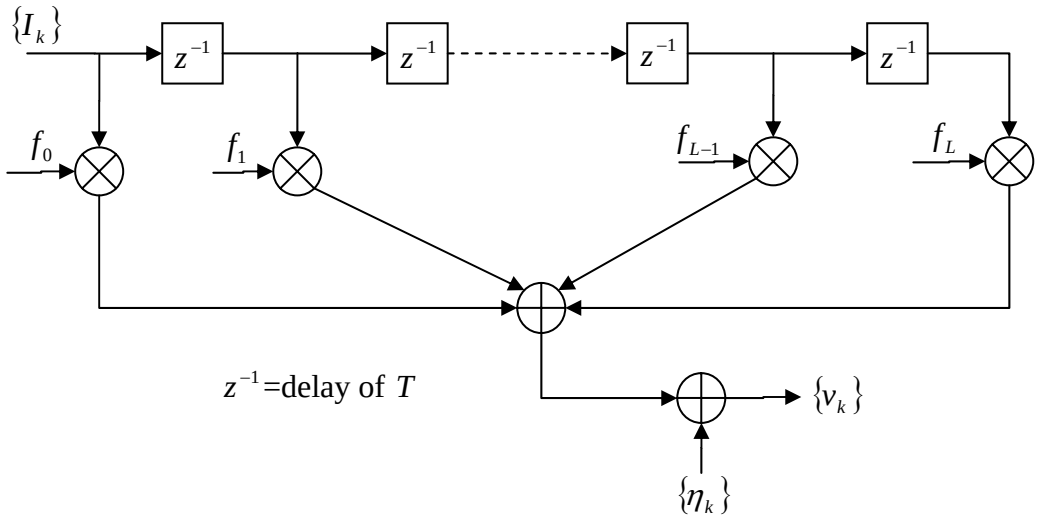

Figure A-1: Equivalent discrete-time model of ISI channel with AWGN

Appendix B: Zero-forcing equalizer

Eq.A.7 is rewritten here.

$$v_k = \sum_{n=0}^{L} f_n I_{k-n} + \eta_k \tag{B.1}$$

The linear equalization process can be expressed as

$$\hat{I}_k = \sum_{j=-\infty}^{\infty} c_j v_{k-j} \tag{B.2}$$

where $\{c_j\}$ are the complex-valued tap weight coefficients of the linear equalizer. Sequence $\{v_k\}$ is the demodulator output and sequence $\{\hat{I}_k\}$ is the estimate of the information sequence $\{I_k\}$. The equalizer is assumed to have an infinite number of taps.

It is observed that the cascade of the discrete-time linear filter model having an impulse response $\{f_n\}$ and an equalizer having an impulse response $\{c_n\}$ can be represented by a single equivalent filter having the impulse response

$$q_n = \sum_{j=-\infty}^{\infty} c_j f_{n-j} \tag{B.3}$$

$\{q_n\}$ is simply the convolution of $\{c_n\}$ and $\{f_n\}$. Its output at the k^{th} sampling instant can be expressed in the form

$$\hat{I}_k = q_0 I_k + \sum_{n \neq k} I_n q_{k-n} + \sum_{j=-\infty}^{\infty} c_j \eta_{k-j} \tag{B.4}$$

The first term in Eq.B.3 represents a scaled version of the desired symbol. The second term is the inter-symbol interference. The peak value of this interference, which is called peak distortion, is

$$D(c) = \sum_{n \neq 0} |q_n|$$

$$= \sum_{n \neq 0} \left| \sum_{j=-\infty}^{\infty} c_j f_{n-j} \right| \tag{B.5}$$

Where $D(c)$ is a function of the equalizer tap coefficients.

With an equalizer having an infinite number of taps, it is possible to select the tap weights so that $D(c) = 0$, i.e., $q_n = 0$ for all n except $n = 0$. That is, the inter-symbol interference can be completely eliminated. The values of the tap weights to accomplish this goal are determined from the condition

$$q_n = \sum_{j=-\infty}^{\infty} c_j f_{n-j} = \begin{Bmatrix} 1 & (n = 0) \\ 0 & (n \neq 0) \end{Bmatrix} \tag{B.6}$$

By taking the z transform of Eq.B-5, it is obtained

$$Q(z) = C(z)F(z) = 1 \tag{B.7}$$

$$C(z) = \frac{1}{F(z)} \tag{B.8}$$

where $C(z)$ denotes the z transform of the $\{c_j\}$. Note that the equalizer, with transfer function $C(z)$, is simply the inverse filter to the linear filter model $F(z)$. In other words, complete elimination of the inter-symbol interference requires the use of an inverse filter to $F(z)$. Such equalizer is called a zero-forcing equalizer.

Appendix C: Mean-square-error (MSE) criterion linear equalizer

In the MSE criterion, the tap weight coefficients $\{c_j\}$ of the equalizer are adjusted to minimize the mean square value of the error

$$J = E|\varepsilon_k|^2 = E|I_k - \hat{I}_k|^2 \tag{C.1}$$

where I_k is the information symbol transmitted in the k^{th} signaling interval and $\hat{I}_k$ is the estimate of that symbol at the output of the equalizer. Here the principle of orthogonality, one of the most elegant theorems in the subject of linear optimum filtering, was stated:

"The necessary and sufficient condition for the cost function J to obtain its minimum value is for the corresponding value of the estimation error ε_k to be orthogonal to each input sample that enters into the estimation of the desired response at time k."

When the equalizer is assumed to have a finite number of taps, the linear equalization process can be expressed as

$$\hat{I}_k = \sum_{j=-K}^{K} c_j v_{k-j} \tag{C.2}$$

where $\{c_j\}$ are the complex-valued tap weight coefficients of the linear equalizer. Sequence $\{v_k\}$ is the demodulator output. For the cost function J to obtain its minimum value, the orthogonal condition which must be satisfied is expressed as:

$$E(\varepsilon_k v_{k-l}^*) = 0, \qquad -K < l < K \tag{C.3}$$

Substitution for ε_k in Eq.C.3 yields

$$E\left[\left(I_k - \sum_{j=-K}^{K} c_j v_{k-j}\right) v_{k-l}^*\right] = 0 \tag{C.4}$$

equivalently,

$$\sum_{j=-K}^{K} c_j E\left(v_{k-j} v_{k-l}^*\right) = E\left(I_k v_{k-l}^*\right), \qquad -K < l < K \tag{C.5}$$

It is convenient to express the set of linear equations in matrix form. Thus,

$$\Gamma C = \mathrm{P} \tag{C.6}$$

Let Γ denote the (2K+1)-by-(2K+1) correlation matrix of the demodulator output sequence $\{v_k\}$:

$$\Gamma = E\left[V^*(k) V^T(k)\right] \tag{C.7}$$

Where $V(k) = \left[v_{k-K}, v_{k-(K-1)}, \ldots, v_k, \ldots, v_{k+(K-1)}, v_{k+K}\right]^T$ is the (2k+1)-by-1 demodulator output sequence $\{v_k\}$ vector at time *k*.

Correspondingly, let P denote the (2k+1)-by-1 cross-correlation vector between the demodulator output sequence $\{v_k\}$ vector and the information signal I_k:

$$\mathrm{P} = E\left[V^*(k) I_k\right] \tag{C.8}$$

$C = \left[c_K, c_{K-1}, \ldots, c_0, \ldots, c_{-(K-1)}, c_{-K}\right]^T$ is the (2k+1)-by-1 equalizer coefficients vector.

The solution of Eq.C.6 is

$$C_{optimum} = \Gamma^{-1}\mathrm{P} \tag{C.9}$$

where Γ^{-1} is the inverse matrix of Γ.

Appendix D: Procedure to calculate a gradient vector

Gradient vector of a cost function $J(\vec{w})$, which is denoted by $\nabla J(\vec{w})$, is written.

$$\nabla J(\vec{w}) = \frac{\partial J(\vec{w})}{\partial \vec{w}} = \begin{bmatrix} \frac{\partial J(\vec{w})}{\partial a_1} + j\frac{\partial J(\vec{w})}{\partial b_1} \\ \frac{\partial J(\vec{w})}{\partial a_2} + j\frac{\partial J(\vec{w})}{\partial b_2} \\ \vdots \\ \frac{\partial J(\vec{w})}{\partial a_M} + j\frac{\partial J(\vec{w})}{\partial b_M} \end{bmatrix} \tag{D.1}$$

where $\vec{w} = [a_1 + jb_1, \quad a_2 + jb_2, \quad \cdots \quad , a_M + jb_M]$ is a complex valued vector.

The linear equalization process can be expressed as

$$\hat{I}_k = \sum_{j=-K}^{K} c_j v_{k-j} \tag{D.2}$$

where $\{c_j\} = \{a_j + jb_j\}$ are the complex-valued tap weight coefficients of the linear equalizer. Sequence $\{v_k\}$ is the demodulator output.

The cost function J is

$$J = E|\varepsilon_k|^2 = E|I_k - \hat{I}_k|^2$$

$$= E[\varepsilon_k \varepsilon_k^*] = E[(I_k - \hat{I}_k)(I_k - \hat{I}_k)^*]$$

substituting Eq.D.2.

$$= E[|I_k|^2] - \sum_{j=-K}^{K} c_j^* E[v_{k-j}^* I_k] - \sum_{j=-K}^{K} c_j E[v_{k-j} I_k^*] + \sum_{j=-K}^{K} \sum_{i=-K}^{K} c_j c_i^* E[v_{k-j} v_{k-i}^*] \tag{D.3}$$

The gradient vector of the cost function J based on the equalizer coefficients vector $C = \left[c_K, c_{K-1}, \ldots, c_0, \ldots, c_{-(K-1)}, c_{-K}\right]^T$ is

$$\nabla J(C) = \frac{\partial J(C)}{\partial C} = \frac{\partial\left(E\left[\left|I_k\right|^2\right]\right)}{\partial C} - \frac{\partial\left(\sum_{j=-K}^{K} c_j^* E\left[v_{k-j}^* I_k\right]\right)}{\partial C} - \frac{\partial\left(\sum_{j=-K}^{K} c_j E\left[v_{k-j} I_k^*\right]\right)}{\partial C} + \frac{\partial\left(\sum_{j=-K}^{K}\sum_{i=-K}^{K} c_j c_i^* E\left[v_{k-j} v_{k-i}^*\right]\right)}{\partial C} \quad \text{(D.4)}$$

Now the four parts on the right-hand side will be calculated separately:

1. for the first part,

$\frac{\partial\left(E\left[\left|I_k\right|^2\right]\right)}{\partial C} = \begin{bmatrix} 0 \\ 0 \\ \vdots \\ 0 \end{bmatrix}$ is a (2k+1)-by-1 null vector.

2. for the second part,

$$\frac{\partial\left(\sum_{j=-K}^{K} c_j^* E\left[v_{k-j}^* I_k\right]\right)}{\partial C} = \begin{bmatrix} \frac{\partial\left(\sum_{j=-K}^{K} c_j^* E\left[v_{k-j}^* I_k\right]\right)}{\partial a_K} + j\frac{\partial\left(\sum_{j=-K}^{K} c_j^* E\left[v_{k-j}^* I_k\right]\right)}{\partial b_K} \\ \frac{\partial\left(\sum_{j=-K}^{K} c_j^* E\left[v_{k-j}^* I_k\right]\right)}{\partial a_{K-1}} + j\frac{\partial\left(\sum_{j=-K}^{K} c_j^* E\left[v_{k-j}^* I_k\right]\right)}{\partial b_{K-1}} \\ \vdots \\ \frac{\partial\left(\sum_{j=-K}^{K} c_j^* E\left[v_{k-j}^* I_k\right]\right)}{\partial a_{-K}} + j\frac{\partial\left(\sum_{j=-K}^{K} c_j^* E\left[v_{k-j}^* I_k\right]\right)}{\partial b_{-K}} \end{bmatrix}$$

$$= \begin{bmatrix} \frac{\partial\left(c_K^* E\left[v_{k-K}^* I_k\right]\right)}{\partial a_K} + j\frac{\partial\left(c_K^* E\left[v_{k-K}^* I_k\right]\right)}{\partial b_K} \\ \frac{\partial\left(c_{K-1}^* E\left[v_{k-(K-1)}^* I_k\right]\right)}{\partial a_{K-1}} + j\frac{\partial\left(c_{K-1}^* E\left[v_{k-(K-1)}^* I_k\right]\right)}{\partial b_{K-1}} \\ \vdots \\ \frac{\partial\left(c_{-K}^* E\left[v_{k+K}^* I_k\right]\right)}{\partial a_{-K}} + j\frac{\partial\left(c_{-K}^* E\left[v_{k+K}^* I_k\right]\right)}{\partial b_{-K}} \end{bmatrix}$$

$$= \begin{bmatrix} \frac{\partial\left((a_K - jb_K)E\left[v_{k-K}^* I_k\right]\right)}{\partial a_K} + j\frac{\partial\left((a_K - jb_K)E\left[v_{k-K}^* I_k\right]\right)}{\partial b_K} \\ \frac{\partial\left((a_{K-1} - jb_{K-1})E\left[v_{k-(K-1)}^* I_k\right]\right)}{\partial a_{K-1}} + j\frac{\partial\left((a_{K-1} - jb_{K-1})E\left[v_{k-(K-1)}^* I_k\right]\right)}{\partial b_{K-1}} \\ \vdots \\ \frac{\partial\left((a_{-K} - jb_{-K})E\left[v_{k+K}^* I_k\right]\right)}{\partial a_{-K}} + j\frac{\partial\left((a_{-K} - jb_{-K})E\left[v_{k+K}^* I_k\right]\right)}{\partial b_{-K}} \end{bmatrix}$$

$$= \begin{bmatrix} E\left[v_{k-K}^* I_k\right] + j(-j)E\left[v_{k-K}^* I_k\right] \\ E\left[v_{k-(K-1)}^* I_k\right] + j(-j)E\left[v_{k-(K-1)}^* I_k\right] \\ \vdots \\ E\left[v_{k+K}^* I_k\right] + j(-j)E\left[v_{k+K}^* I_k\right] \end{bmatrix}$$

$$= 2\begin{bmatrix} E\left[v_{k-K}^* I_k\right] \\ E\left[v_{k-(K-1)}^* I_k\right] \\ \vdots \\ E\left[v_{k+K}^* I_k\right] \end{bmatrix}$$

3. for the third part,

$$\frac{\partial\left(\sum_{j=-K}^{K} c_j E\left[v_{k-j} I_k^*\right]\right)}{\partial C} = \begin{bmatrix} \frac{\partial\left(\sum_{j=-K}^{K} c_j E\left[v_{k-j} I_k^*\right]\right)}{\partial a_K} + j\frac{\partial\left(\sum_{j=-K}^{K} c_j E\left[v_{k-j} I_k^*\right]\right)}{\partial b_K} \\ \frac{\partial\left(\sum_{j=-K}^{K} c_j E\left[v_{k-j} I_k^*\right]\right)}{\partial a_{K-1}} + j\frac{\partial\left(\sum_{j=-K}^{K} c_j E\left[v_{k-j} I_k^*\right]\right)}{\partial b_{K-1}} \\ \vdots \\ \frac{\partial\left(\sum_{j=-K}^{K} c_j E\left[v_{k-j} I_k^*\right]\right)}{\partial a_{-K}} + j\frac{\partial\left(\sum_{j=-K}^{K} c_j E\left[v_{k-j} I_k^*\right]\right)}{\partial b_{-K}} \end{bmatrix}$$

$$= \begin{bmatrix} \frac{\partial\left(c_K E\left[v_{k-K} I_k^*\right]\right)}{\partial a_K} + j\frac{\partial\left(c_K E\left[v_{k-K} I_k^*\right]\right)}{\partial b_K} \\ \frac{\partial\left(c_{K-1} E\left[v_{k-(K-1)} I_k^*\right]\right)}{\partial a_{K-1}} + j\frac{\partial\left(c_{K-1} E\left[v_{k-(K-1)} I_k^*\right]\right)}{\partial b_{K-1}} \\ \vdots \\ \frac{\partial\left(c_{-K} E\left[v_{k+K} I_k^*\right]\right)}{\partial a_{-K}} + j\frac{\partial\left(c_{-K} E\left[v_{k+K} I_k^*\right]\right)}{\partial b_{-K}} \end{bmatrix}$$

$$= \begin{bmatrix} \frac{\partial\left((a_K + jb_K) E\left[v_{k-K} I_k^*\right]\right)}{\partial a_K} + j\frac{\partial\left((a_K + jb_K) E\left[v_{k-K} I_k^*\right]\right)}{\partial b_K} \\ \frac{\partial\left((a_{K-1} + jb_{K-1}) E\left[v_{k-(K-1)} I_k^*\right]\right)}{\partial a_{K-1}} + j\frac{\partial\left((a_{K-1} + jb_{K-1}) E\left[v_{k-(K-1)} I_k^*\right]\right)}{\partial b_{K-1}} \\ \vdots \\ \frac{\partial\left((a_{-K} + jb_{-K}) E\left[v_{k+K} I_k^*\right]\right)}{\partial a_{-K}} + j\frac{\partial\left((a_{-K} + jb_{-K}) E\left[v_{k+K} I_k^*\right]\right)}{\partial b_{-K}} \end{bmatrix}$$

$$= \begin{bmatrix} E\left[v_{k-K} I_k^*\right] + j(j) E\left[v_{k-K} I_k^*\right] \\ E\left[v_{k-(K-1)} I_k^*\right] + j(j) E\left[v_{k-(K-1)} I_k^*\right] \\ \vdots \\ E\left[v_{k+K} I_k^*\right] + j(j) E\left[v_{k+K} I_k^*\right] \end{bmatrix}$$

$$= \begin{bmatrix} 0 \\ 0 \\ \vdots \\ 0 \end{bmatrix}$$ is a (2k+1)-by-1 null vector.

4. for the fourth part,

$$\frac{\partial\left(\sum_{j=-K}^{K}\sum_{i=-K}^{K} c_j c_i^* E\left[v_{k-j} v_{k-i}^*\right]\right)}{\partial C} = \begin{bmatrix} \frac{\partial\left(\sum_{j=-K}^{K}\sum_{i=-K}^{K} c_j c_i^* E\left[v_{k-j} v_{k-i}^*\right]\right)}{\partial a_K} + j\frac{\partial\left(\sum_{j=-K}^{K}\sum_{i=-K}^{K} c_j c_i^* E\left[v_{k-j} v_{k-i}^*\right]\right)}{\partial b_K} \\ \frac{\partial\left(\sum_{j=-K}^{K}\sum_{i=-K}^{K} c_j c_i^* E\left[v_{k-j} v_{k-i}^*\right]\right)}{\partial a_{K-1}} + j\frac{\partial\left(\sum_{j=-K}^{K}\sum_{i=-K}^{K} c_j c_i^* E\left[v_{k-j} v_{k-i}^*\right]\right)}{\partial b_{K-1}} \\ \vdots \\ \frac{\partial\left(\sum_{j=-K}^{K}\sum_{i=-K}^{K} c_j c_i^* E\left[v_{k-j} v_{k-i}^*\right]\right)}{\partial a_{-K}} + j\frac{\partial\left(\sum_{j=-K}^{K}\sum_{i=-K}^{K} c_j c_i^* E\left[v_{k-j} v_{k-i}^*\right]\right)}{\partial b_{-K}} \end{bmatrix}$$

$$= \begin{bmatrix} \dfrac{\overbrace{\partial\left(c_K \sum_{i\neq K} c_i^* E\left[v_{k-K} v_{k-i}^*\right] + c_K^* \sum_{j\neq K} c_j E\left[v_{k-j} v_{k-K}^*\right] + c_K c_K^* E\left[v_{k-K} v_{k-K}^*\right]\right)}^{\Psi_K}}{\partial a_K} + j\frac{\Psi_K}{\partial b_K} \\ \dfrac{\overbrace{\partial\left(c_{K-1} \sum_{i\neq K-1} c_i^* E\left[v_{k-(K-1)} v_{k-i}^*\right] + c_{K-1}^* \sum_{j\neq K-1} c_j E\left[v_{k-j} v_{k-(K-1)}^*\right] + c_{K-1} c_{K-1}^* E\left[v_{k-(K-1)} v_{k-(K-1)}^*\right]\right)}^{\Psi_{K-1}}}{\partial a_{K-1}} + j\frac{\Psi_{K-1}}{\partial b_{K-1}} \\ \vdots \\ \dfrac{\overbrace{\partial\left(c_{-K} \sum_{i\neq -K} c_i^* E\left[v_{k+K} v_{k-i}^*\right] + c_{-K}^* \sum_{j\neq -K} c_j E\left[v_{k-j} v_{k+K}^*\right] + c_{-K} c_{-K}^* E\left[v_{k+K} v_{k+K}^*\right]\right)}^{\Psi_{-K}}}{\partial a_{-K}} + j\frac{\Psi_{-K}}{\partial b_{-K}} \end{bmatrix}$$

$$= \begin{bmatrix} 2\sum_{j\neq K} c_j E\left[v_{k-j} v_{k-K}^*\right] + \dfrac{(a_K^2 + b_K^2) E\left[v_{k-K} v_{k-K}^*\right]}{\partial a_K} + j\dfrac{(a_K^2 + b_K^2) E\left[v_{k-K} v_{k-K}^*\right]}{\partial b_K} \\ 2\sum_{j\neq K-1} c_j E\left[v_{k-j} v_{k-(K-1)}^*\right] + \dfrac{(a_{K-1}^2 + b_{K-1}^2) E\left[v_{k-(K-1)} v_{k-(K-1)}^*\right]}{\partial a_{K-1}} + j\dfrac{(a_{K-1}^2 + b_{K-1}^2) E\left[v_{k-(K-1)} v_{k-(K-1)}^*\right]}{\partial b_{K-1}} \\ \vdots \\ 2\sum_{j\neq -K} c_j E\left[v_{k-j} v_{k+K}^*\right] + \dfrac{(a_{-K}^2 + b_{-K}^2) E\left[v_{k+K} v_{k+K}^*\right]}{\partial a_{-K}} + j\dfrac{(a_{-K}^2 + b_{-K}^2) E\left[v_{k+K} v_{k+K}^*\right]}{\partial b_{-K}} \end{bmatrix}$$

$$= 2\begin{bmatrix} \sum_{j=-K}^{K} c_j E\left[v_{k-j} v_{k-K}^*\right] \\ \sum_{j=-K}^{K} c_j E\left[v_{k-j} v_{k-(K-1)}^*\right] \\ \vdots \\ \sum_{j=-K}^{K} c_j E\left[v_{k-j} v_{k+K}^*\right] \end{bmatrix}$$

The gradient vector of the cost function J based on the equalizer coefficients vector $C = \left[c_K, c_{K-1}, \ldots, c_0, \ldots, c_{-(K-1)}, c_{-K}\right]^T$ can be rewritten

$$\nabla J(C) = -2\begin{bmatrix} E\left[v_{k-K}^* I_k\right] \\ E\left[v_{k-(K-1)}^* I_k\right] \\ \vdots \\ E\left[v_{k+K}^* I_k\right] \end{bmatrix} + 2\begin{bmatrix} \sum_{j=-K}^{K} c_j E\left[v_{k-j} v_{k-K}^*\right] \\ \sum_{j=-K}^{K} c_j E\left[v_{k-j} v_{k-(K-1)}^*\right] \\ \vdots \\ \sum_{j=-K}^{K} c_j E\left[v_{k-j} v_{k+K}^*\right] \end{bmatrix} = -2\mathrm{P} + 2\Gamma C \qquad \text{(D.5)}$$

Let Γ denote the (2K+1)-by-(2K+1) correlation matrix of the demodulator output sequence $\{v_k\}$:

$$\Gamma = E\left[V^*(k)V^T(k)\right]$$

where $V(k) = \left[v_{k-K}, v_{k-(K-1)}, \ldots, v_k, \ldots, v_{k+(K-1)}, v_{k+K}\right]^T$ is the (2k+1)-by-1 demodulator output sequence $\{v_k\}$ vector at time *k*.

Correspondingly, let P denote the (2k+1)-by-1 cross-correlation vector between the demodulator output sequence $\{v_k\}$ vector and the information signal I_k:

$$\mathrm{P} = E\left[V^*(k)I_k\right]$$

$C = \left[c_K, c_{K-1}, \ldots, c_0, \ldots, c_{-(K-1)}, c_{-K}\right]^T$ is the (2k+1)-by-1 equalizer coefficients vector.